SYSTEM IDENTIFICATION OF SITE AMPLIFICATION

A THESIS

Submitted by

N. K. SATYANARAYANA

for the award of the degree
of

MASTER of SCIENCE

(by Research)

Under the guidance of

Dr. G. V. RAMANA

GEOTECHNICAL ENGINEERING DIVISION

DEPARTMENT OF CIVIL ENGINEERING

INDIAN INSTITUTE OF TECHNOLOGY, DELHI

NEW DELHI – 110 016

CERTIFICATE

This is to certify that the thesis entitled "SYSTEM IDENTIFICATION OF SITE AMPLIFICATION", submitted by Nagampalli Krishna Satyanarayana to the Indian Institute of Technology, Delhi for the degree of Master of Science by Research is a bonafide record of research work carried out by him under my supervision. The contents of the thesis, in full or in part, have not been submitted to any other Institute or University for the award of degree or diploma.

New Delhi

Date: 10/4/01

(Dr. G. V. Ramana)

(Supervisor)

ACKNOWLEDGEMENTS

As I pray Supreme power, it means everyone who are directly or indirectly helped me will be acknowledged since I feel the supreme power precontrols all my (our) moments and acknowledging assumed to be fulfilled to everyone without specification. But it would be a pleasure for me to say few words from my heart. First I thank Dr. G.V. Ramana, Assistant Professor of Civil Engineering Department for his unbounded patience, constant help and I felt innovative to work under him. I can not show my inexpressible heart feelings on my friends K. Satyanarayana, Sashidhar and Anjan Kumar for their invaluable help at crisis. I thank Dr. Akhila Sinha, Dr. Savita Goel, Dr. Kamal Punn of CSC, IIT Delhi for their timely help in using computer software. Finally I thank Professors of Geotechnical Engineering Division for their encouragement.

Krishna Satyanarayana Nagampalli

TABLE OF CONTENTS

ABSTRACT

The Institute of Industrial Science, Tokyo, Japan, initiated the Chiba downhole array, in 1982. This was instrumented with several densely spaced free field and downhole accelerometers, thus constituting a three dimensional array. In this study, the seismic site response during 27 earthquakes recorded at the site with varying peak ground accelerations, frequency content and duration is analyzed. Correlation analyses of the recorded downhole accelerations are performed to calculate the average shear and primary wave velocity profile. A two-layer solution was also employed to calculate the average shear wave profile. In addition, the seismic shear stress-strain histories are directly calculated from the downhole lateral accelerations. These histories are then used to estimate the soil stiffness and material damping in the linear, small strain range. The identified shear wave as well as primary wave velocity profile was compared with the geophysical measurements and with those reported by other researchers. The observed non-softening of the soil below 10 m depth even during the strongest recorded earthquake was explained.

LIST OF TABLES

LIST OF FIGURES

Assessment of site amplification effects necessitates a thorough understanding of the associated soil dynamic response characteristics and mechanisms. In-situ testing procedures currently followed, provide convenient means of measuring soil low-strain properties such as shear wave propagation velocities. At larger strain levels, soil properties are often evaluated through laboratory testing. However, due to limitations in undisturbed soil sampling techniques and difficulties in reproducing in-situ stress-strain and seismic loading history, data provided by laboratory tests may not reflect the site actual behavior, especially when subjected to strong-motion excitations.

Recorded site seismic response is a valuable complement to in-situ and laboratory geotechnical investigation techniques. In particular, analysis of downhole seismic array data provides unique information of actual soil (and overall site) behavior over a range of loading conditions that are not readily covered by in-situ or laboratory experimentation procedures. In view of the need for a better understanding of site dynamic response, downhole instrumentation is being increasingly deployed at seismically active locations especially in the United States, Japan, Mexico, and Taiwan. The recent fast accumulation of earthquake records from seismic arrays in well-documented sites provide a powerful new tool to measure and investigate the soil properties of interest (site characterization / amplification characteristics) under actual earthquake condition.

An earthquake may be viewed as a full-scale experiment and recorded input and output may be used to identify the stiffness and damping properties, and is a valuable complement to other geotechnical investigations. Evaluation of soil properties from earthquake records provide information on soil behavior over a range of excitation that are not readily covered by in-situ or laboratory experimentation and more importantly without resorting to in-situ sampling (Kramer et al. [32]), which may not be a very representation of the overall composition.

Once the array station established and seismometers installed, sequential earthquake records can be obtained for further analysis, unlike as in the case of laboratory analysis where the samples would be required every time from the required depth at which the in-situ test results are needed. Further the analysis done on borehole recordings may be correlated with results of laboratory testing.

In 1982, a unique three dimensional array system was installed at Chiba experiment station of Institution of Industrial Science, University of Tokyo. A database of acceleration time history of 27 earthquake events was made available for various boreholes (C0, C1, C2, C3, C4, P1, P2, P3, P4, P5, P6, P7, P8, P9, and P0). The site location was selected because of its intense seismic activity and the presence of thick soil strata above bedrock. In the present study, acceleration time history records of the borehole C0, where the Peak Ground Acceleration (PGA) is greater than 10 cm/sec^2, are used for estimating the dynamic soil properties. These earthquakes were found to vary in peak acceleration, shaking duration and frequency content bandwidth; thus providing a valuable source over a broad range of excitations.

1.2 Objectives

The main objectives of this study were to analyze the Chiba seismic records and to identify the site dynamic response properties and mechanisms. Free field surface and downhole acceleration records were used,

- to identify the site resonant frequencies
- to evaluate the site shear wave propagation characteristics
- to document the presence of nonlinear response at large Peak Ground Acceleration (PGA) levels and
- to evaluate the variations of soil stiffness and damping properties.

1.3 Methodology

Identification of site dynamic response properties and mechanisms from seismic records requires preliminary analyses to assess data quality and classify the recorded response and loading conditions. The identification methodology consists of:

- Pattern recognition and classification of the recorded response.
- Selection of a class of appropriate analytical / computational models and assessment of the most influential dynamic response parameters.
- Estimation of these parameters.

Assessment of site amplification effects necessitates a thorough understanding of the associated soil dynamic response characteristics and mechanisms. In-situ testing procedures currently followed, provide convenient means of measuring soil low-strain properties such as shear wave propagation velocities. At larger strain levels, soil properties are often evaluated through laboratory testing. However, due to limitations in undisturbed soil sampling techniques and difficulties in reproducing in-situ stress-strain and seismic loading history, data provided by laboratory tests may not reflect the site actual behavior, especially when subjected to strong-motion excitations.

Recorded site seismic response is a valuable complement to in-situ and laboratory geotechnical investigation techniques. In particular, analysis of downhole seismic array data provides unique information of actual soil (and overall site) behavior over a range of loading conditions that are not readily covered by in-situ or laboratory experimentation procedures. In view of the need for a better understanding of site dynamic response, downhole instrumentation is being increasingly deployed at seismically active locations especially in the United States, Japan, Mexico, and Taiwan. The recent fast accumulation of earthquake records from seismic arrays in well-documented sites provide a powerful new tool to measure and investigate the soil properties of interest (site characterization / amplification characteristics) under actual earthquake condition.

An earthquake may be viewed as a full-scale experiment and recorded input and output may be used to identify the stiffness and damping properties, and is a valuable complement to other geotechnical investigations. Evaluation of soil properties from earthquake records provide information on soil behavior over a range of excitation that are not readily covered by in-situ or laboratory experimentation and more importantly without resorting to in-situ sampling (Kramer et al. [32]), which may not be a very representation of the overall composition.

Once the array station established and seismometers installed, sequential earthquake records can be obtained for further analysis, unlike as in the case of laboratory analysis where the samples would be required every time from the required depth at which the in-situ test results are needed. Further the analysis done on borehole recordings may be correlated with results of laboratory testing.

In 1982, a unique three dimensional array system was installed at Chiba experiment station of Institution of Industrial Science, University of Tokyo. A database of acceleration time history of 27 earthquake events was made available for various boreholes (C0, C1, C2, C3, C4, P1, P2, P3, P4, P5, P6, P7, P8, P9, and P0). The site location was selected because of its intense seismic activity and the presence of thick soil strata above bedrock. In the present study, acceleration time history records of the borehole C0, where the Peak Ground Acceleration (PGA) is greater than 10 cm/sec^2, are used for estimating the dynamic soil properties. These earthquakes were found to vary in peak acceleration, shaking duration and frequency content bandwidth; thus providing a valuable source over a broad range of excitations.

1.2 Objectives

The main objectives of this study were to analyze the Chiba seismic records and to identify the site dynamic response properties and mechanisms. Free field surface and downhole acceleration records were used,

- to identify the site resonant frequencies
- to evaluate the site shear wave propagation characteristics
- to document the presence of nonlinear response at large Peak Ground Acceleration (PGA) levels and
- to evaluate the variations of soil stiffness and damping properties.

1.3 Methodology

Identification of site dynamic response properties and mechanisms from seismic records requires preliminary analyses to assess data quality and classify the recorded response and loading conditions. The identification methodology consists of:

- Pattern recognition and classification of the recorded response.
- Selection of a class of appropriate analytical / computational models and assessment of the most influential dynamic response parameters.
- Estimation of these parameters.

The conducted analyses fall within the pattern recognition phase. They are based on non-parametric identifications to classify the recorded seismic response at Chiba and evaluate the most influential response parameters and mechanisms.

1.4 Analyses Techniques

As stated above, the objectives of this study were to analyze the recorded seismic soil response at Chiba array and to identify the site dynamic response properties. Two classes of techniques were employed to attain these objectives:

- Correlation and spectral techniques to estimate site low-strain parameters such as shear wave velocities, resonant frequencies and to assess the effects of non-linearities on these parameters.

- A simple non-parametric identification technique was developed to estimate the site shear stress-strain histories and to evaluate variations of stiffness and damping.

Spectral analysis was based on the Fourier transforms of the recorded data (using a fast Fourier transform algorithm). Welch technique was employed in estimating energy spectra to reduce random errors. A new non-parametric identification procedure recently developed was used to evaluate seismic shear stress-strain histories directly from downhole acceleration records.

This procedure is simple to implement and is well suited to site geometry and downhole accelerometer spacing. Furthermore, it does not require the availability of bedrock (input) motions, in contrast to many conventional techniques. At Chiba site no input records are available. In estimating stress and strain histories, filtering was performed using non-recursive zero-phase digital time-domain filters through Hanning window.

1.5 Organization of the Report

In this study report, site geotechnical profile geophysical measurements at borehole C0 and acceleration data of Chiba array are presented in Chapter 2. Literature review covering similar research work in the area of downhole arrays is presented in chapter 3. Shear and primary wave velocities estimated using a non-parametric identification technique (cross-correlation method) are compared with geophysical measurements in chapter 4.

Recorded acceleration time histories are used to identify the stiffness and damping properties of in-situ soil under actual earthquake conditions and the computed shear stress-strain histories are presented in chapter 5. Using a two-layer solution (a non-parametric identification), shear wave velocity profile between two downhole stations is estimated and compared with geophysical measurement profile in chapter 6. Summary and conclusions based on the results of three analyses techniques are presented in chapter 7.

Chapter 2

STRONG MOTION DATA – CHIBA ARRAY

2.1 Introduction

One of the state-of-the-art technologies in strong ground motion measurement is array installation and monitoring the data. The array observation system is an ideal tool for accumulating the strong-motion data. An array system provides information regarding strong-motion parameters viz. acceleration, velocity and sometimes strain by using systematically placed instruments oriented deep below the ground surface to monitor the peak earthquake signals as per the requirement.

The aim of observation dictates the arrangement of seismometers. One of the typical types is a two-dimensional surface array SMART-1 on thick alluvial site at Lotung, Taiwan and SMART-2 array on hard site in the Haulien area (Yeon-Tein et al. [51]). Another arrangement used for the present analysis is a dense seismograph array network installed at Chiba experiment station (Nagata et al. [36]). In this array, seismometers are placed very densely both on the ground surface and in the boreholes, constituting a three-dimensional network. The records obtained from this array are useful in evaluating the spatial correlations and in examining the amplification theory.

Arrays are also useful for studying earthquake response mechanisms and spatial distribution of many important earthquake parameters such as,

- Amplitude parameters (Peak acceleration, peak velocity, peak displacement, Sustained maximum acceleration and velocity, Effective design acceleration)
- Frequency content parameters (Ground motion spectra, Fourier spectra, Power spectra, and Response spectra)
- Spectral parameters (Predominant period, Bandwidth, Central frequency, Shape factor)
- Duration.

In addition, these records offer a solid basis for,

- Calculation of in-situ dynamic properties
- Refinement of empirical and computational predictive techniques
- Calibration of numerical models

The Chiba array has been successfully operating since 1982 and over 160 events have been recorded. A database has been created for the effective utilization of these earthquake records, which can be obtained from University of Tokyo, Japan.

2.2 Geotechnical profile

The Chiba experiment station is located about 30 km east of Tokyo as shown in Figure 2.1. The longitude of the station is $140^{\circ}\,6'\,37''\,E$ and the latitude is $35^{\circ}\,37'\,17''\,N$.

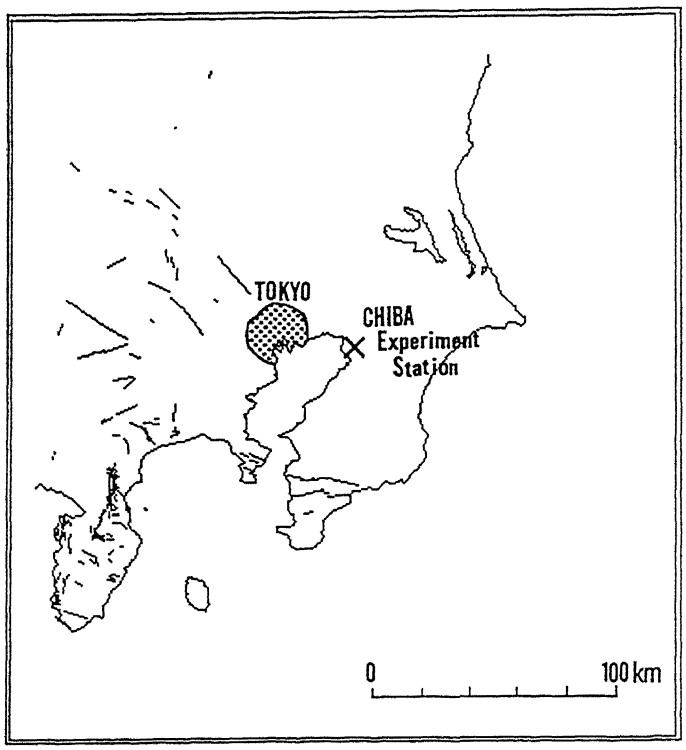

Figure 2.1: Location of Chiba experiment station

The layout of the boreholes instrumented with accelerometers is shown in Figure 2.2. The co-ordinates of each borehole at ground surface are listed in Table 2.1. The data obtained from borehole C0 is used in the analysis for the present work. Seismometers are placed in the boreholes at various depths and the location of borehole accelerometers is given in Table 2.2.

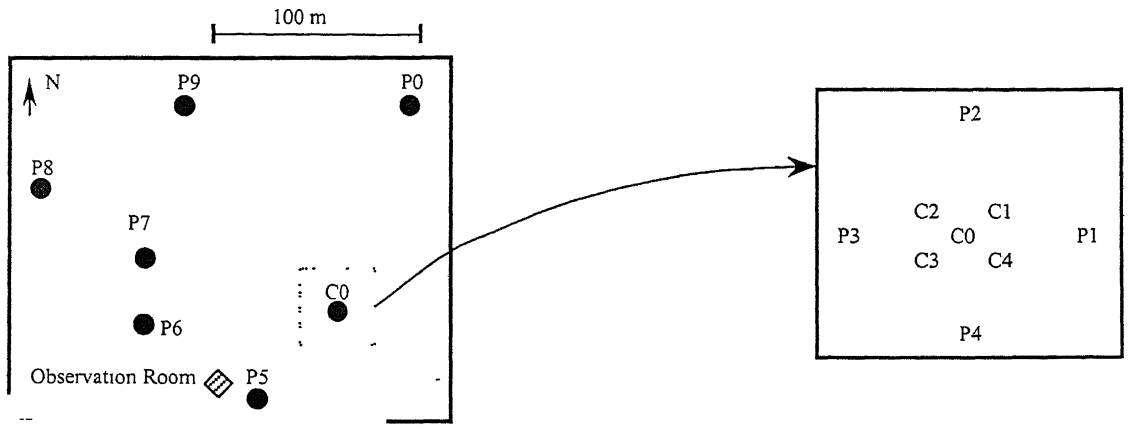

Figure 2.2: Layout of boreholes

Table 2.1: Co-ordinates of boreholes at ground surface

Borehole	Relative to C0		Elevation (m)
	East (m)	East (m)	
C0	0.00	0.00	13.52
C1	3.54	3.54	13.52
C2	-3.54	3.54	13.52
C3	-3.54	-3.54	13.52
C4	3.54	-3.54	13.52
P1	15.00	0.00	13.52
P2	0.00	15.00	13.52
P3	-15.00	0.00	13.52
P4	0.00	-15.00	13.52
P5	-45.13	-115.38	12.59
P6	-128.92	-61.42	12.64
P7	-120.43	4.67	13.65
P8	-216 13	120.73	11.91
P9	-109.01	178.74	10.92
P0	44.94	190.90	12.10

Table 2.2: Location of borehole accelerometers

Depth	Borehole														
	C0	C1	C2	C3	C4	P1	P2	P3	P4	P5	P6	P7	P8	P9	P0
1	O	O	O	O	O	O	O	O	O	O	O	O	O	O	O
5	O	O	O	O	O										
10	O	O	O	O	O	O	O	O	O	O	O				
20	O					O	O	O	O	O	O	O	O	O	O
40	O									O					

Extensive geotechnical site characterization was carried out at these locations in terms SPT and geophysical measurements. Topographical and geological conditions of the site are generally simple, as the ground surface is almost flat. Figure 2.3 shows the soil profile of borehole C0 and the elastic wave velocities measured by downhole shooting method.

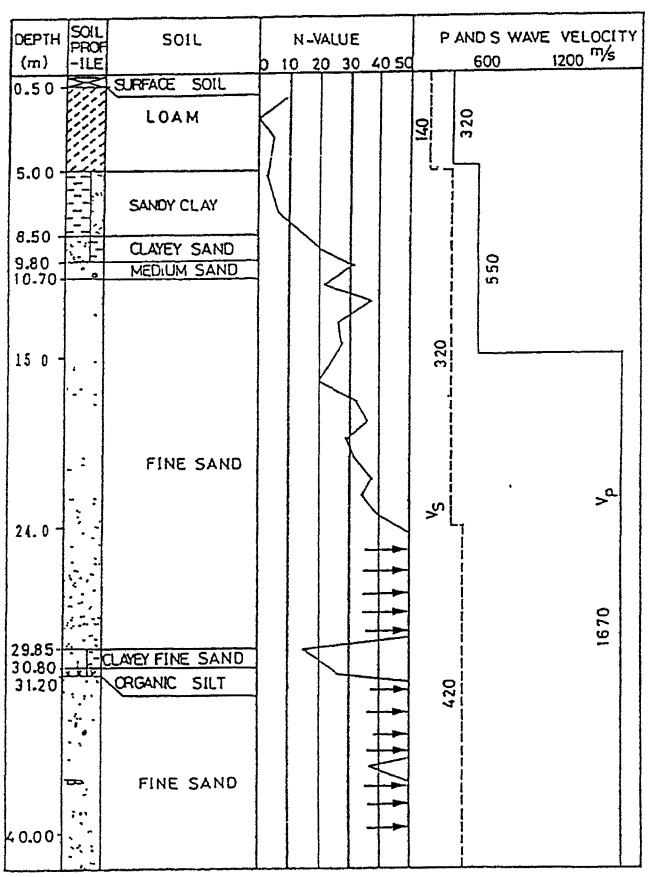

Figure2.3: Soil profile and geophysical measurements at borehole C0

Top 3 – 5 m of the site contained loam with standard penetration (N) value less than 10 and sandy clay underlies this loam layer with a thickness of 2 – 4 m, again with N values less than 10. A diluvium sand layer lies under the clay layer with N values greater than 20 – 30. The sand layer (whose stiffness increased with depth) is interspersed with clayey layers of relatively small N values. In spite of slight differences in the depth of boundaries between different layers from one borehole to another, an overall agreement indicates a relatively simple soil structure. The ground water table was found to be lower than GL–5.0 m.

2.3 Instrumentation

A piezoelectric type acceleration transducer was used in the array observation. Three transducers (two horizontal in East-West (EW), North-South (NS) and one in Up-Down (UD) directions) and their amplifiers are installed in cylindrical steel casing with an external diameter of 65 mm and a length of 335 mm. The accelerometers were installed in boreholes with diameters of 116 mm. Maximum of five accelerometers in each borehole was installed and fixed at predetermined depths (1, 5, 10, 20 & 40 m) using cement mortar.

Signals from the seismometers (placed in the boreholes to record signals in three directions viz. EW, NS and UD) were recorded at every 0.005 seconds by three units of 64 channel digital recorder. The system is always kept in a full operational status. Recording devices are activated the moment any one of the three components at p540 (GL – 40 m in p5 borehole) exceeds an acceleration of $1.0 cm \sec^{-2}$.

The system continues in operation for 30 seconds after the motion falls below this trigger threshold level. The recorder consists of a magnetic tape with a recording capacity of 30 minutes. Timing information is internally generated, and in addition the absolute time is corrected hourly by using the signal from NHK radio station. Detailed layout of accelerometers at different depths in the borehole C0 is shown Figure.2.4.

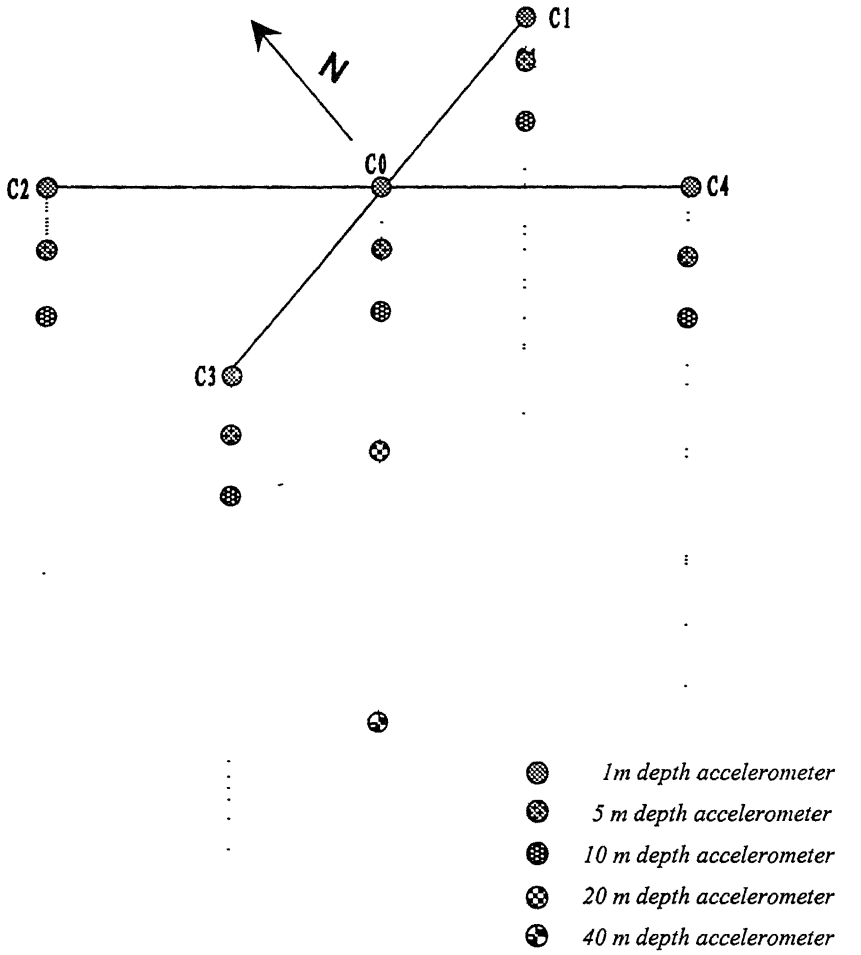

Figure 2.4: Layout of accelerometers at borehole C0

2.4 Database development of Chiba array

The Chiba array database consists of the data on major earthquakes whose peak ground acceleration at C0 (GL – 1 m) is larger than $20 cm\sec^{-2}$ or whose maximum steel pipe strains are larger than $5x10^{-6}$. The basic information on included earthquake records (only 25 events are considered) of the Chiba array database is listed in Table 2.3. Voltage signals from the seismometers are stored in digital magnetic tapes. These voltage values are multiplied with the conversion factor to give the values of acceleration, velocity and strain. Baseline correction is applied in this stage to have zero-mean for acceleration records.

If a seismograph does not start until a triggering level of motion is reached, the entire accelerogram is in error by the level of motion at the time of triggering. Integration of an uncorrected acceleration time history will produce a linear error in velocity and quadratic error in displacement. Comparing the same signals recorded in the three tape units, the time lag correction is applied. The recording time is sometimes too long to store a whole record in the database. Then the recording duration is truncated at the time when the cumulative power of horizontal acceleration records at C0 exceeds 99% of the total recording time. After these operations, the strain and velocity records are stored in the database. However, further corrections are applied to the acceleration records and a high cut-off filter is employed considering the sensitivity of the accelerometer.

Table 2.3: Basic information on earthquake records

S. no	Event no.	Focal Depth (Km)	JMA magnitude	Epicentral Distance (Km)	Max acceleration on surface at C0 (cm/sec^2)		
					EW	NS	UD
1	8205	30	7.0	178	28.3	26.1	11.7
2	8307	72	6.0	35	47.4	55.7	13.2
3	8401	388	7.3	373	25.5	24.2	12.7
4	8406	452	7.9	702	22.3	28.0	7.8
5	8416	13	6.6	219	13.8	14.5	7.8
6	8420	78	4.9	5	22.1	24.1	40.8
7	8510	64	4.8	16	27.4	29.6	12.6
8	8519	78	6.1	28	59.2	82.2	23.5
9	8525	63	5.0	32	75.7	71.6	28.3
10	8601	44	6.1	125	15.4	14.3	5.2
11	8602	73	6.5	105	54.0	40.7	21.5
12	8706	35	6.7	219	11.3	14.0	6.3
13	8717	57	4.9	62	20.7	33.5	12.1
14	8722	58	6.7	45	213.6	327.1	124.8
15	8723	52	4.6	46	17.2	21.2	16 4
16	8725	58	4.4	42	23.8	13.8	9.3
17	8726	42	4.0	52	22.5	30.4	18.0
18	8802	42	4.2	37	40.6	40.8	10.1
19	8806	48	5.2	38	54.9	97.8	19.8
20	8808	32	4.1	17	19.0	26.2	9.6
21	8816	96	6.0	42	48.4	59.8	15.2
22	8823	69	5.3	62	46.4	35.2	12.0
23	8901	55	5.6	48	55.7	49.1	25.4
24	8903	56	6.0	55	27.5	28.9	13.2
25	8904	45	4.9	52	41.0	21.9	15.3

The installation of seismographs in the borehole is very important because they are installed at great depths (up to 40 meters) in the boreholes without any visual observation. While setting the seismograph in borehole, utmost care is taken to give it the correct orientation, but still orientation errors do occur and were reflected in the seismograms. To correct these erroneous seismograms, orientation errors for the faultily oriented instruments are estimated and the records are corrected.

2.5 Organization of Database

Two databases, one for acceleration and the other for strain and velocity are stored in magnetic tapes. Each database consists of 27 sequential data sets corresponding to the 27 events as shown in Figure 2.5. Each data set includes 135 records for the acceleration database and 37 records for the strain and velocity database.

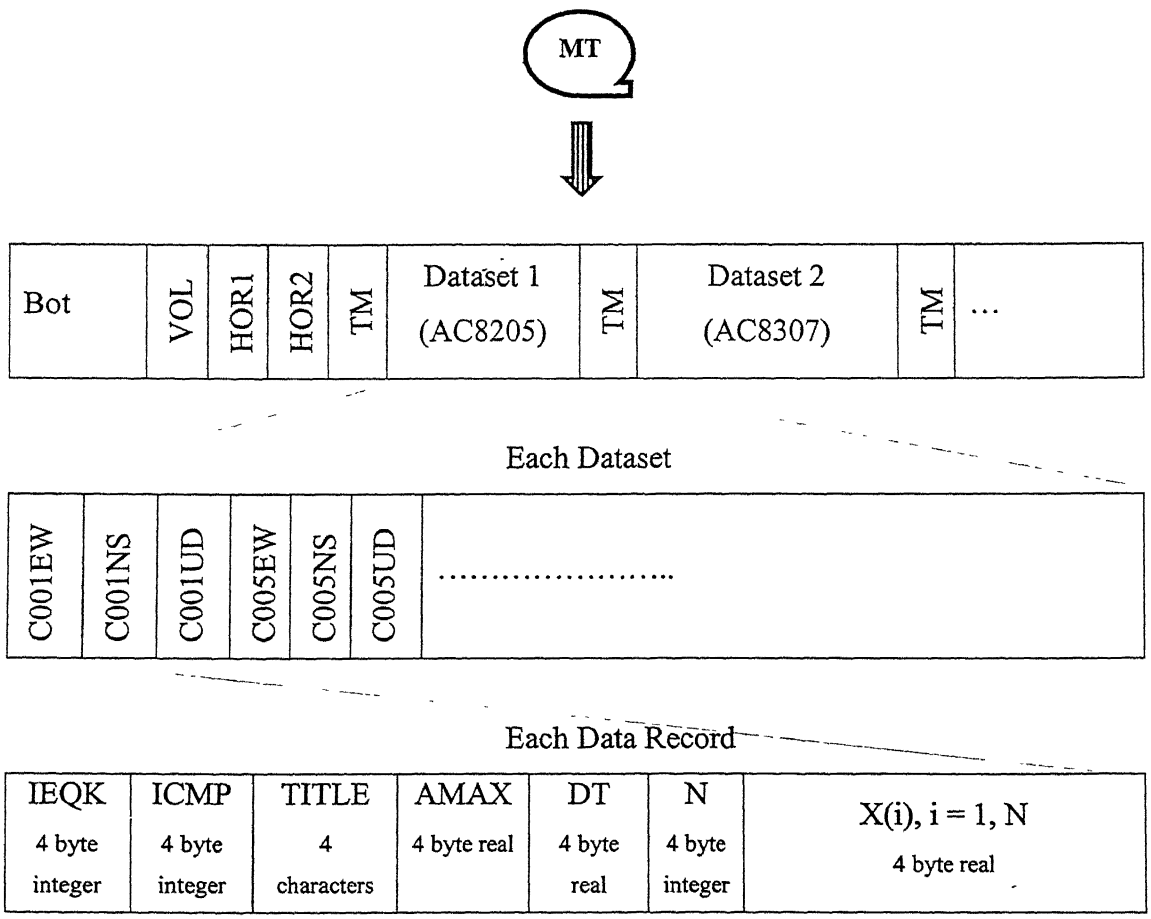

Figure: 2.5 Organization of Chiba array database

Each time history data is composed with a heading data that includes the event code (IEQK), the component code (ICMP), the title of the record, the maximum value of the record, the time interval (sampling interval) and the number of time steps. The details of the event and component codes are shown in Figure 2.6 and the combination code is unique for each record. The time history data is followed after the heading data.

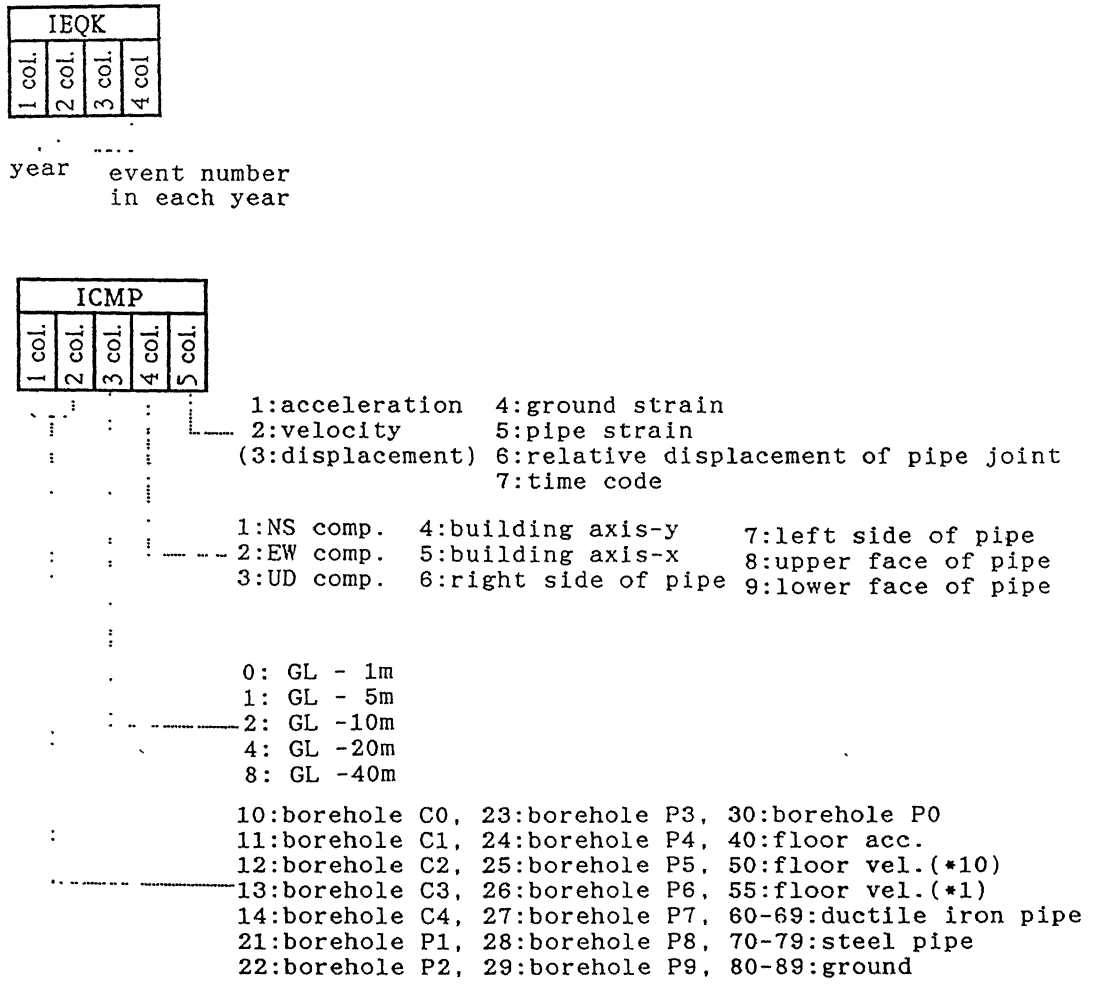

Figure 2.6: Event and Component codes

2.6 Data Procurement / Retrieval

Data records of 27 events recorded at various boreholes are made available in a magnetic tape storage device in the compressed form (Zip format). The records at 1, 5, 10, 20 & 40 m depths in EW, NS and UD directions at borehole C0 were separated from each data set. Using SUN Solaris SPARC work station at IIT Delhi, each compressed data set of the database is unzipped and the required data records are copied. 5-10 Mb hard disc space is required for each data set (after unzipping) and is about 80 Mb for all the records, hence sufficient memory space should be ensured. Storage and management of data records is very essential before proceeding to the analysis work when the disc space is constrained and CD-ROMs can come in handy.

2.7 Plots of Selected Database and Observations

Five different events were selected for plotting the acceleration time histories and Fourier spectra as shown in Figures 2.7 – 2.16. These events are:

- 8706 where PGA is 14 cm/sec^2 in NS direction
- 8903 where PGA is 28.9 cm/sec^2 in NS direction
- 8519 where PGA is 82.2 cm/sec^2 in NS direction
- 8525 where PGA is 75.7 cm/sec^2 in EW direction
- 8722 where PGA is 327.1 cm/sec^2 in NS direction

The amplitude of acceleration is observed to be higher at surface than at 40 m depth as can be seen from the Figure 2.7-2.16. The acceleration at the ground surface is about 3 – 4 times more than the acceleration at the 40 m depth. The Fourier spectrum shows that the frequency content of the record at 40 m depth and at the surface are different and also the energy of different waves is being considerable only up to a maximum frequency of 10 Hz. The energy and frequency content of the wave is getting modified gradually as it reaches the surface. Therefore it can be said that the soil behavior under earthquake loading at the ground surface is different than the soil at other depths, also considerable changes in acceleration and frequency content could be observed mostly in surface and 5 m records.

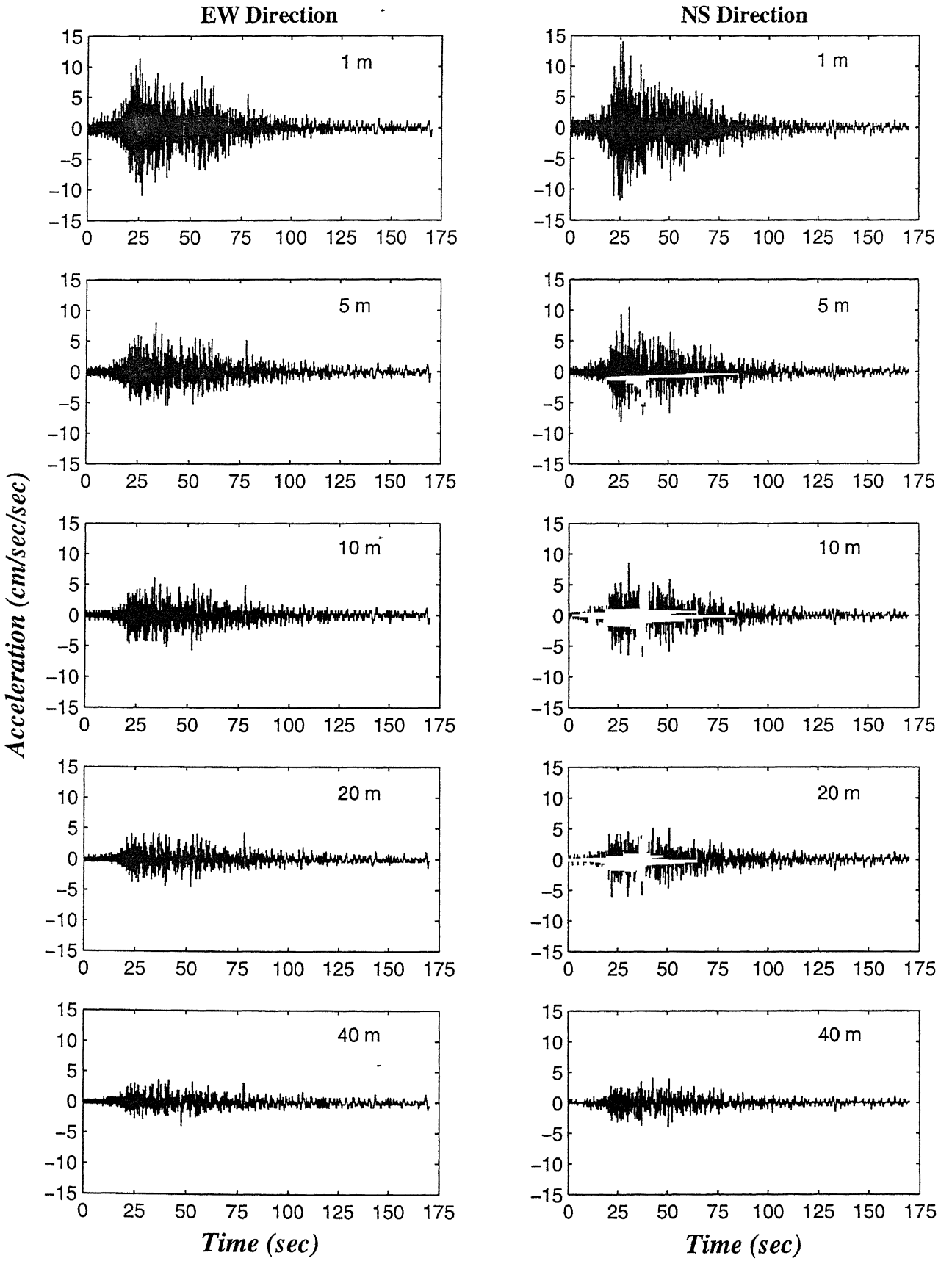

Figure 2.7: Acceleration time histories during the earthquake event 8706 at borehole C0

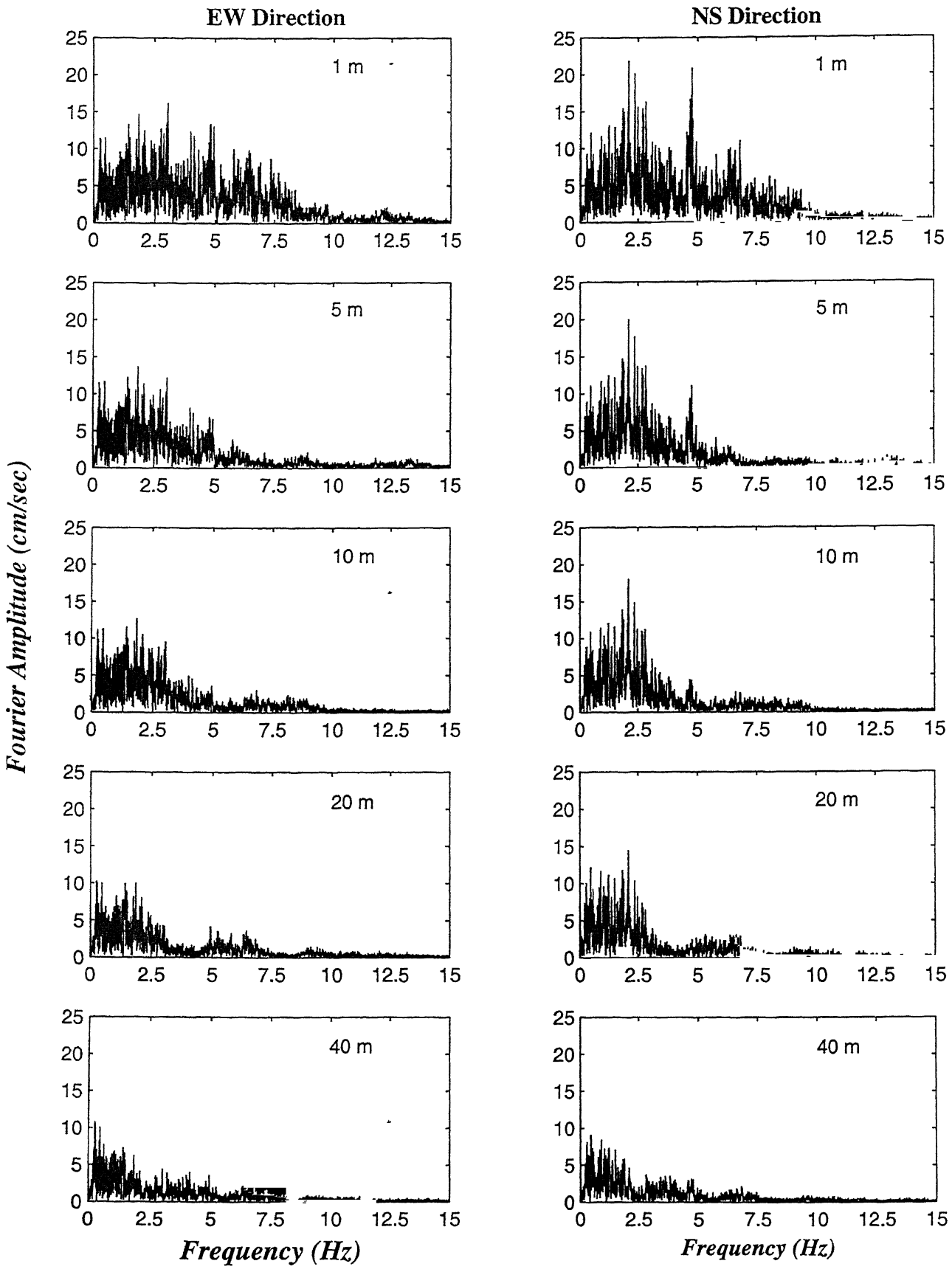

Figure 2.8: Fourier Spectra during the earthquake event 8706 at borehole C0

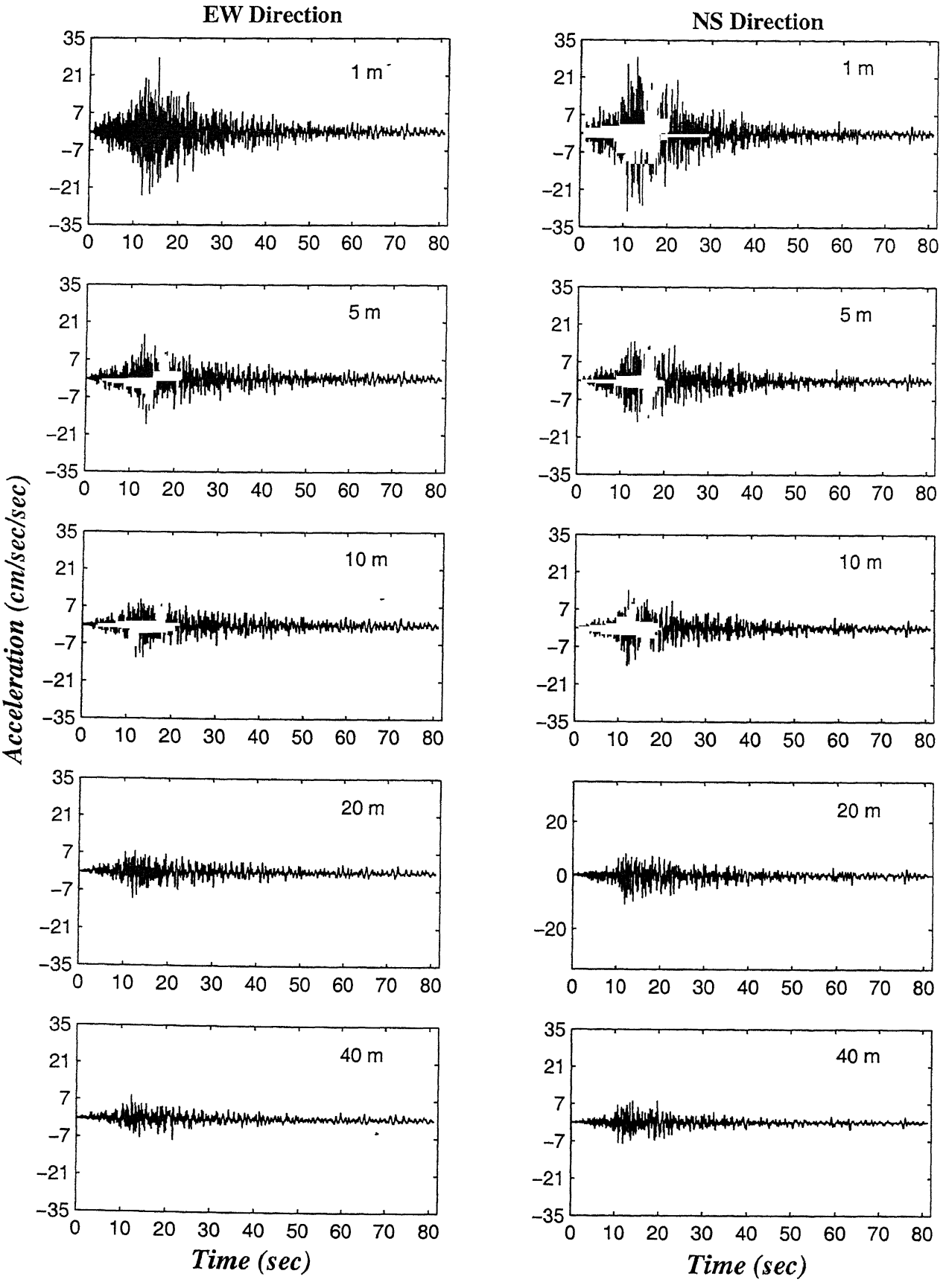

Figure 2.9: Acceleration time histories during the earthquake event 8903 at borehole C0

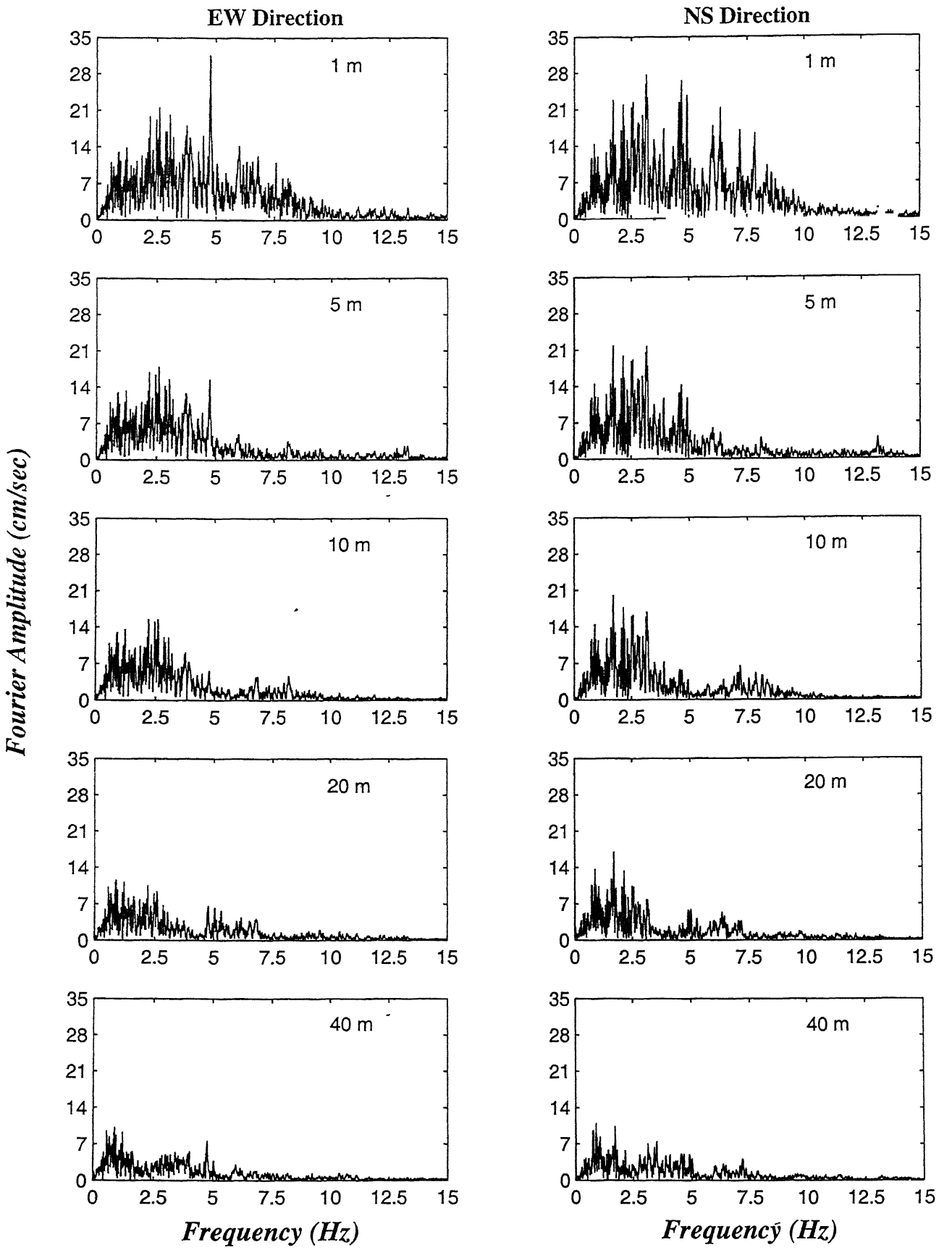

Figure 2.10: Fourier Spectra during the earthquake event 8903 at borehole C0

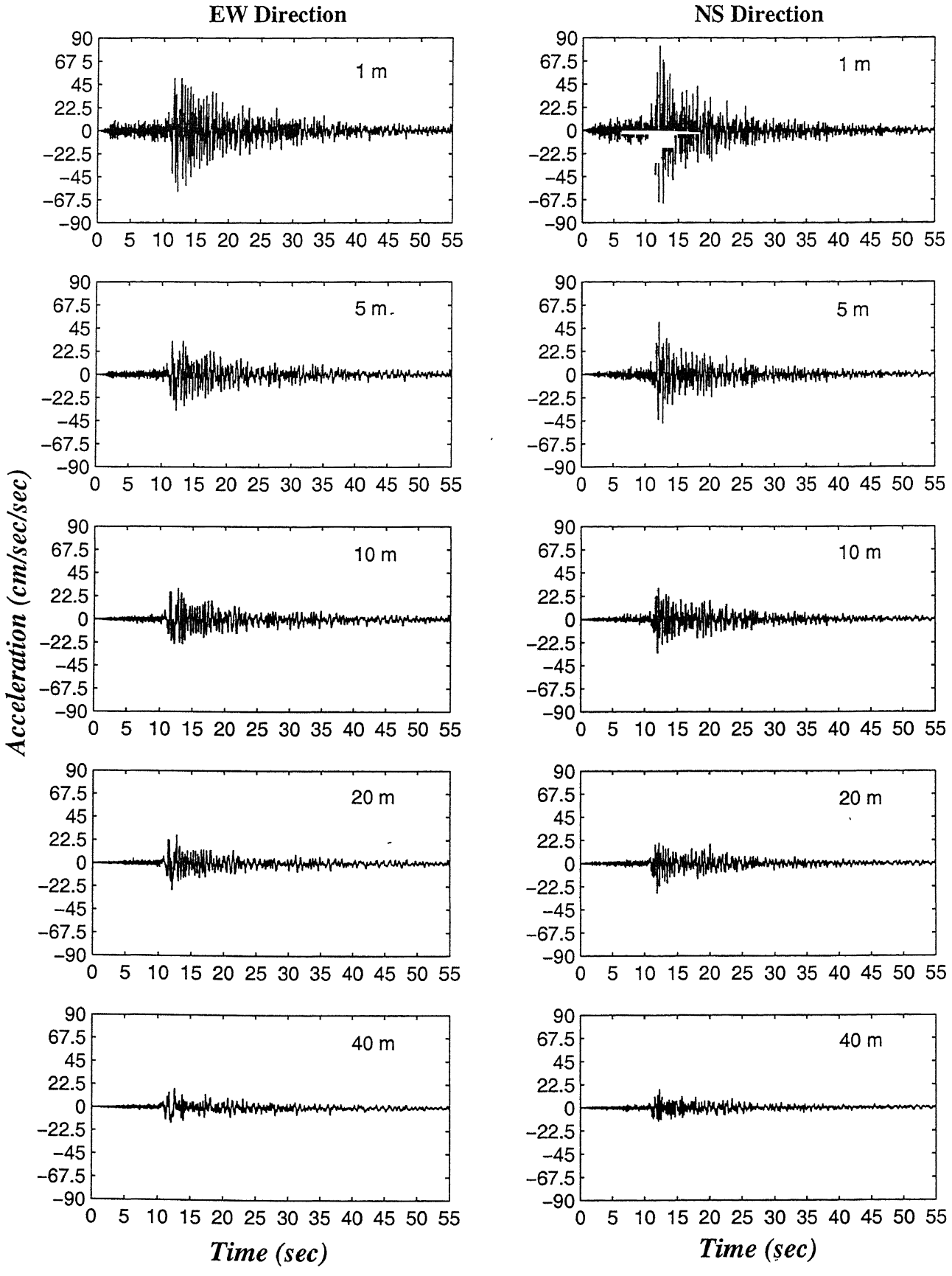

Figure 2.11: Acceleration time histories during the earthquake event 8519 at borehole C0

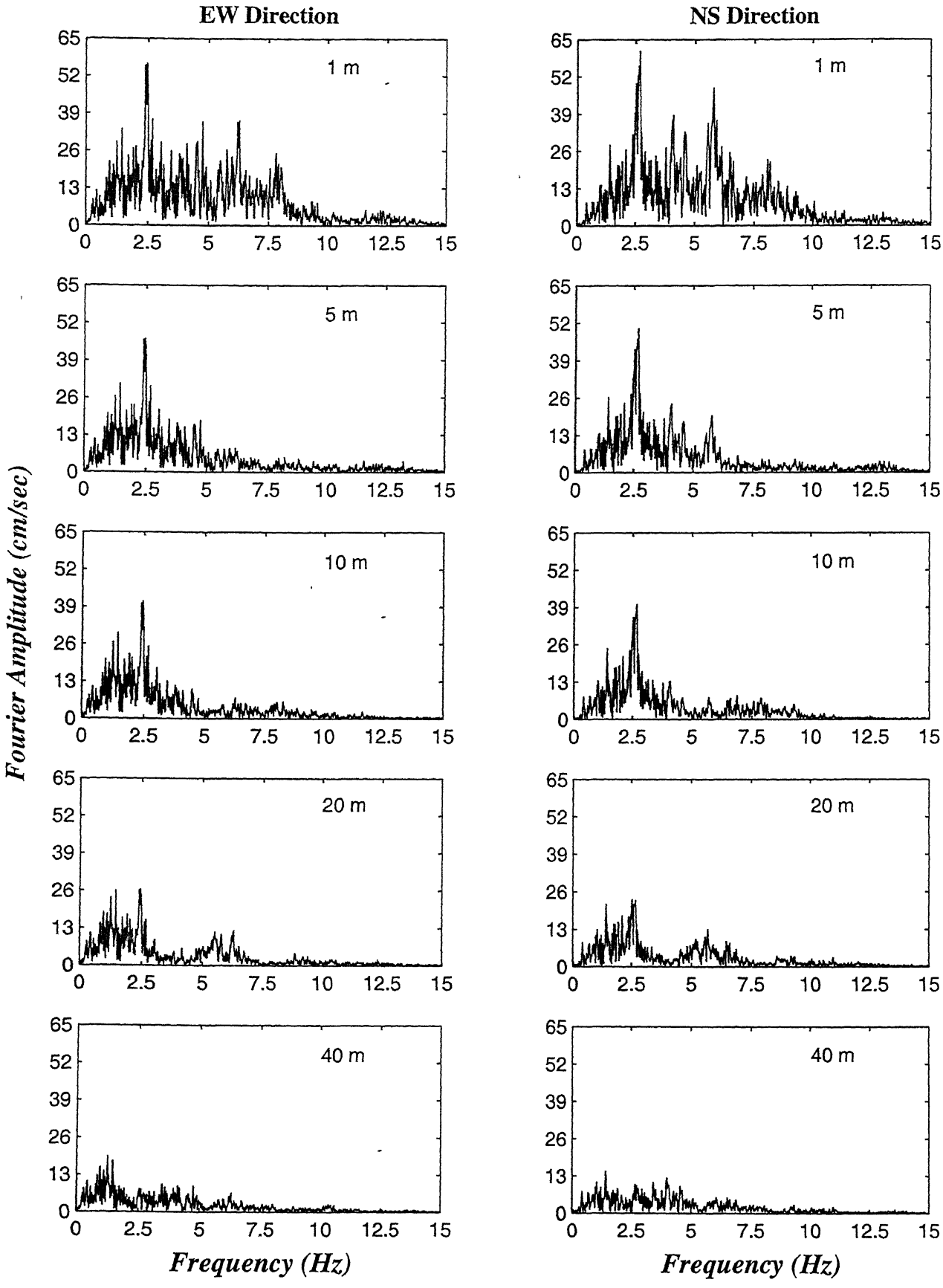

Figure 2.12: Fourier Spectra during the earthquake event 8519 at borehole C0

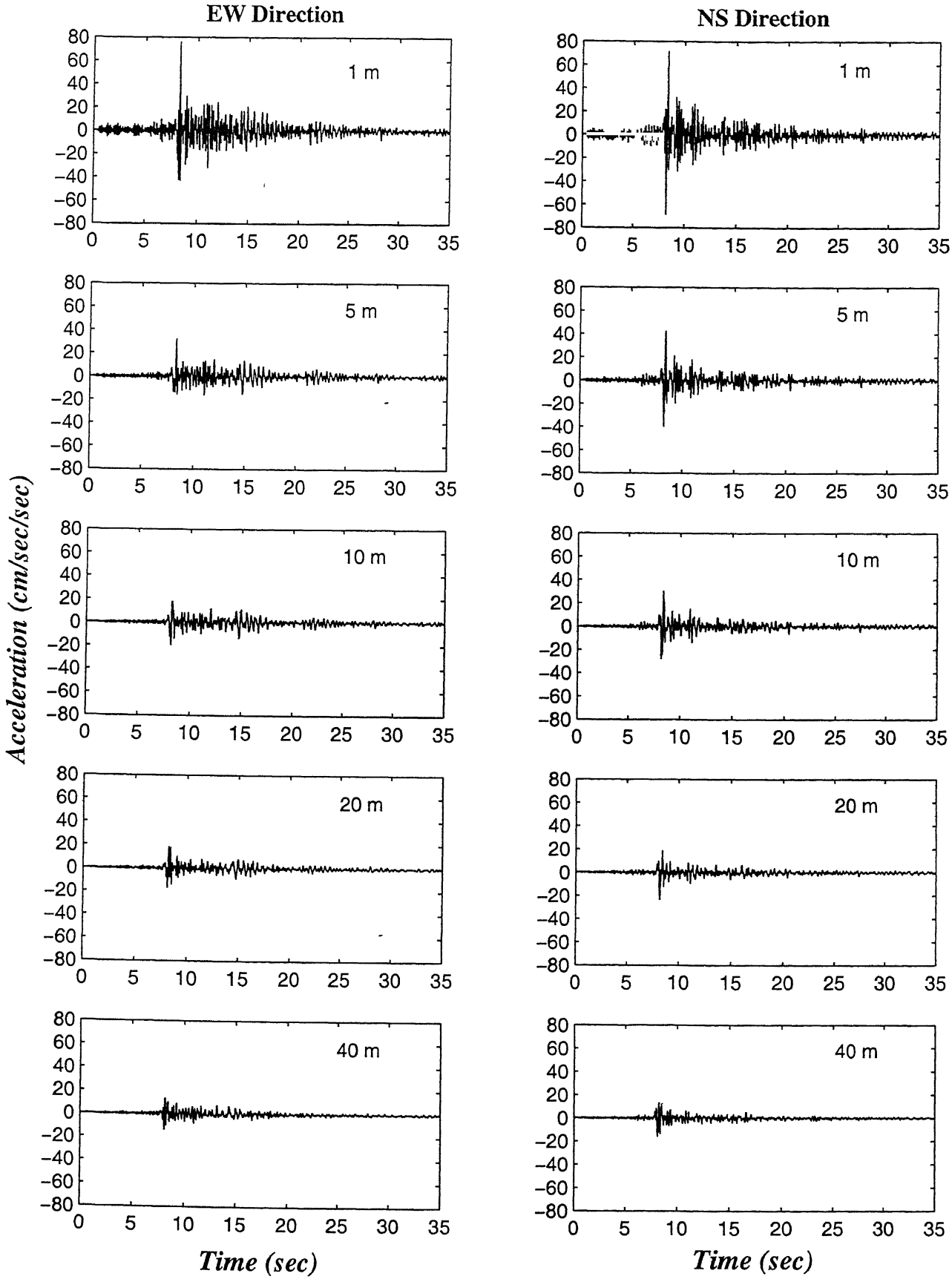

Figure 2.13: Acceleration time histories during the earthquake event 8525 at borehole C0

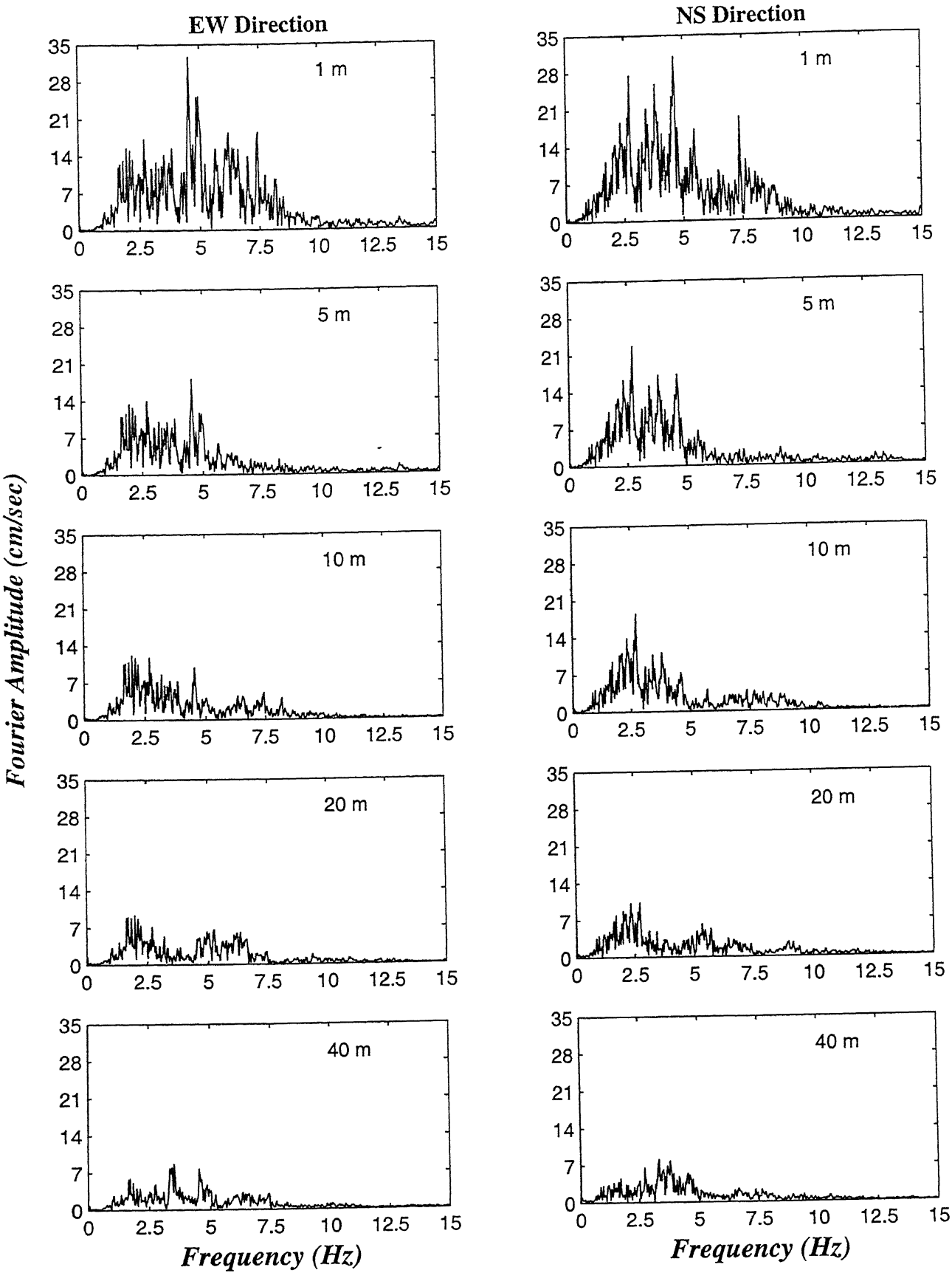

Figure 2.14: Fourier Spectra during the earthquake event 8525 at borehole C0

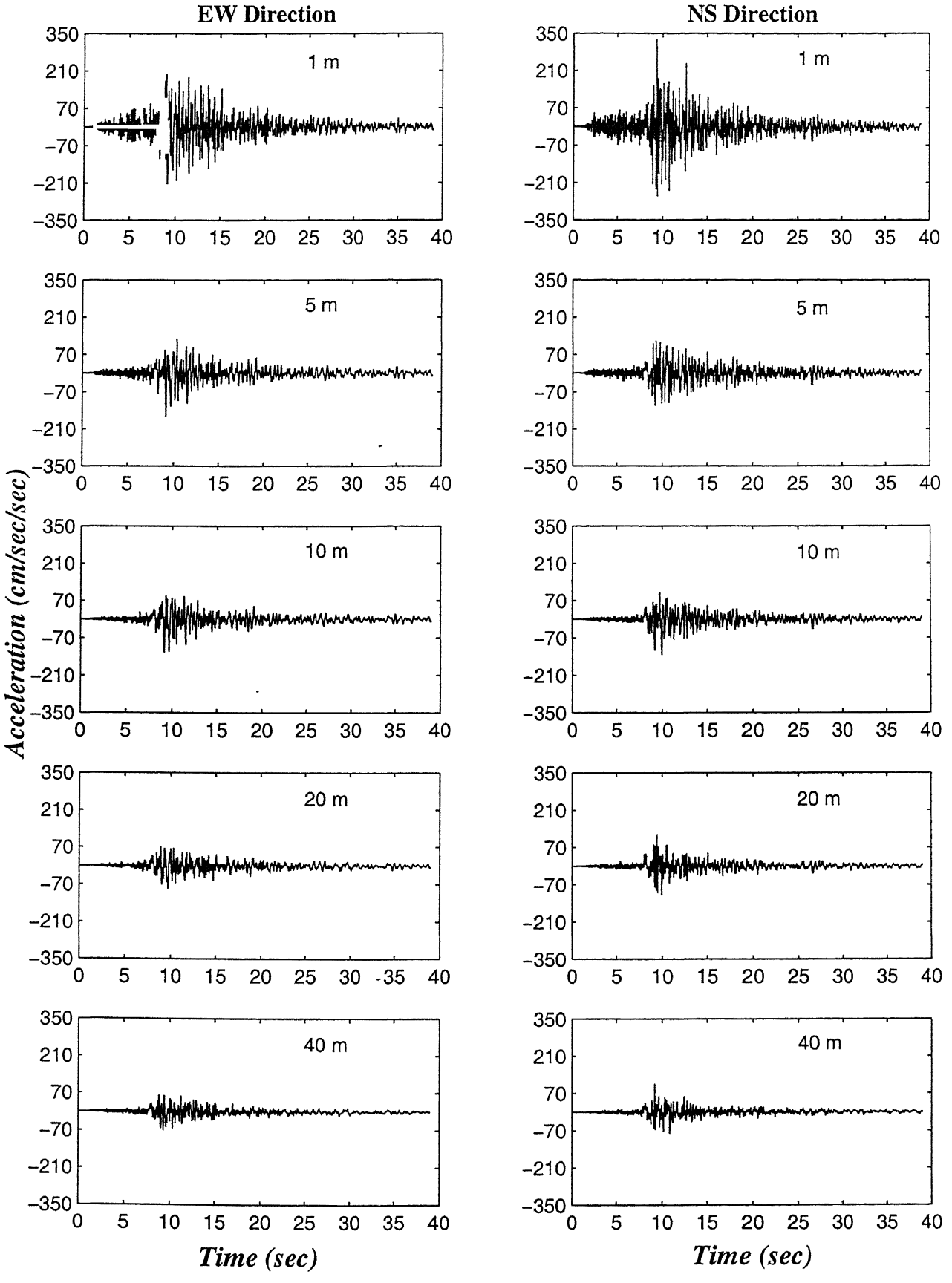

Figure 2.15: Acceleration time histories during the earthquake event 8722 at borehole C0

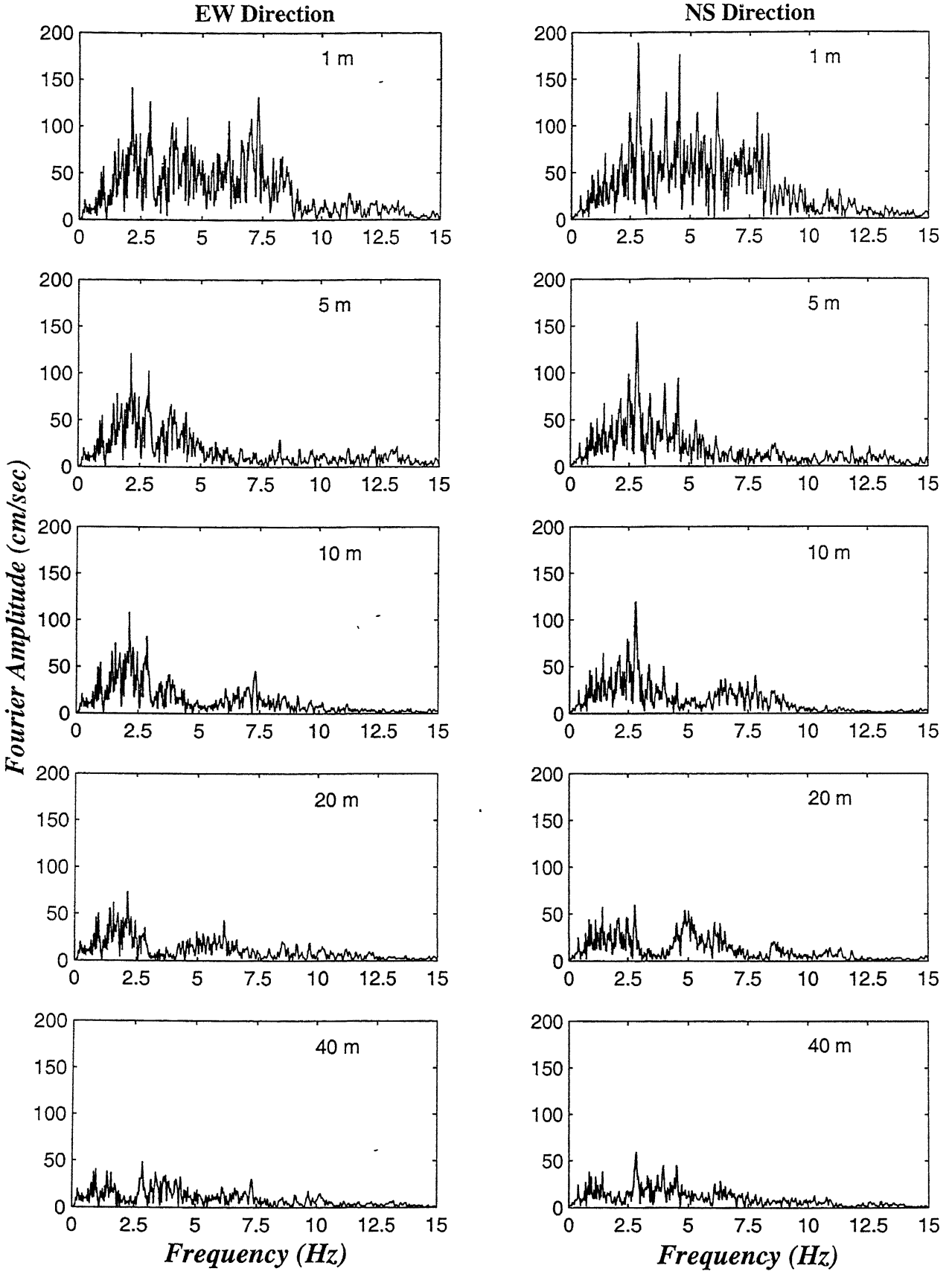

Figure 2.16: Fourier Spectra during the earthquake event 8722 at borehole C0

Chapter 3

LITERATURE REVIEW

3.1 Introduction

Parameter estimation of soils [1, 2, 18, 33, 34, 45, 52, 53, 54, 55] and structures [6, 13, 16, 19, 31, 37, 39, 41] from dynamic response data has enjoyed considerable attention in recent years. The techniques that have been developed range from linear deterministic models to nonlinear stochastic models. The applications vary from improving models for damage detection to identifying inputs to a system in order to control its response. This notable surge in related research activity is largely due to recent trends towards increased availability of computational resources and availability of experimental data and earthquake records.

In this chapter, a brief bibliographic review is outlined. This review is intended to give an overall idea about the research activities in the fields that are directly related to this investigation i.e., identification of dynamic soil properties using downhole array data. Work related to estimation of dynamic soil properties of an earth dam using strong motion data, first of this kind, is presented in section 3.2.

Several efforts in recent years to use downhole array data for parameter estimation are compiled in section 3.3. Research work that was reported on Chiba array data is compiled in section 3.4. Section 3.5 describes other studies conducted on downhole seismic data, that may not directly be related the current work, for the sake of completeness. A brief summary is presented in section 3.6.

3.2 The First Attempt

Research efforts to identify soil behavior from earthquake records are scarce. An early success at estimating dynamic soil properties using measured earth dam response was reported by Abdel - Ghaffar and Scott [1, 2].

A shear beam model was used to estimate the shear moduli and damping ratio for the gravely and rolled-fill Santa Felicia earth dam. The soil was modeled as a hysteretic SDOF system with a nonlinear restoring force, and narrow band-pass filtering of the data isolated fundamental frequency of dam. An estimate of shear modulus and damping (Figure. 3.1) was obtained by plotting absolute accelerating of the dam against crest displacement relative to the base.

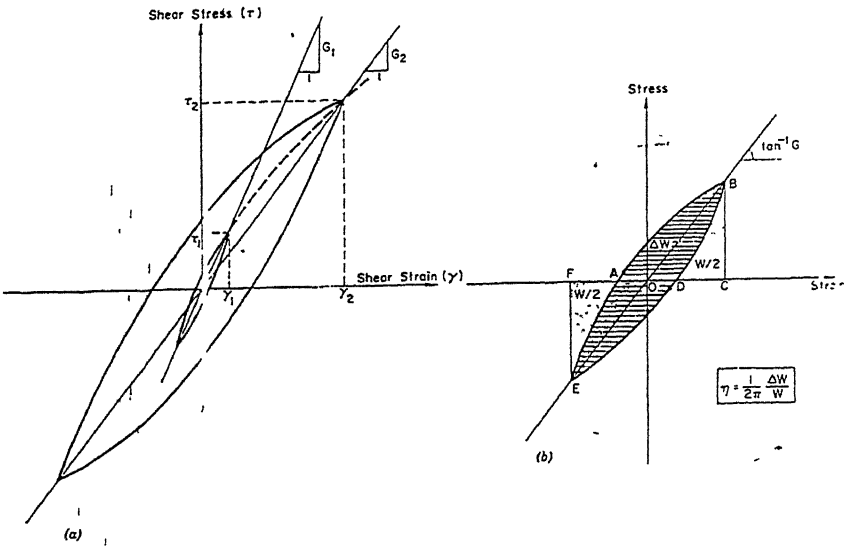

Figure 3.1: Hysteretic stress-strain relationships used to calculate the shear moduli and damping factors of earth dam (Abdel - Ghaffar et al. [2])

Recently, Lin and Chao et al. [33] suggested guidelines to improve the hysteresis loops, that were observed to be distorted in Abdel - Ghaffer et al. [2] study, based on a numerical simulation on earth dam as a non-linear, purely hysteretic SDOF structure subjected to a given base motion. From the calculation of shear moduli and damping factors, it was observed that the loops obtained were undistorted for the same time window in comparison between Abdel - Ghaffer analysis and present analysis. It was concluded that to minimize errors, only those loops of larger strain amplitudes only should be used.

3.3 Work related to Downhole arrays

Strong motion earthquake records provide one of the few sources of information on the dynamic behavior of soil / overall site behavior at large amplitude response. Under earthquake conditions, soil may sustain unpredicted damage or may display unanticipated strengths; such information is not available through other means. This has motivated an extensive deployment of instrumentation to record soil response / site amplification in seismic regions. Currently, high quality records of well-instrumented soil sites (Japan, USA, Mexico, and Taiwan) are available, which are being used for a verity of research observations. This section describes some of these efforts related to current study.

Zeghal and Elgamal [53] used a non-parametric identification technique to evaluate the mechanism of wildlife refuge site liquefaction. Surface and downhole accelerations and pore water pressures recorded during the 1987 earthquakes were used to obtain direct estimates of average shear stress-strain and effective stress path histories, which provided valuable insight in to the site seismic behavior during liquefaction and associated loss of stiffness.

Elgamal et al. [14] used the cross-correlation method to calculate the shear wave velocity and propagation mechanism using Lotung free-field surface and downhole acceleration records. Resonant and modal configurations were estimated using spectral analyses. It was concluded that spectral and correlation techniques may be utilized to identify soil low-strain properties and site resonant characteristics.

Matsunaga et al. [35] adopted cross-correlation method and ray theory for calculating time lag and phase velocities of body waves using downhole array records established in the Tokyo international airport, Japan. In both the studies, the computed S wave propagation velocity values are in good agreement with the measured values (geophysical tests).

Campanella et al. [8] has given the frequency domain calculation to obtain the timelag for the wave to travel between the two adjacent stations. Crossover methods and Cross-correlation methods were applied on signals from downhole seismic cone analysis. It was established that the Cross-correlation method of obtaining the time lag is more reliable than the Crossover method.

Huang and Chiu [21] analyzed four-level Dahan downhole array recordings (at 0, 50, 100 and 200 m depth) to investigate site amplification due to the near-surface structure. They used eight sets of data to study site amplification. Five techniques of spectral ratios have been tested to determine the most reliable way to estimate site response. The study reported the superiority of Ratio of Root-Mean-Square (RMS) Fourier amplitude spectra. Results show that the amplification factors are nearly uniform at the depths of 50 and 100 m and agree well with those from time-domain analyses and the transmission-coefficient estimation.

Bersenev et al. [7] studied the soil nonlinear behavior under dynamic loading conditions and carried out spectral ratio analysis on weak and strong motion data at SMART1 and SMART2 array at Lotung and Haulien. In SMART1 analysis, amplification of soft alluvial site relative to the rock and in SMART2 analysis, amplification of terrace deposits with respect to alluvium deposits was calculated. In both the cases, significant differences between the weak and strong motion application functions were observed. When the thickness of the surface layers is significantly less, the low frequency contribution from nonlinearity was less important and long period waves were not observed.

Honjo et al. [20] given Extended Bayesian Method (EBM) to study the propagation characteristics of earthquake motion from bedrock. The accuracy of the method was compared with the conventional Least Square Method (LSM). The array records available from downtown Tokyo, Japan were used in the analysis. Transfer functions were smoothened using Parzen window. The estimated shear modulus and damping ratio by inverse analysis (EBM) were in good agreement with the observed records, but not in the case of conventional analysis (LSM) and hence proved the effectiveness of the EBM over LSM.

Chang et al. [11] estimated the in-situ dynamic properties to provide field evidence of non-linear soil behavior during earthquake excitation and to evaluate the accuracy of dynamic properties obtained from geophysical measurements and laboratory tests. From the Lotung downhole array data, shear wave velocities were estimated from the fundamental resonant frequencies identifiable from Fourier spectral ratios. Non-linear behavior of shear strain was observed, which was estimated by linear ground response deconvolution analysis based on inferred shear wave velocity profiles. Analysis on low excitation and high excitation levels were calculated in different time windows. The back-calculated shear wave velocity, moduli

values were compared with the velocity obtained from geophysical tests and shear modulus reduction curves respectively. Substantial drop in shear wave velocity at high excitation levels was observed, when compared with the shear wave velocity from geophysical tests and hence the results clearly indicated the non-linear behavior of soil during strong motion earthquake.

Directly assessing the non-stationary data, Glaser [18] found that parametric modeling of the system is superior to the traditional Fourier methods, to estimate in-situ soil properties, especially when soil is subjected to large strains.

3.4 Studies on Chiba Downhole array

Katayama et al. [22] and Nagata et al. [36] described the dense seismograph array network installed at Chiba experiment station, Institute of Industrial Science, University of Tokyo in 1982. It measured earthquake records in three dimensions, which can be used in evaluating the spatial correlation of earthquake ground motions and in the study of soil amplification. Katayama et al. [24] had given a detailed description of Chiba array strong motion database and its effective use.

Yamazaki et al. [49] provided information about location, site condition at Chiba experiment station, corrections for orientation errors, process of development & organization of database and emphasized the use of event codes in determining engineering properties of strong ground motion.

Tsujihara et al. [47] studied the subsurface soil properties based on Chiba downhole array data and formulated a 'frequency domain problem' and implemented the 'transfer function method' in obtaining the shear wave velocity (Vs) & quality factor (Q). Estimated shear wave velocity (V_s) was less than the elastic wave velocity (Fig. 3.2). Events with varying PGA were analyzed and the study reported that the soils below 10m depth are relatively stiff (e.g. Vs > 300 m/sec) and no non-linearity was observed even during large excitation of the ground. The quality factor (Q) obtained was different in every event, so that the identification could bot be carried out accurately to make a definite conclusion.

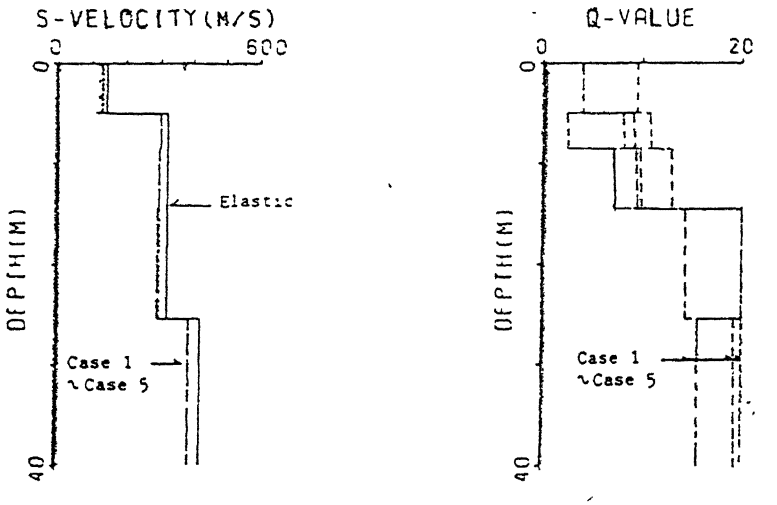

Figure 3.2: Profiles of identified Shear wave velocity and Quality factor (Tsujihara et al. [47])

Sawada et al. [44] formulated multiple reflection theory in frequency domain to estimate the dynamic soil properties. Chiba array records were analyzed and identified Shear wave velocity (Vs) was in reasonable agreement with that of PS logging test (Fig. 3.3). However, there was a large scatter in identified Quality factor (Q) values indicating the less reliability of the employed method.

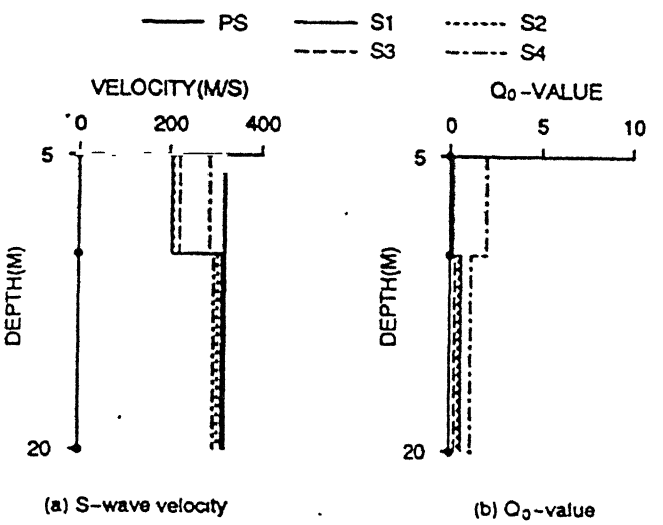

(S1, S3 & S4 correspond to events 8307, 8510 and 8519 with PGA values of 55.7, 29.6 & 82.2 cm/sec^2)

Figure 3.3: Estimated values of Shear wave velocity and Quality factor (Sawada et al. [44])

Katayama et al. [28], in his Soil amplification study report on Chiba array downhole data, showed that the soft soil layer few meters (0 – 5 m) below the ground surface got amplified more than the rest of the stiff layers below it. Katayama and others [23, 25, 26, 27] used the three dimensional nature of Chiba array records to study the behavior of wave propagation, spatial correlation and affect of separation distance between two stations.

Ghayamghamian et al. [17] used downhole ground motions recorded at five vertical sites in Japan to investigate the nonlinear site response and in-situ dynamic soil properties. The hysteresis behavior of soil was found to be changed for different time windows (i.e. for different levels of shaking) (Figure. 3.4) and determined nonlinear behavior of the site. The shear moduli inferred from the events producing strong ground motions were substantially lower than that producing weak ground motions.

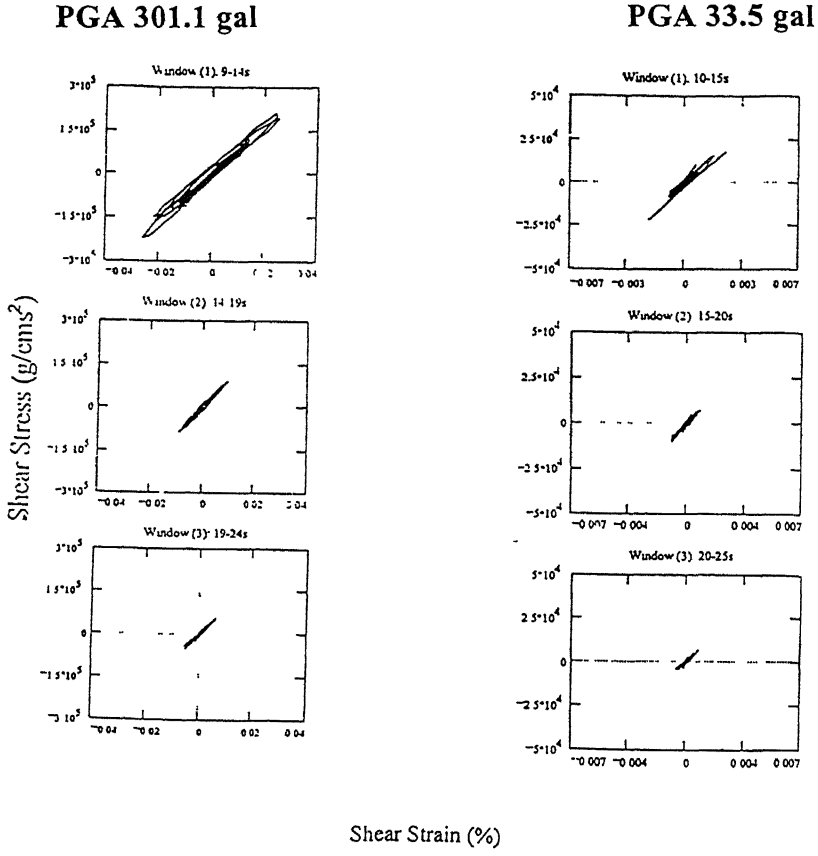

Figure 3.4: Shear stress verses Shear strain for different time windows (Ghayamghamian [17])

Two records of Chiba vertical array where PGA recorded was 33.5 gal and 301.1 gal were used. Shear stress-strain hysteresis loops were plotted for earthquakes with PGA 301.1 gal (in 9-14, 14-19 & 19-24 sec time windows) and PGA 33.5 gal (in 10-15, 15-20 & 20-25 sec time windows) and shown in Figure 3.4. A mild detectable non-linear behavior was recorded during the event with PGA 301.1 gal, which could be observed by changing shear modulus and damping ratios in different time windows. However, this phenomenon was not observed during PGA 33.5 gal due to the small levels of shaking.

Katayama et al. [28, 29] investigated the soil amplification characteristics in terms of peak ground acceleration and transfer function based on the Chiba array observation records. The recorded peak accelerations at borehole C0 at GL -1, -5, -10 and -20 m were normalized by those at GL -40 m for the 27 events (Chiba database) to study the amplification of peak acceleration. The ratios for the three components i.e. East-West (EW), North-South (NS) and Up-Down (UD) for individual events are shown in Figure 3.5.

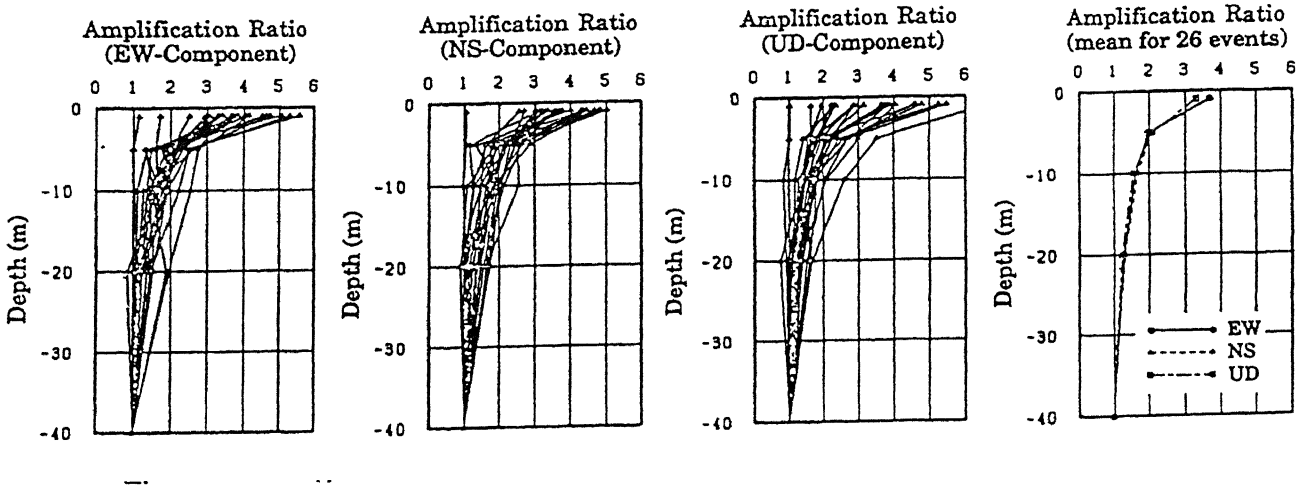

Figure 3.5: Amplification ratios of peak ground acceleration for 27 events at borehole C0 (Katayama et al. [29])

Amplification took place mostly with in the few meters below ground level due to top 5m soil and the underlying layers are relatively denser and not subjected to considerable amplification. Transfer functions of two events (8722 with PGA 327.1 cm/sec^2 and 8725 with PGA 24 cm/sec^2) were compared to study the possible effects of non-linear response of soil deposits on the transfer function. Smoothened transfer function for these two events is shown in Figure 3.6. Effect of non-linear response of soil was observed to be small for the soil below 10 m depth due to the denser sub soil layer.

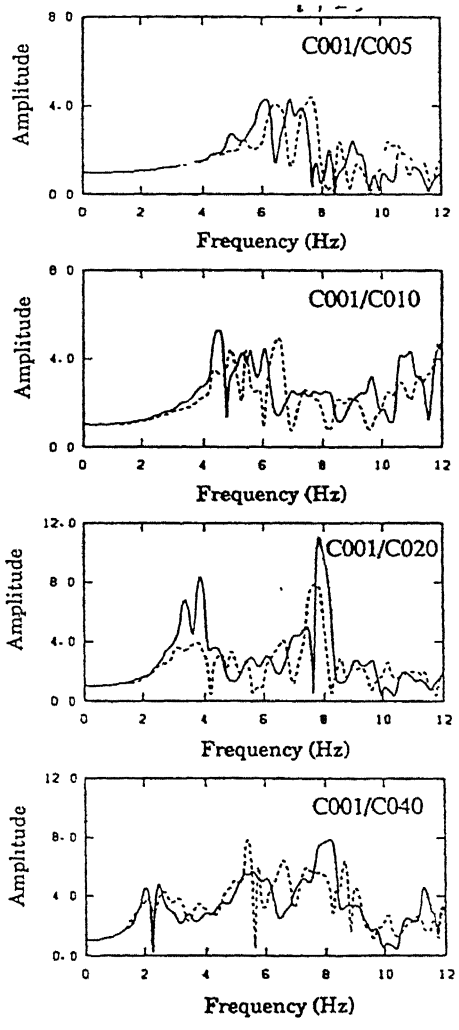

Figure 3.6: Smoothened transfer functions estimated from NS component of the 1987 east off Chiba prefecture earthquake and one of its after shocks in borehole C0 (Katayama et al. [29])

3.5 Other studies on Downhole arrays

Yeon - Tein et al. [51] described the strong motion array in Haulien, Taiwan called SMART-2 and development of LSST (Large Scale Seismic Testing) experiment on hard site in the Haulien area. SMART-2 was designed for studying the rupture process of earthquake faulting and near field ground motions. Haulien LSST experiment was designed for soil structure interaction research.

Ansary et al. [3] discussed the characteristics of microtremors based on the spectral analysis on Haulien LSST microtremor data. The amplification characteristics were observed in the free field as well as in the back fill. The amplitude ratio of theoretical rayleigh wave matching with the observed amplitude ratio of microtremors clearly indicated the influence of rayleigh wave except for some low and high frequency microtremors which may consists of low waves. Back fill soil microtremor records did not reflect good matching of amplitude ratio between theoretical rayliegh wave and observed, alluding the difficulty in predicting the characteristics of microtremors in the case of back fill soil.

Cheng et al. [12] used Haulien vertical free-field arrays to study the response of soil during strong motion earthquake. The geological profile is very typical consists of loose sands for the top 5 m underlying gravel deposits of unconsolidated conglomerate composed of pebbles varying in diameter 10 cm to 20 cm. The assumption was that the horizontal ground motions were because of vertically propagating Shear wave and hence One-dimensional shear beam model was employed.

Amplitude spectrum and phase spectrums were estimated from spectral analysis to calculate the modal frequency from amplitude spectrum and phase angle from phase spectrum. Single and two layer characteristic equations for transfer function were derived from wave propagation theory been used to calculate the parameters for system identification by substituting the predominant frequencies obtained from amplitude spectrum. The velocities obtained in EW direction between different layers were lower than the velocities obtained in the NS direction, clearly indicated the anisotropic behavior of the soil.

Archuleta et al. [4] conducted site amplification study on Garner valley downhole array and observed the modification in the amplitude of the acceleration in the surface layers, which is basically soil overlain by weathered granite. Garner valley downhole array of accelerometers was used to measure the effects of local site conditions on the amplification and attenuation of seismic waves.

Archuleta et al. [5] studied the Garner valley accelerometer records for amplification phenomenon. The amplitude of waves will not be effected by the layer when the thickness is less than the wavelength, moreover the amplification occurs when the frequencies whose quarter wavelength is less than the layer thickness. Analysis shown that larger earthquake was amplified less than the smaller earthquakes. This is due to the lower corner frequency in the larger earthquakes, as the corner frequency decreases, the wavelength increase and hence the amplitude decreases.

Pecker et al. [38] used the weak motion records of Garner valley array to validate the low strain soil properties obtained from soil survey at the experiment site. Spectral ratio technique was used to analyze the weak ground motion records, consequently to compare with the results obtained from elastic behavior from soil survey. The soil behavior was isotropic and yielded in reasonable validation of results from the geotechnical survey.

Peter et al. [40] analyzed seismic signals using multiple signal characterization (MUSIC) method. Results showed that the method was capable of resolving multiple closely spaced source and work well with both stationary and non-stationary signals.

Yasuyuki et al. [50] investigated the behavior of embankment model resting on sandy ground, using the measured records from buried instruments in the model. Pore water pressure was found to be proportionate to the input acceleration characteristics. Ground beneath the embankment has not undergone cyclic mobility effect unlike it was found in free ground and large settlement was observed in the embankment due to vibrational earthquake motion than a shake-type motion.

Toshimi et al. [46] defined engineering bedrock as a linear behavior regime even during the strongest shaking after studying the bedrock waves from the Sendai region borehole observation network, Japan, using 1-D soil modeling. Such waves estimated from site amplification were observed to be much lower than the observed surface & borehole records themselves. Therefore they could be used in aseismic analysis of important structures and used in the study of source characteristics of the observed events as well as the path effects between the seismological bedrock and the engineering bedrock.

Safak [42] has given discrete time wave propagation analysis to investigate the site amplification in layered media. The model uses only three parameters for determining the site amplification, viz. R (reflection coefficient), τ (one way travel time of waves in the layer), and Q (quality factor). This method is much simpler and more accurate than the frequency domain techniques and useful in applications such as random vibration studies, site effects on response spectra and in identification of site characteristics from recorded motions.

3.6 Summary

From the review of literature carried out directly related to the current problem, it can be summarized that,

- Tangible and reasonable information on dynamic site behavior can be obtained from the study of downhole array records.
- Downhole array observation is a useful tool in estimating the in-situ dynamic properties.
- Direct analysis of the downhole records can overcome the constraints involved in preparation and testing of laboratory procedures to simulate the exact field conditions.
- Downhole array earthquake records are powerful tools that complement lab testing to study the dynamic behavior of soil.

Chapter 4

CORRELATION ANALYSES

4.1 Introduction

Correlation analyses have several useful applications in the area of seismic wave propagation such as,

- Identifying similarities in signals,
- Determination of travel times (time lag),
- Identifying replicas in noisy signals and
- To characterize multiple travel paths, lossy and dispersive media.

Several other researchers had earlier employed Cross-correlation technique, to estimate the time lag. Few among them that directly related the current study are:

- Campanella et al.[8] in seismic cone penetration testing using frequency domain method
- Elgamal et al. [14] in estimating site dynamic properties
- Matsunaga et al. [35] in calculating phase velocities.

As was indicated in the review of literature, in identifying sub surface shear wave profile (using time & frequency domain techniques), Cross-correlation technique is a very reliable procedure and enjoyed popularity among the researchers (Santamarina et al. [43]).

In this study, Cross-correlation technique in time domain method is used in estimating the average Shear and Primary wave velocity distribution profiles between the downhole stations at different depths. The advantage of this technique is its ability to identify the replicas of a signal in other signals, even in the presence of significant background noise. These profiles were then compared with those obtained from the Geo-physical measurements (Figure.2.3).

4.2 Methodology

The purpose of employing Cross-correlation in the present work is to identify the time taken by the wave to travel between two downhole stations. If a_i and a_j are two acceleration histories recorded at two different stations i and j, then the Cross-correlation in continuous time is a function of the time shift τ and is given as:

$$C_{a_i a_j}(\tau) = \int_{-\infty}^{\infty} a_i(t).a_j(t+\tau).dt \tag{4.1}$$

where, $a_i(t)$ and $a_j(t)$ represent the time records of wave passing through the first and second receivers placed z m apart (in depth) as shown in Figure. 4.1. τ represents the time delay between the two records and t is the domain of integration. However, in reality, limits of integration in the time domain will be finite and above Cross-correlation can be normalized, to keep the maximum absolute value of $C_{a_i a_j}$ to be less than one.

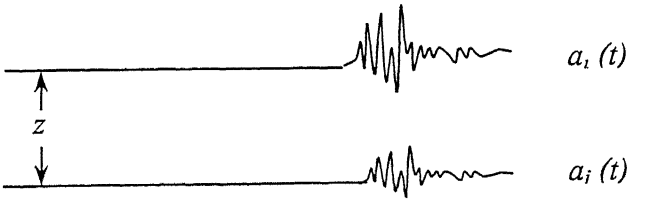

Figure 4.1: The recorded signals at z m apart for time domain Cross-correlation

Cross-correlation function between downhole acceleration time histories $a_i(t)$ *and* $a_j(t)$ recorded at stations i and j may be expressed as:

$$C_{a_i a_j}(t) = \frac{\frac{1}{N-m}\sum_{n=1}^{N-m} a_i(n\Delta t)\,a_j((n+m)\Delta t)}{\sqrt{\frac{1}{N}\sum_{n=1}^{N} a_i^2(n\Delta t)}\sqrt{\frac{1}{N}\sum_{n=1}^{N} a_j^2(n\Delta t)}} \tag{4.2}$$

Here, time delay, $\tau = m \cdot \Delta t$, where m = 0,1,2,3.....N. N represents the total number of records and Δt is the time step of digital data.

In principle, the Cross-correlation of signals at adjacent depths is determined by shifting the lower signal, relative to the upper signal, in steps equal to the time interval between the digitized points of the signals (Campanella et al. [8]).

At each shift, the sum of the products of the signal amplitudes at each interval gives the cross-correlation for that shift. After shifting through all the time intervals, Cross-correlation function verses Time-shift can be plotted, and the time shift interval is used to calculate the interval velocity.

The process is shown schematically in Figure 4.2, where the lower signal has been shifted to the left giving the maximum correlation.

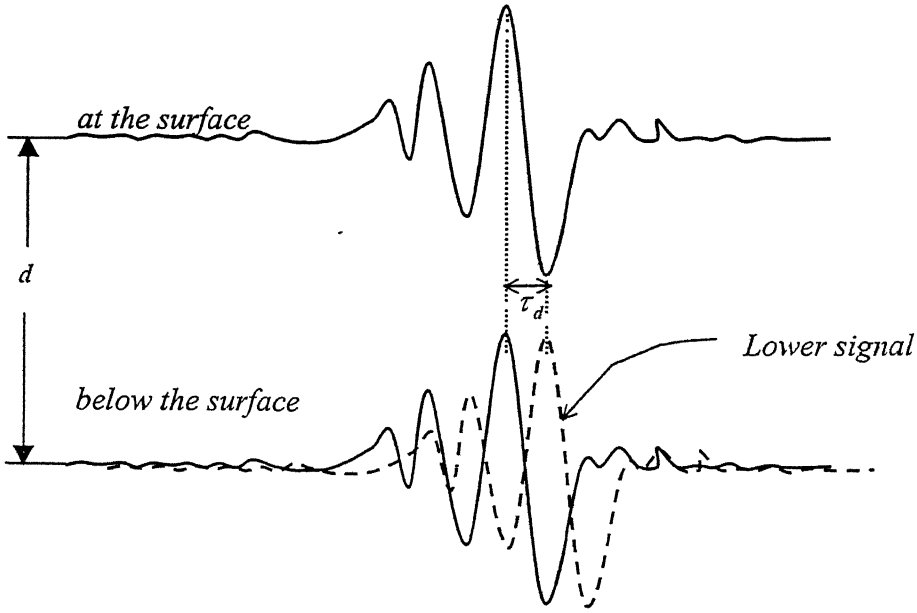

Figure 4.2: Cross-correlation method to obtain Time interval (τ_d)

Cross-correlation function can be calculated in frequency or time domain. In the present work, 'time domain approach' is adopted and the process of Cross-correlation calculation is shown in Figure 4.3.

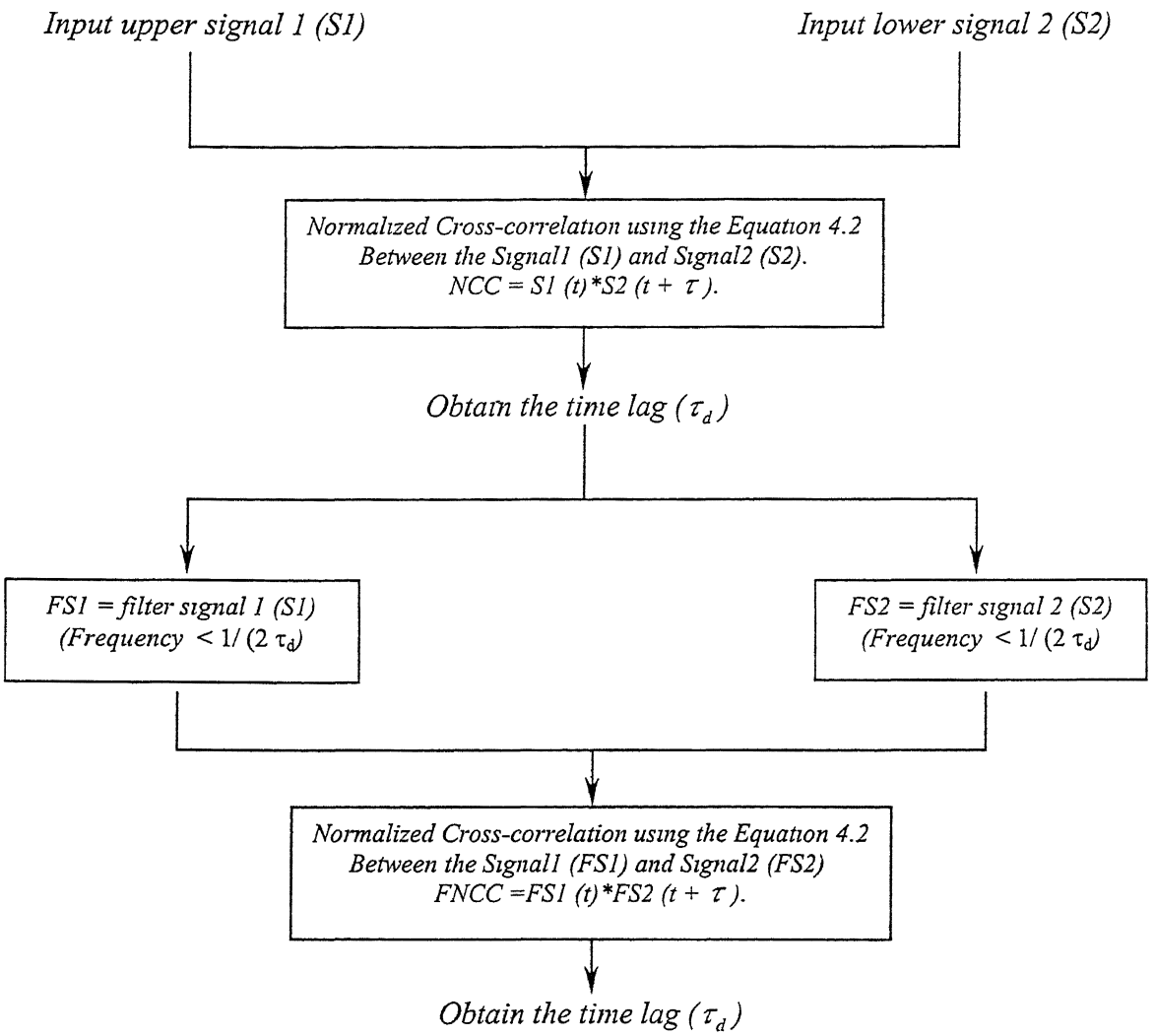

Figure 4.3: Cross-correlation calculation in time domain

Cross-correlation function reaches a major peak at a time delay $\tau = \tau_d$, where τ_d is the time for seismic waves to travel from station i to station j. Then, the apparent velocity V_d of wave propagation between stations i and j may be estimated as,

$$V_d = \frac{d}{\tau_d} \tag{4.3}$$

where, d is the known distance between i and j stations.

Acceleration frequency content records for each event can greatly influence the shape of the Cross-correlation function. Extraneous noise at the input or output reduces the relative contribution of individual correlation peaks and increases the random error in the analysis, but it does not distort or bias the results.

Cross-correlation function obtains sharp peaks and is effective, when the low frequency content ($f < 1/ (2\ \tau_d)$) were filtered out, to distinguish the incident & reflected peaks. Such filtering was necessary to allow separation of incident and reflected wave peaks, in view of:

- the relatively narrow bandwidth of large amplitude frequency components and
- the relatively close spacing of upper most accelerometers.

Assuming the time required for the wave to travel from seismograph a_i to surface is $\tau_{d(a_i \to s)}$, where a_i refers seismograph station at the specified depth, i refers to the station index from surface (1,2,3...n stations). The velocity between the station to the surface is given by:

$$V_{s(a_i \to s)} = \frac{d_{(a_i \to s)}}{\tau_{d(a_i \to s)}} \tag{4.4}$$

where, $d_{(a_i \to s)}$ is the depth of the station from the surface and $V_{s(a_i \to s)}$ is the velocity between the station to the surface. Therefore the average velocity between any two consecutive stations is given by:

$$V_{s(a_i \to a_{i-1})} = \frac{d_{(a_i \to a_{i-1})}}{\tau_{d(a_i \to a_{i-1})}} \quad where, \tag{4.5}$$

$$d_{(a_i \to a_{i-1})} = d_{(a_i \to s)} - d_{(a_{i-1} \to s)} \tag{4.6a}$$

$$\tau_{d(a_i \to a_{i-1})} = \tau_{d(a_i \to s)} - \tau_{d(a_{i-1} \to s)} \tag{4.6b}$$

4.3 Characteristics of Cross-correlation Function

- The value of shift for the peak (positive or negative) in Cross-correlation indicates the time delay between the replicas.

- If the maximum Cross-correlation function has a higher value, the peaks in both the records have similar magnitudes and if it has a smaller value, the two peaks have large variation in magnitude and their wave shapes are different.

- When the Cross-correlation function is maximum, time lag is represented by the phase difference between the two records.

- The peak close to the origin represents the case where transducer is very close to the discontinuity such as free surface or a close spacing between transducers.

- Cross-correlation function magnitude represents the energy carried by the waves. Reflected waves have smaller magnitude, as some energy is lost due to damping.

- If the signal and its replica were of opposite polarity ($-a_i$), the maximum value of $C_{a_i a_j}$ would be negative. Polarity reversal can be caused by the wiring of transducers, or physical reasons such as the reflection of a signal at a free boundary.

4.4 Limitations

Cross-correlation technique provides average shear wave velocity between two downhole stations. In general, the estimates of shear wave velocity are reliable only if,

- The earthquake records are of broad frequency bandwidth,
- Propagation velocities allow for sufficient separation between incident and reflected wave components,
- Low amplitude excitation prevails so as to avoid non-linear soil response and
- Signal is dominated by body shear waves (rather than the surface waves).

4.5 Results and Discussions

Cross-correlation technique is reliable when two stations recording acceleration history are reasonably apart. If they are close by, it is very difficult to judge the time lag, because the two records may be similar with in the short distance. In addition, data recorded close to the surface might be effected by the domination of the surface waves, resulting in poor distribution of Cross-correlation function in estimating time lag in 0 - 5 m layer. Therefore, in the present study, time lag was estimated between 0 - 5 m, 0 - 10 m, 0 - 20 m and 0 - 40 m layers rather than in 0 - 5 m, 5 - 10 m, 10 - 20 m, 20 - 40 m layers. These results were then used to calculate the time taken by the waves to travel in 40 – 20 m, 20 – 10 m, 10 – 5 m and 5 – 0 m layers.

Normalized Cross-correlation function is calculated using Equation 4.2. Time lag (τ_d) is calculated from the lagged cross-correlation peak from the center. The frequency components ($f \leq 1/(2\tau_d)$) were filtered-out from the signal 1 and signal 2 to clearly identify the incident and reflected wave peaks. Cut-off frequency values for the records used in this analysis are shown in the Table 4.2 & 4.3. From the Cross-correlation diagrams (Figure 4.4 – 4.13), it is evident that the time lag is decreasing with the depth and vice versa, i.e. the Shear wave velocity decreases as the wave reaches the surface. It can be observed that some records were not used in the calculation of Cross-correlation function especially between the surface and 5 m layer. The reason being this layer is dominated by the surface waves rather than the body waves.

Spectral density function between two time history records may be defined as the Fourier transformation of the correlation function between those records. Good frequency bandwidth distribution can result in getting accurate estimation of cross-correlation function and the time lag. Figures 4.14 – 4.16 illustrate the Cross-spectral density function, in which, the earthquake records did not contain enough frequency bandwidth for a meaningful interpretation of Cross-correlation function. (e.g. the earthquake 8823 for which very narrow frequency bandwidth (3 – 4 Hz) could be observed almost at all depths especially in the NS direction). Such narrow bandwidth of recorded signal produced an unreliable Cross-correlation function and was not used in the analysis.

Figures 4.17 – 4.19 shows the Cross-correlation function used to calculate Primary wave velocity. The amplitude of the function increased with depth and two main peaks can be observed as the incident and reflected waves. As can be seen from the Figures 4.4 – 4.13 and 4.17 – 4.19, that the time lag increased with the depth. The time lag values obtained from the cross-correlation analysis for different depths to the surface in the calculation of shear wave and primary wave velocities are shown in Table 4.4 and 4.5. The calculated shear and primary wave velocities between the consecutive stations are shown in Table 4.6 and 4.7 respectively. Shear and Primary wave velocity profiles were estimated for different events by Cross-correlation analysis and are compared with geophysical measurement velocity profile (Figures 4.20 – 4.21). These velocities in EW & NS directions are in reasonable agreement with the velocities measured using in-situ geophysical method.

4.6 Summary

- Cross-correlation method is a reliable technique in estimating time lag when the recording stations are far apart.

- Filtering was effective in clearly differentiating the incident and reflected wave peaks.

- Estimation of wave propagation velocities were reliable when the signal is dominated by body waves and having large frequency band width.

- The estimated shear wave velocities for the events where the PGA < 41 cm/sec^2 (low amplitude excitation) recorded on the surface, were reasonably in good agreement with the geophysical measurements.

- Shear wave velocities were observed to be higher than the geophysical measurements, especially in 10-20 m and 20-40 m layers.

- Some of the events were not employed to estimate shear wave velocities due to narrow frequency bandwidth.

- The estimated shear wave velocity during an event where recorded PGA (Peak event 8722, PGA is 327.1 cm/sec^2 on the surface) is observed to be in agreement with the geophysical measurements. However, for such a large PGA, significant non-linear response is expected and shear wave velocity should be lower. As observed by other researchers and corroborated in this study, non-linear response of soil is small even during peak PGA due to rigid sub soil layers and hence the velocities were almost coinciding in both higher and lower PGA studies.

Table 4.1: Lower cut-off frequencies employed in the calculation of cross-correlation

(Shear wave velocity estimation)

S. no	Event	PGA (cm/sec^2)		Lower Cut-off Frequency (Hz)							
		EW	NS	EW Direction				NS Direction			
				S and 5m	S and 10m	S and 20m	S and 40m	S and 5m	S and 10m	S and 20m	S and 40m
1	8401	25.5	24.2	*	8	3	3	*	2.5	2.5	3
2	8420	22.1	24.1	*	8	2	3	*	5	2.5	3
3	8510	27.4	29.6	*	5	2.5	1.5	*	2.5	2.5	3
4	8519	59.2	82.2	*	8	4	1.5	*	2.5	2.5	3
5	8525	75.7	71.6	*	5	4	1.5	*	6.5	4.5	1.5
6	8601	15.4	14 3	6.5	3	3	1	7	5	4.5	1.5
7	8717	20.7	33.5	*	6	4	3	*	2	5	3
8	8722	213.6	327.1	8 5	6.25	4	3.57	10	5	5	3
9	8723	17.2	21.2	12	2	4	3.57	8.5	5.5	5	3.57
10	8725	23.8	13.8	*	1	5	3.57	6.75	2	2	3.57
11	8726	22.5	30.4	*	5	5.5	3.57	*	2	5	3
12	8802	40.6	40.8	4	2	2	3.7	9.5	2	2	3.7
13	8806	54.9	97.8	*	2.25	2	3.57	*	5	3	3.5
14	8808	19.0	26.2	3	2	6.5	3.57	10	2	6.67	3.4
15	8816	48.4	59.8	*	4	4	3.57	*	*	*	*
16	8823	46.4	35.2	*	*	*	*	*	4	3.5	3
17	8901	55.7	49.1	*	7.55	4	3.57	*	5	4	3.5
18	8903	27.5	28.9	*	7	5	3.8	*	7	4.5	3.5
19	8904	41.0	21.9	4.5	2	2	3.5	11	5	2	3

* Not used because of narrow low frequency bandwidth

Table 4.2: Lower cut-off frequencies employed in the calculation of cross-correlation

(Primary wave velocity estimation)

S. no	Event	PGA (cm/sec^2)	Lower Cut-off Frequency (Hz)			
		UD	UD Direction			
			Surface and 5m	Surface and 10m	Surface and 20m	Surface and 40m
1	8401	12.7	8	6	4	3
2	8416	7.8	5	7	5	4
3	8510	12.6	8	6	4	3
4	8519	23.5	8	6	4	3
5	8601	5.2	4	6	4	4
6	8602	21.5	5	6	4	3
7	8717	12.1	9	6	4	3
8	8722	124.8	8	7	5	5
9	8723	16.4	7	5	4	3
10	8725	9.3	1	5	4	3
11	8726	18.0	8	6.5	4	5
12	8806	19.8	5	4.5	4.5	4
13	8816	15.2	8	7	5.5	4
14	8823	12.0	8	6	5	7
15	8901	25.4	7	6.5	4.5	3
16	8903	13.2	7.5	6	4	3.5

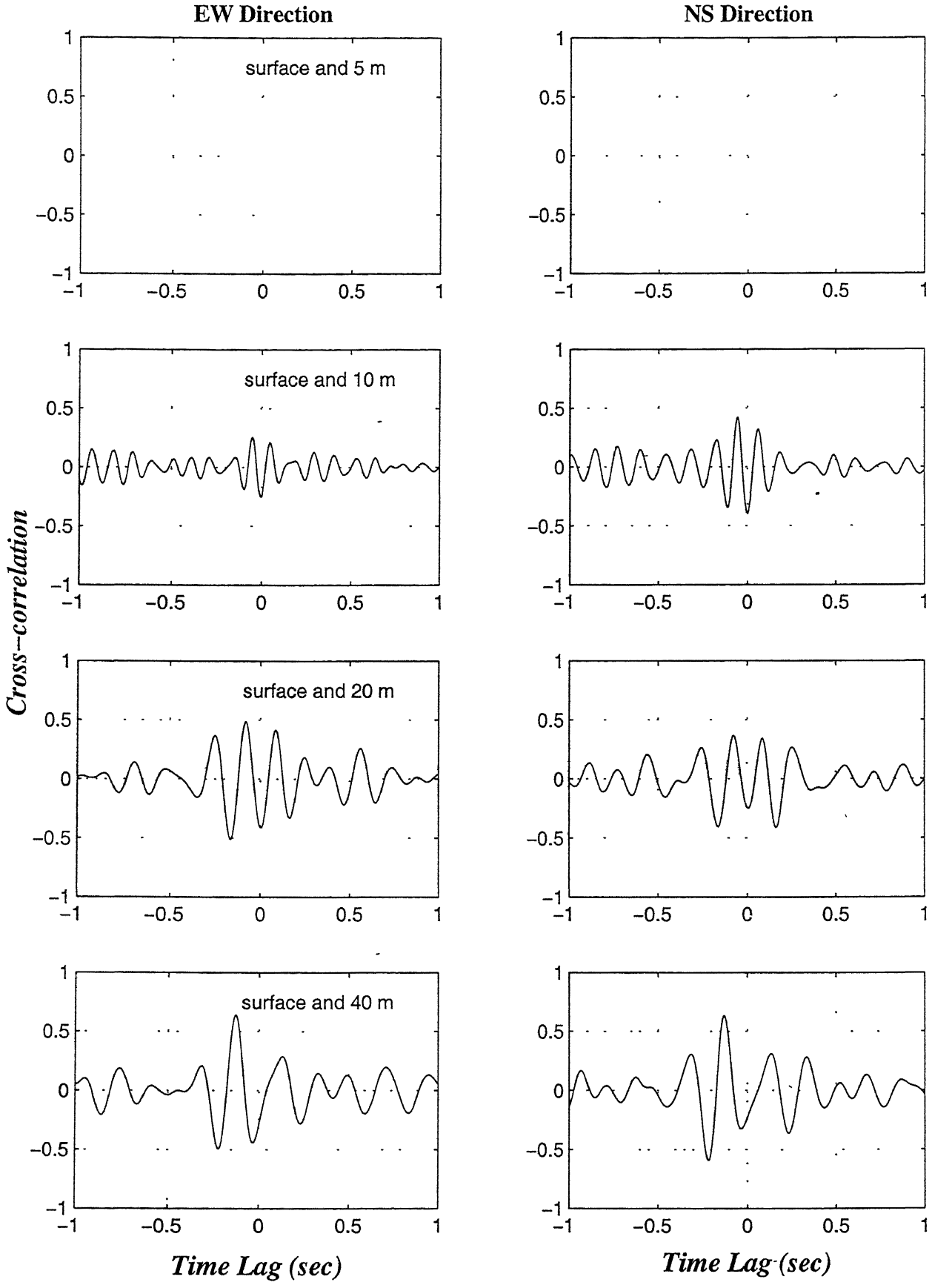

Figure 4.4: Cross-correlation of acceleration histories during the earthquake 8401 at borehole C0

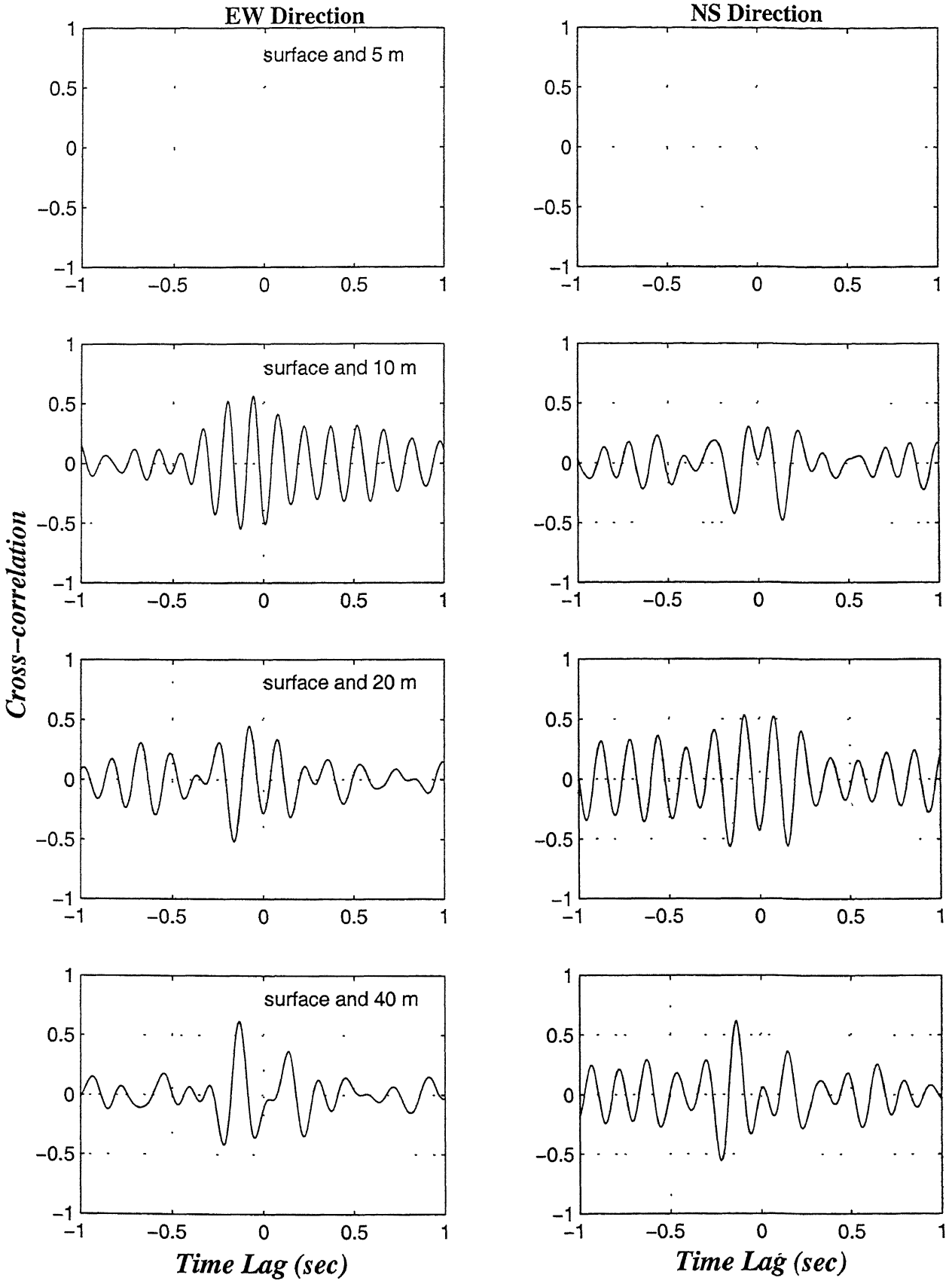

Figure 4.5: Cross-correlation of acceleration histories during the earthquake 8510 at borehole C0

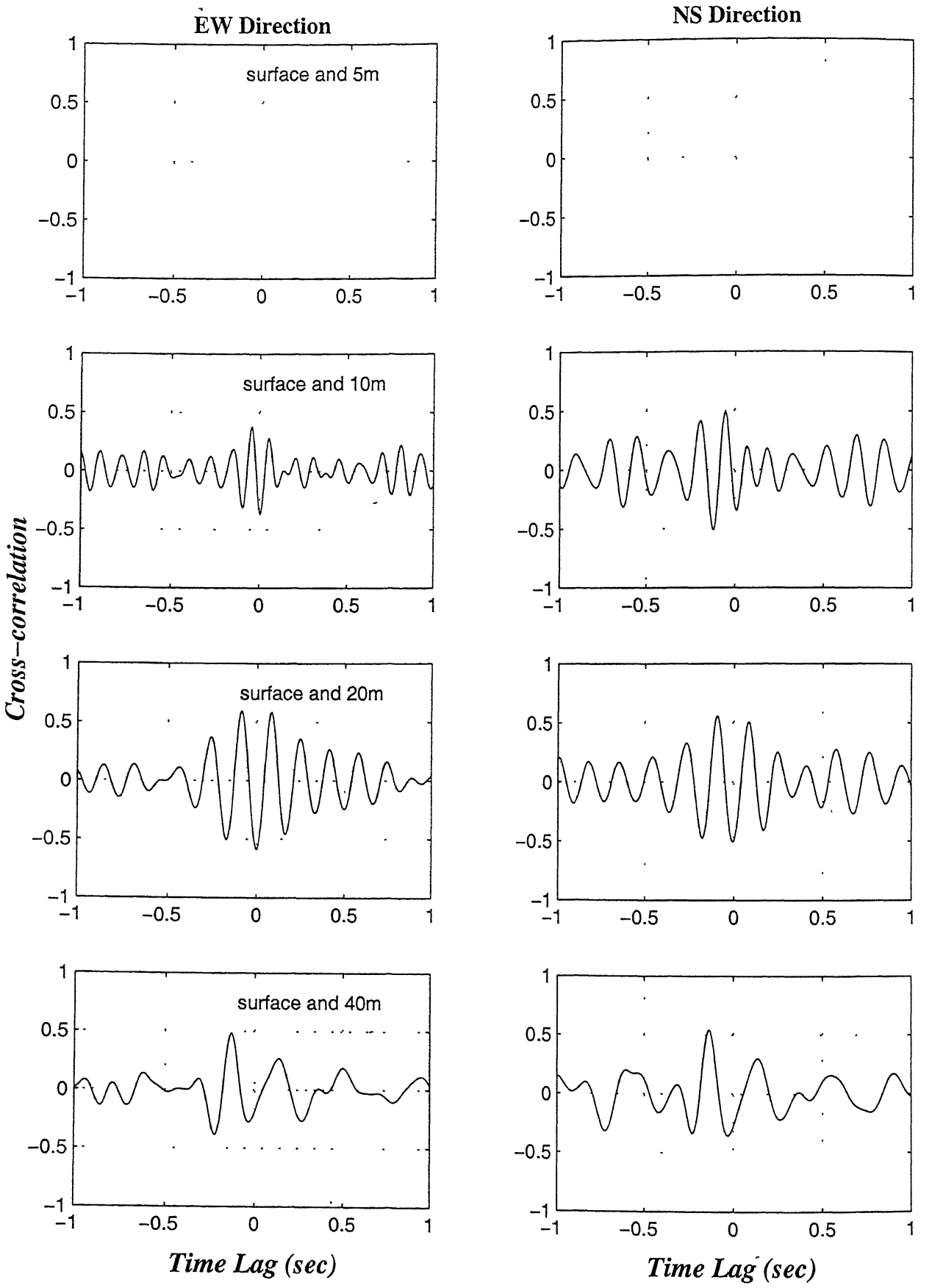

Figure 4.6: **Cross-correlation of acceleration histories during the earthquake 8519 at borehole C0**

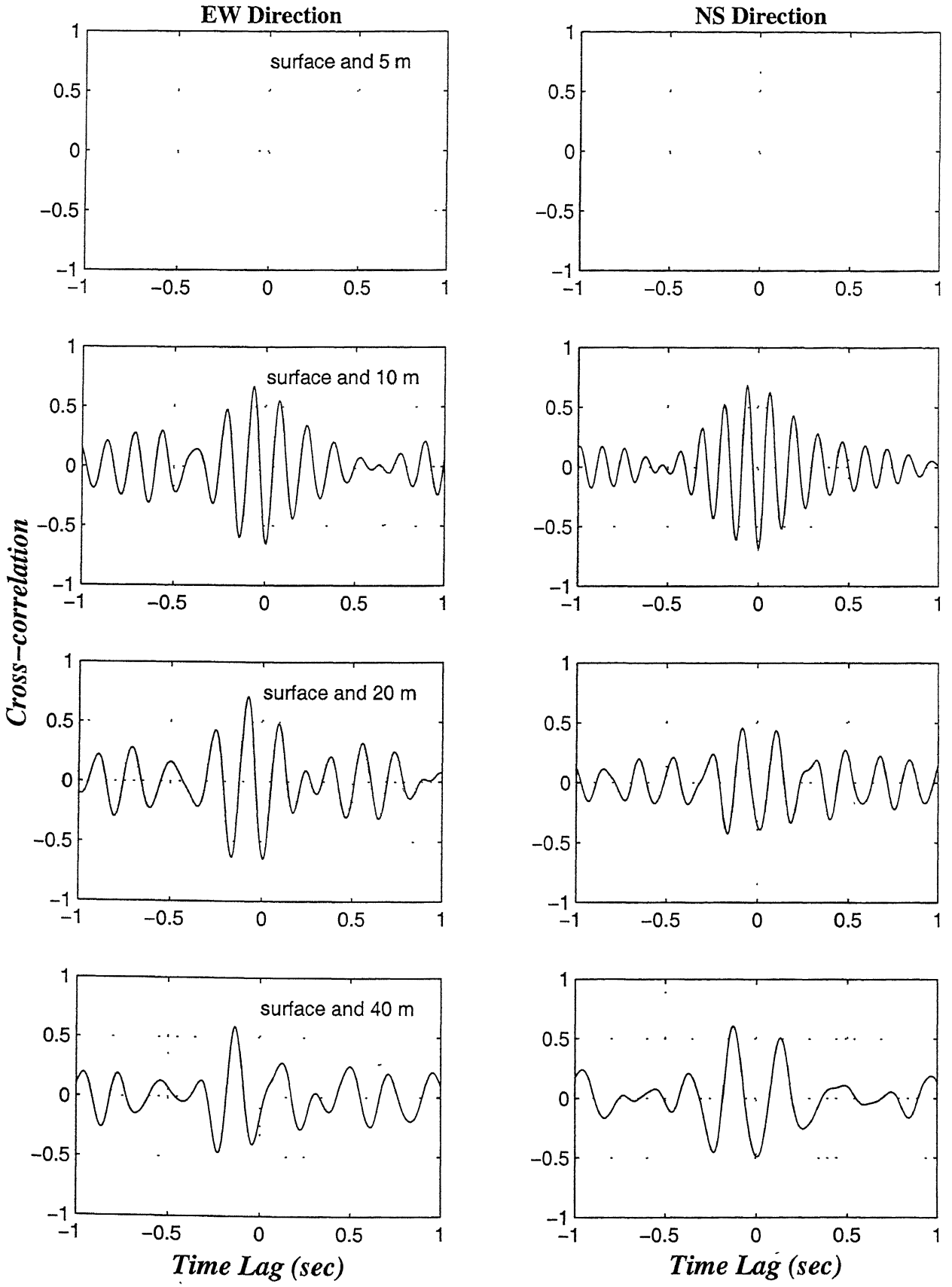

Figure 4.7: **Cross-correlation of acceleration histories during the earthquake 8525 at borehole C0**

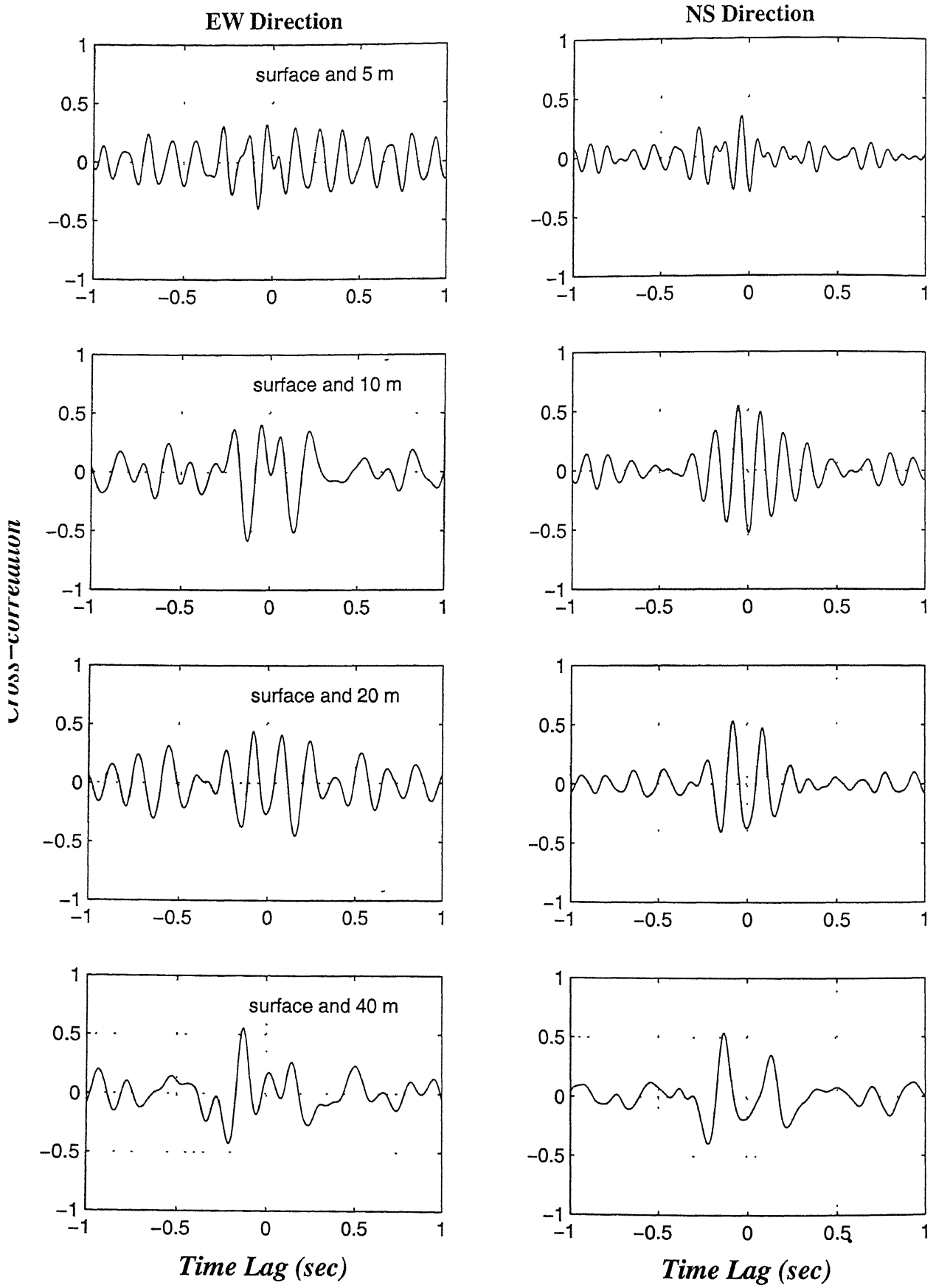

Figure 4.8: **Cross-correlation of acceleration histories during the earthquake 8601 at borehole C0**

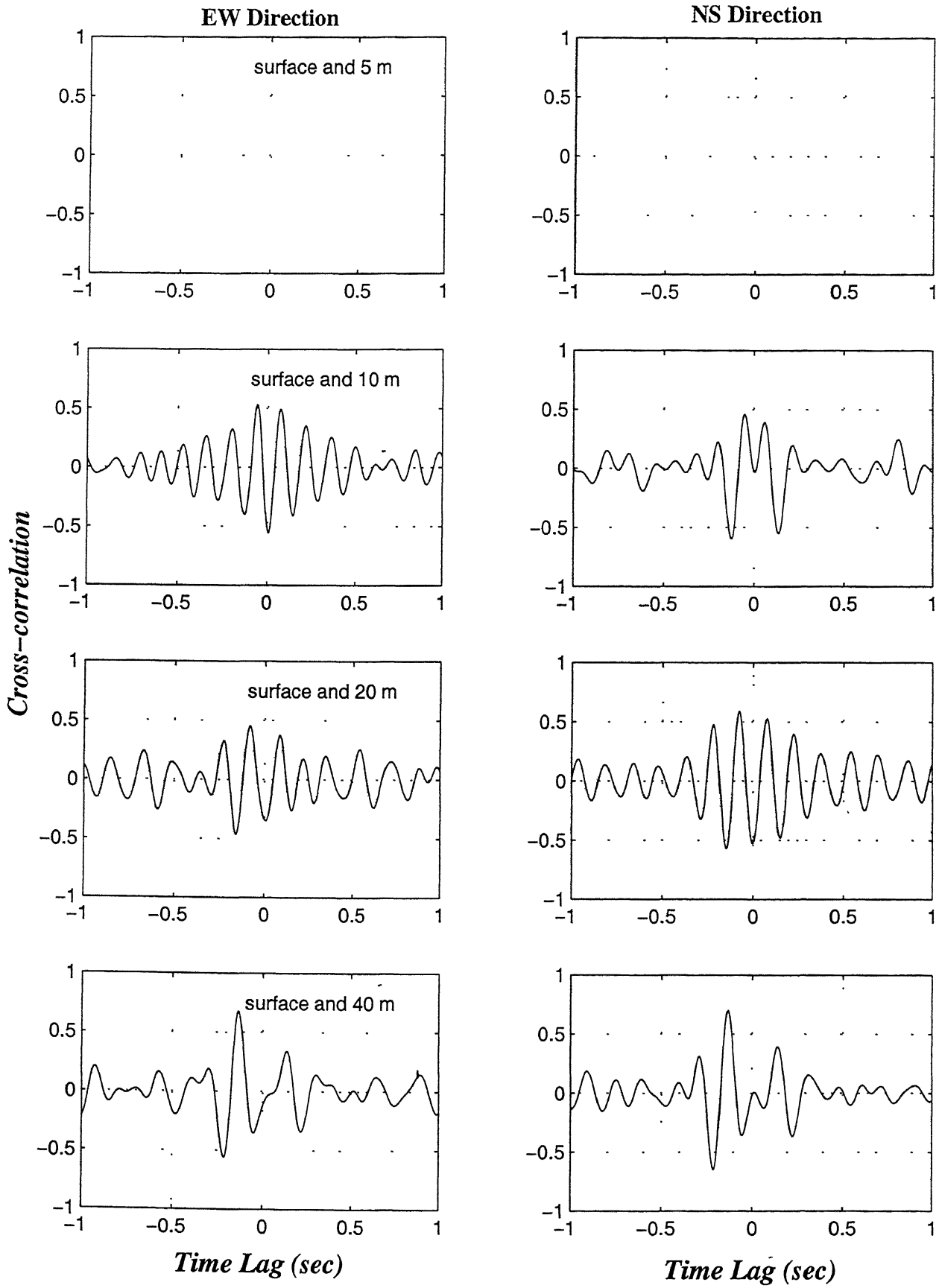

Figure 4.9: **Cross-correlation of acceleration histories during the earthquake 8717 at borehole C0**

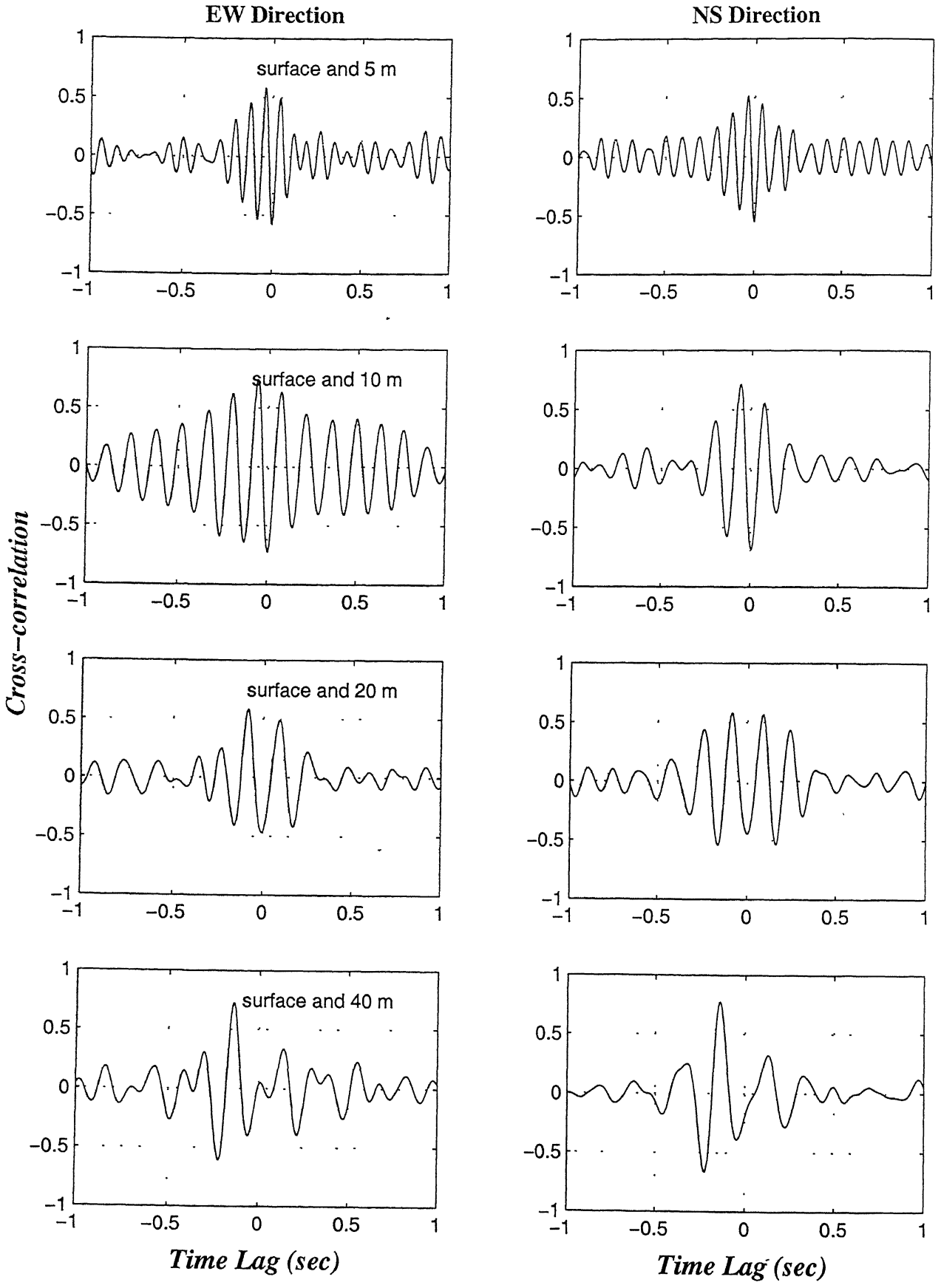

Figure 4.10: Cross-correlation of acceleration histories during the earthquake 8722 at borehole C0

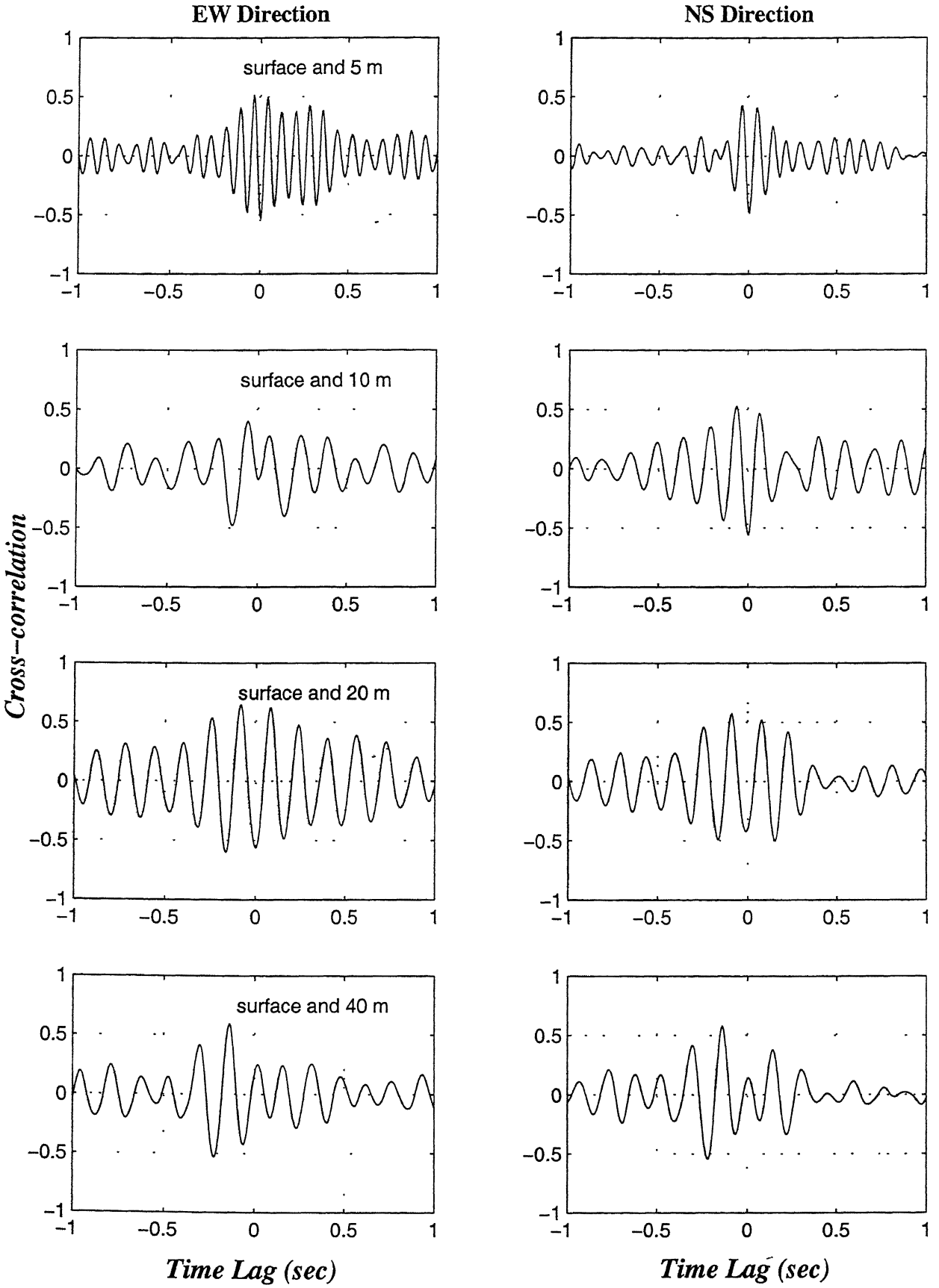

Figure 4.11: Cross-correlation of acceleration histories during the earthquake 8723 at borehole C0

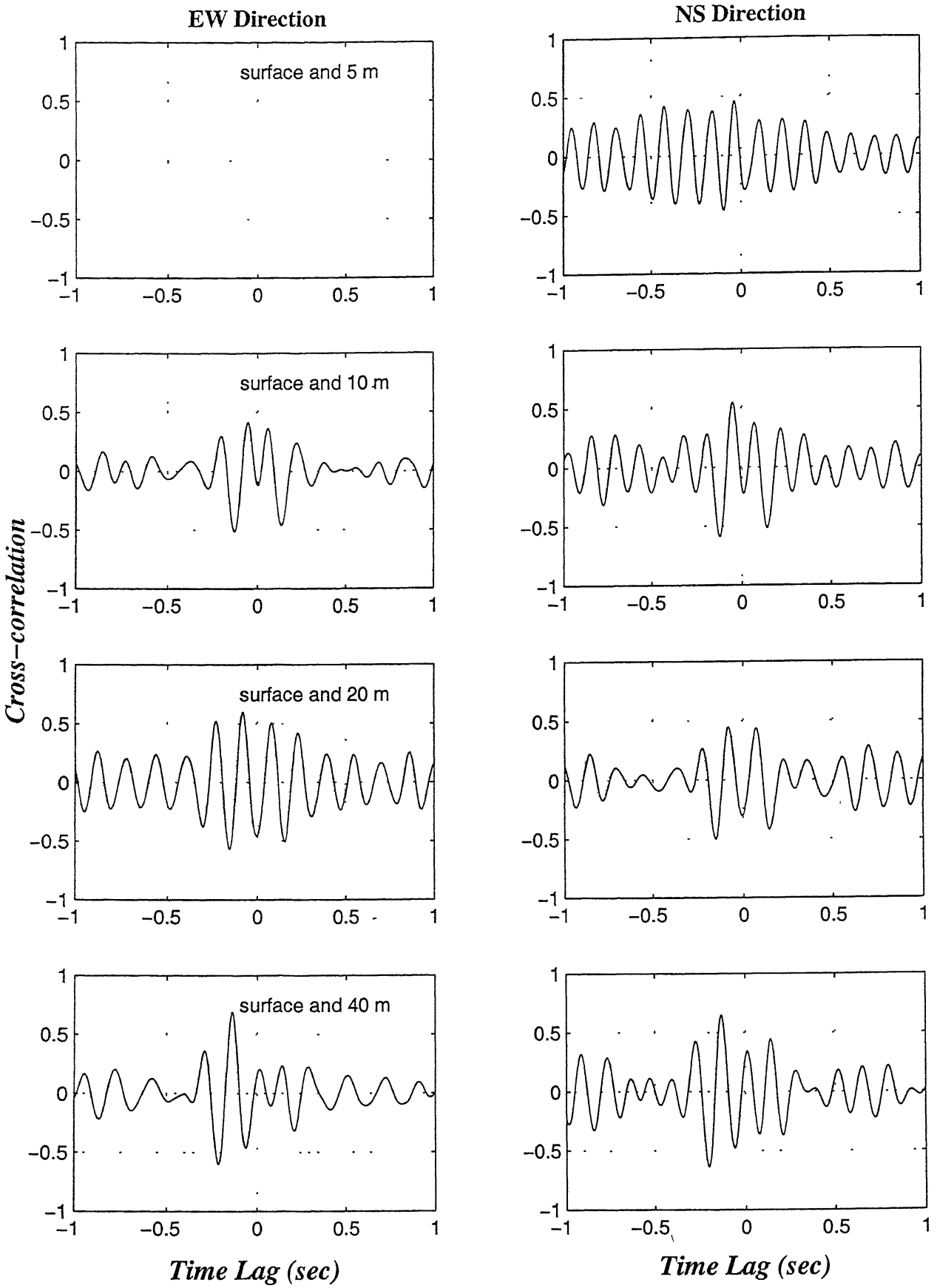

Figure 4.12: Cross-correlation of acceleration histories during the earthquake 8725 at borehole C0

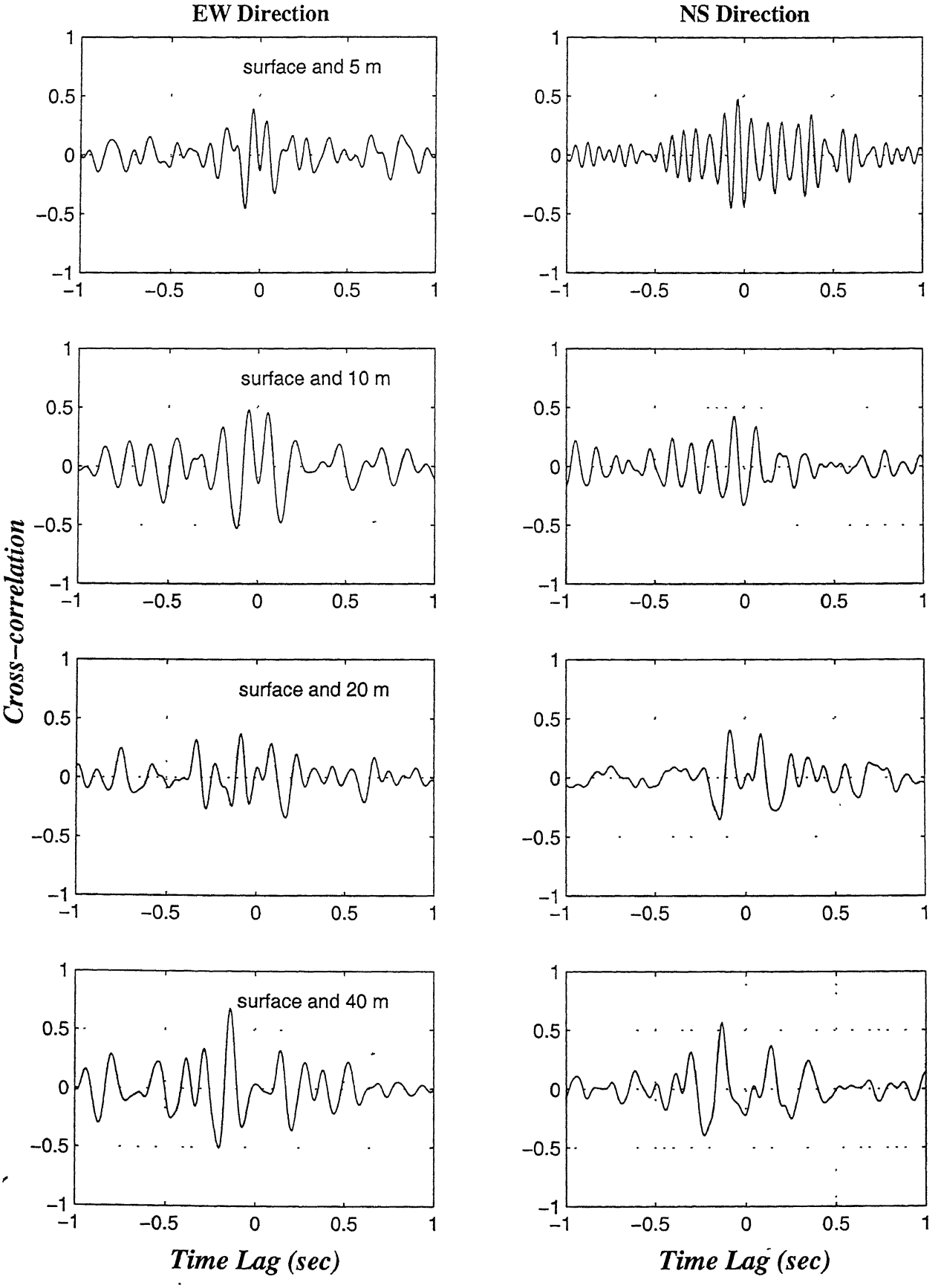

Figure 4.13: Cross-correlation of acceleration histories during the earthquake 8904 at borehole C0

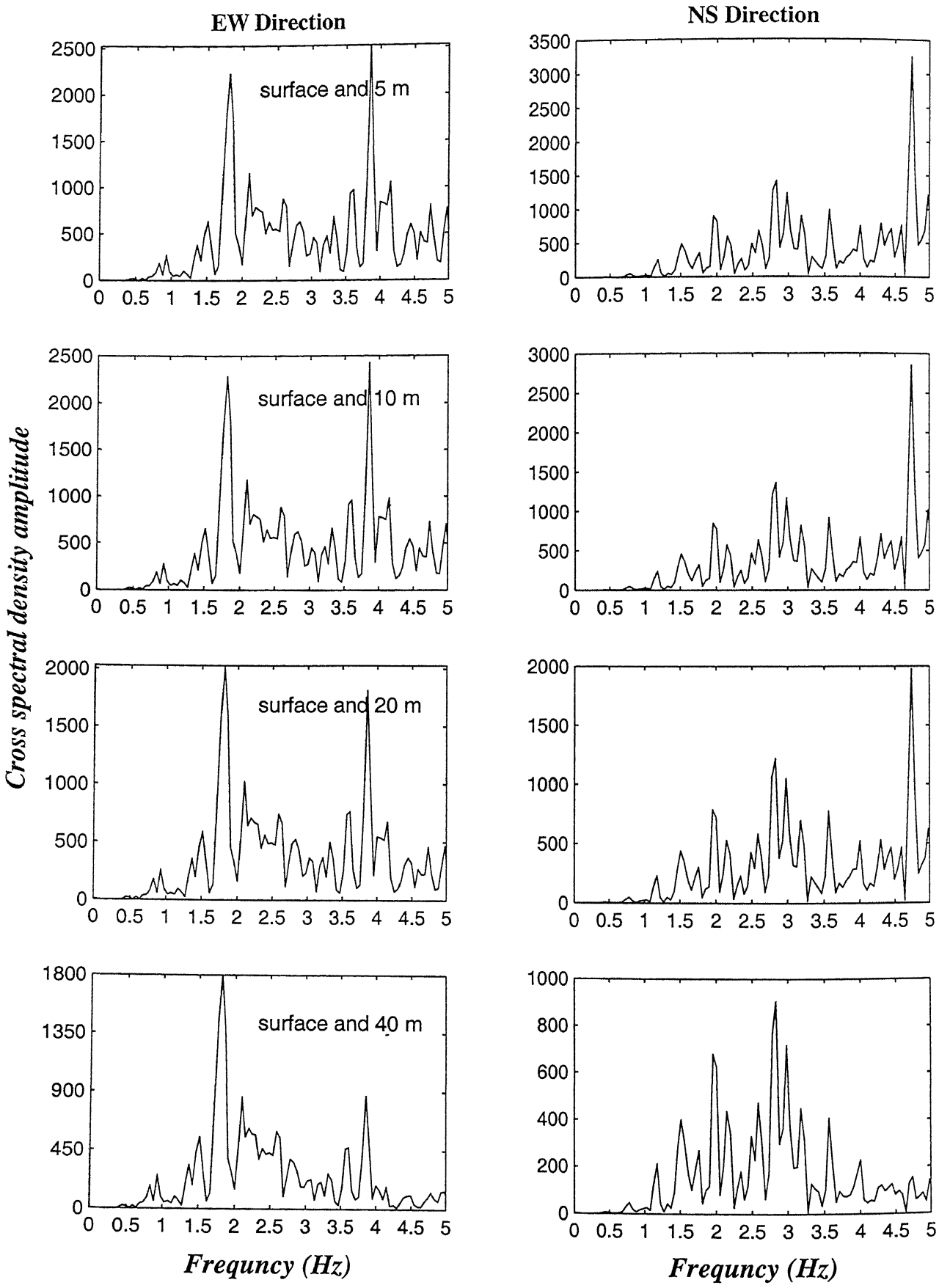

Figure 4.14: Cross-spectral density function during the earthquake 8307 at borehole C0

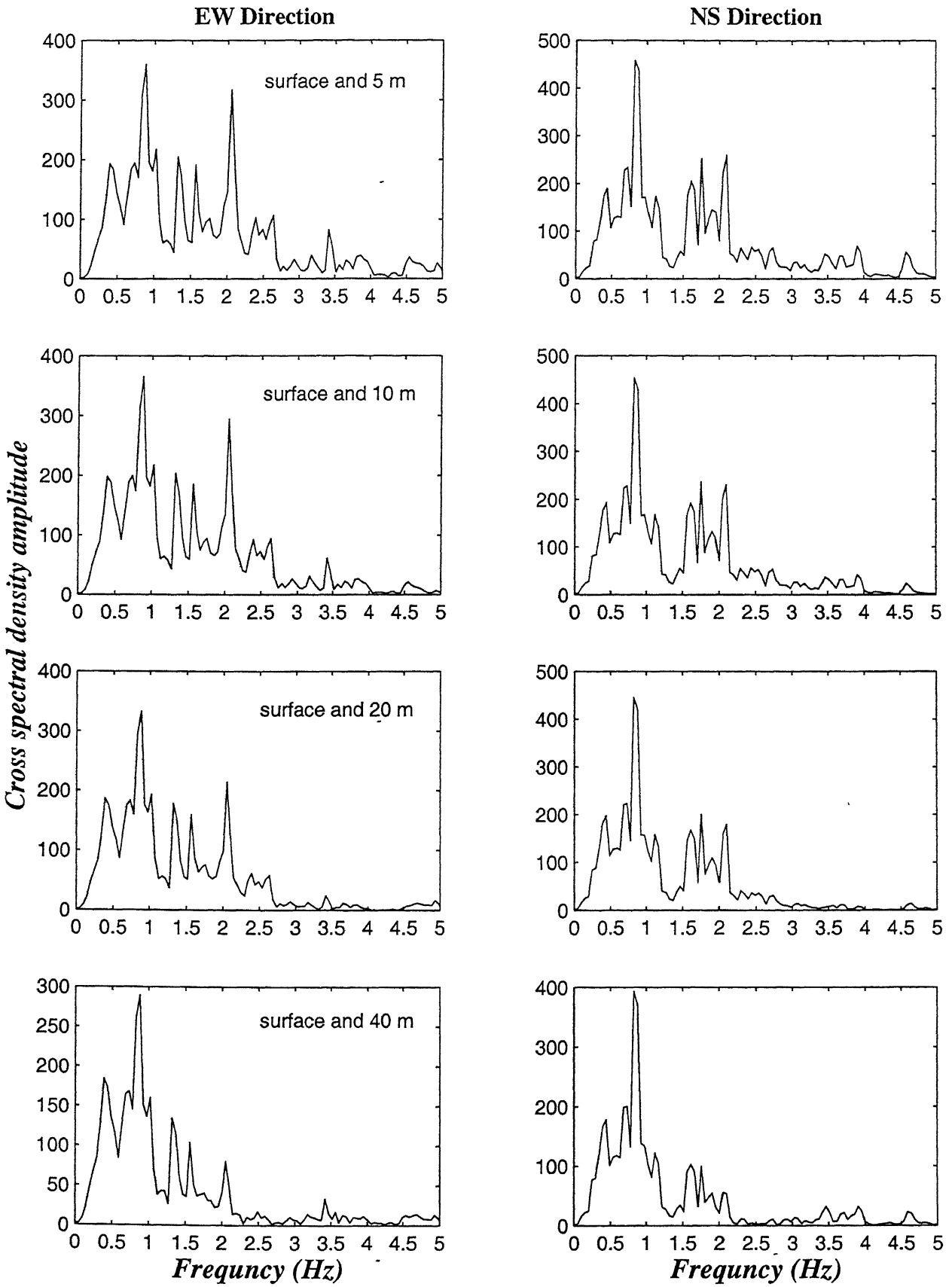

Figure 4.15: Cross-spectral density function during the earthquake 8406 at borehole C0

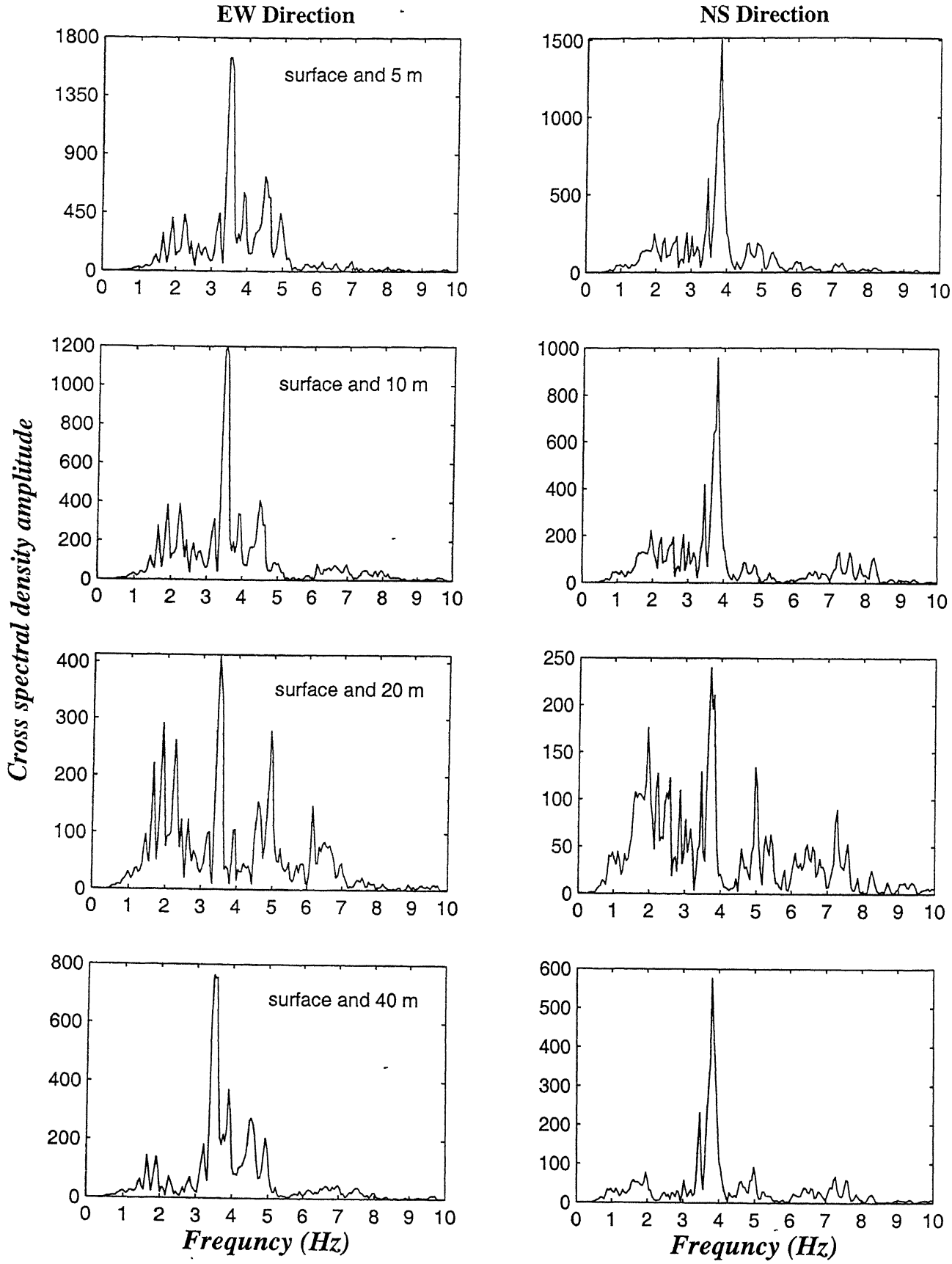

Figure 4.16: Cross-spectral density function during the earthquake 8823 at borehole C0

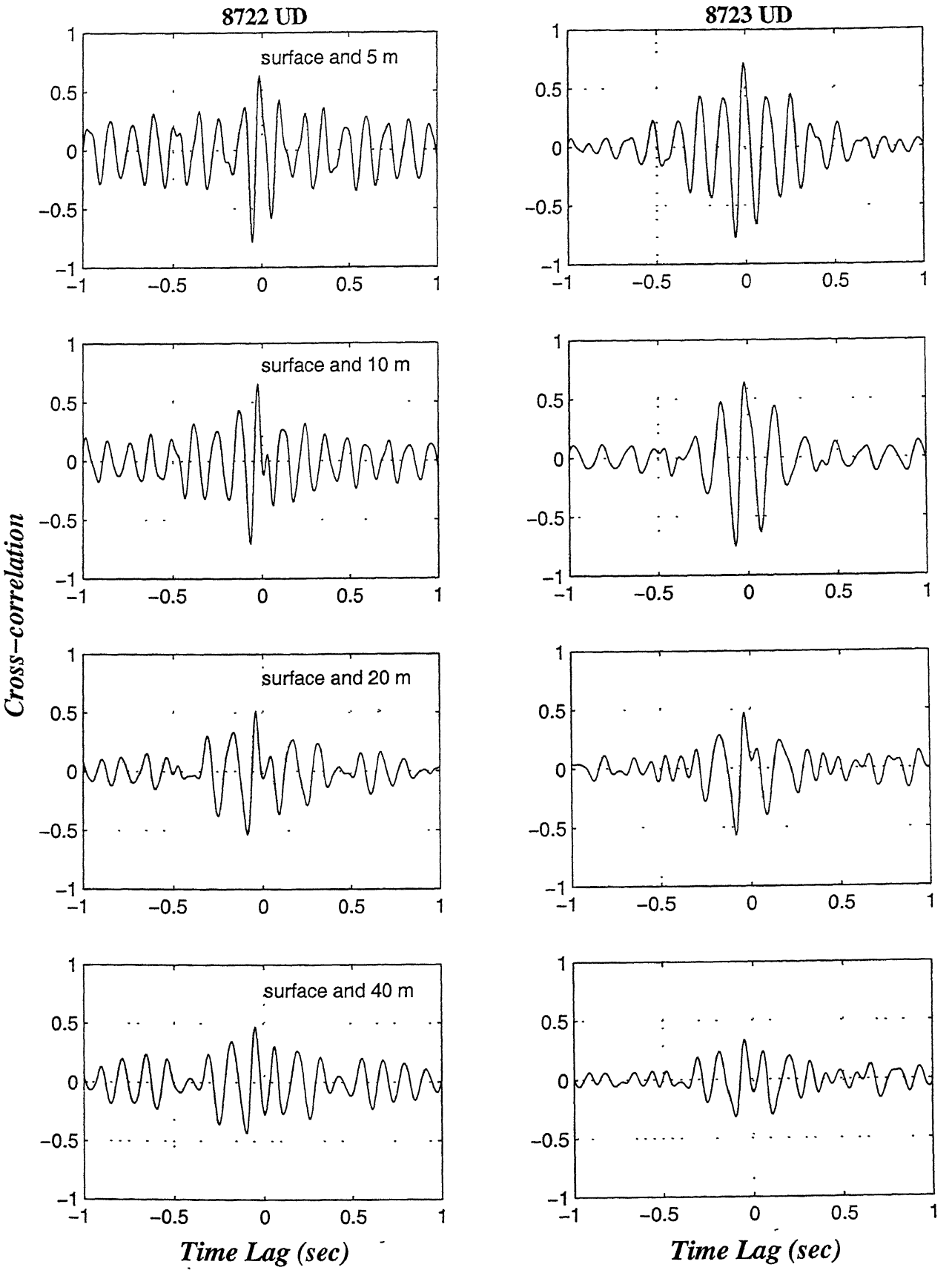

Figure 4.17: Cross-correlation of acceleration histories during the earthquakes 8722 and 8723 at borehole C0

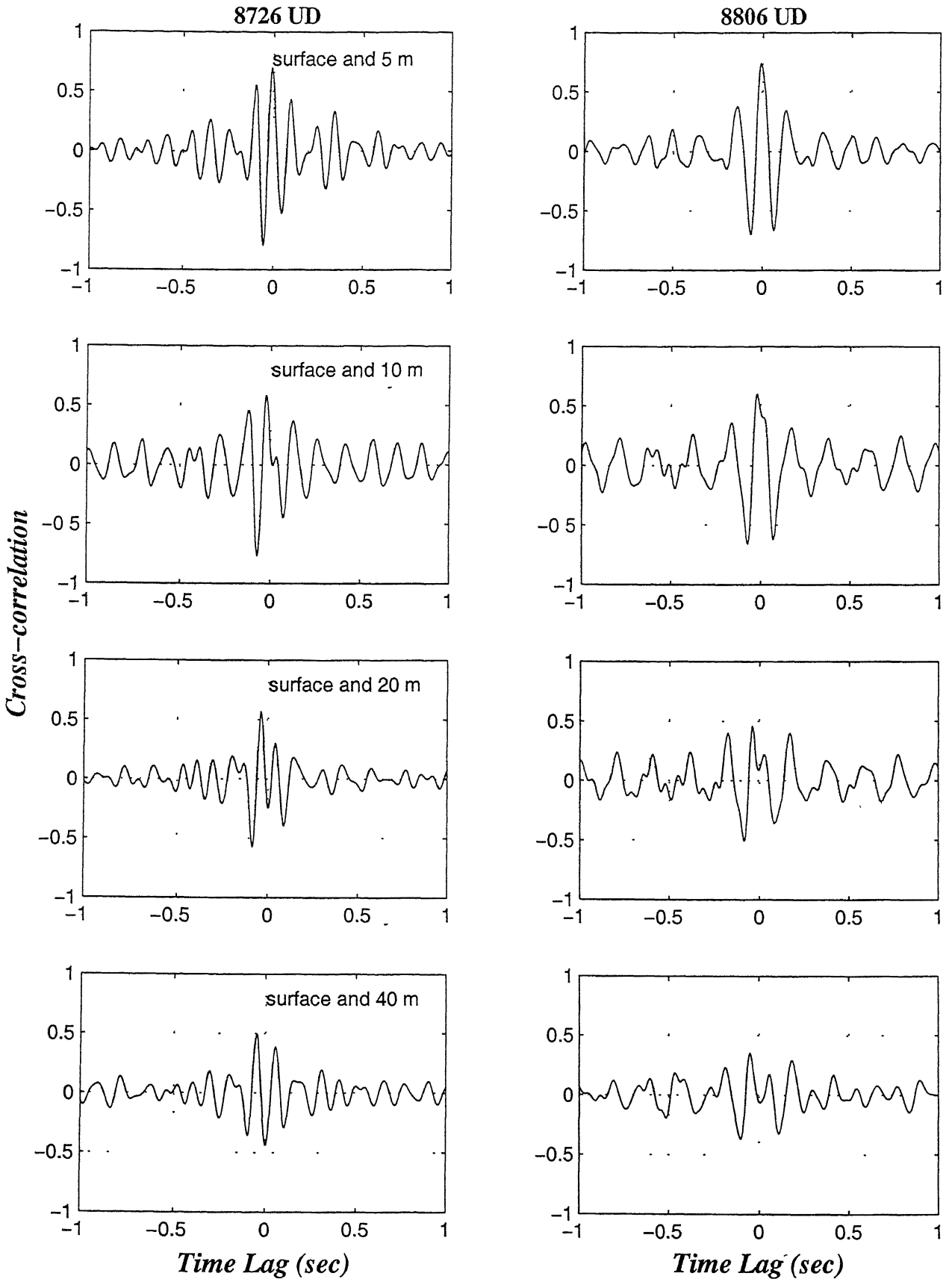

Figure 4.18: Cross-correlation of acceleration histories during the earthquakes 8726 and 8806 at borehole C0

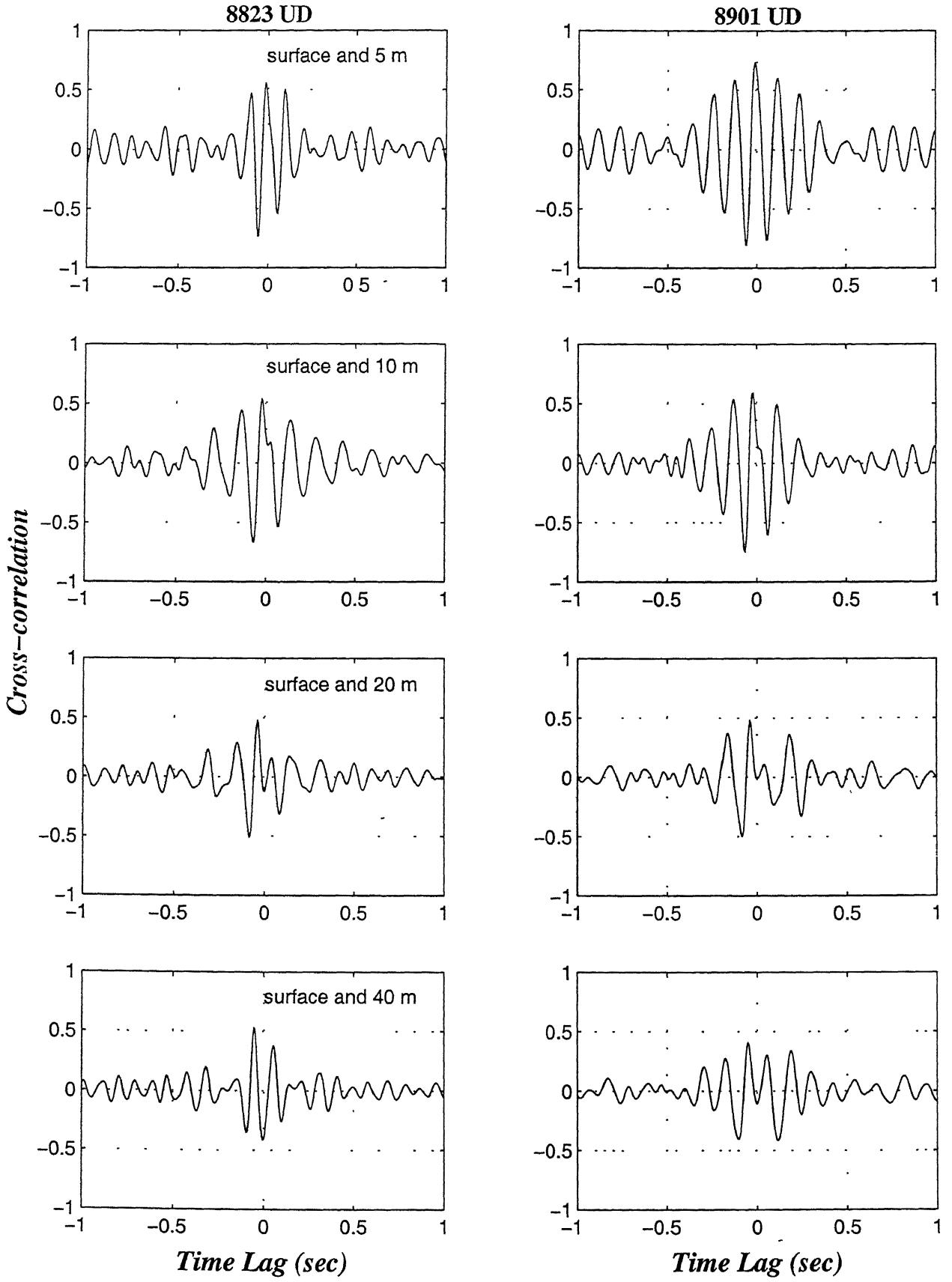

Figure 4.19: Cross-correlation of acceleration histories during the earthquake 8823 and 8901 at borehole C0

Table 4.5: Estimated shear wave velocities between the borehole stations

S. no	Event	PGA (cm/sec^2)		Shear Wave velocity V_s (m/sec)									
				EW Direction					NS Direction				
		EW	NS	S and 5m	S and 10m	5 and 10m	10 and 20m	20 and 40m	S and 5m	S and 10m	5 and 10m	10 and 20m	20 and 40m
1	8401	25.5	24.2	*	200	*	333.3	400	*	181.8	*	333.3	400
2	8420	22.1	24.1	*	153	*	1000~	333.3	*	181.8	*	400	363.6
3	8510	27.4	29.6	*	166.7	*	500~	363.6	*	200	*	285.7	400
4	8519	59.2	82.2	*	222.2	*	250	400	*	181.8	*	285.7	444.4
5	8525	75.7	71.6	*	153.8	*	666.7~	363.6	*	166.7	*	400	500~
6	8601	15.4	14.3	166.7		250	333.3	400	125		333 3	400	400
7	8717	20.7	33.5	*	166.7	*	400	400	*	181.8	*	400	363.6
8	8722	213.6	327.1	111.1		333.3	333.3	400	125		250	333.3	400
9	8723	17.2	21.2	142.8		333.3	333.3	363.6	125		200	400	400
10	8725	23.8	13.8	*	181.8	*	400	333.3	*	285.7	*	400	400
11	8726	22.5	30.4	*	166.7	*	500~	333.3	*	200	*	333.3	363.6
12	8802	40.6	40.8	100		250	400	363.6	125		333.3	333.3	400
13	8806	54.9	97.8	*	166.7	*	400	363.6	*	166.7	*	285.7	666.7~
14	8808	19.0	26.2	142.8		250	400	333.3	142.8		200	400	333.3
15	8816	48.4	59.8	*	166.7	*	500~	444.4	*		*	*	*
16	8823	46.4	35.2	*		*	*	*	*	181.8	*	333.3	444.4
17	8901	55.7	49.1	*	200	*	400	333.3	*	200	*	400	363.6
18	8903	27.5	28.9	*	166.7	*	400	444.4	*	181.8	*	400	363.6
19	8904	41.0	21.9	125		333.3	333.3	363.6	142.8		250	333.3	400

*** Not used in the estimation of shear wave velocity due to narrow frequency bandwidth** **~ Un-reliable estimate**

Table 4.6: Estimated Primary wave velocities between the borehole stations

S. no	Event	PGA (cm/sec^2)	Primary wave velocity V_p (m/sec)			
		UD	UD Direction			
			Surface and 5m	5m and 10m	10m and 20m	20m and 40m
1	8401	12.7	500	1000~	666.7	1333.3
2	8416	7.8	1000~	333.3	1000	1333.3
3	8510	12.6	500	1000~	666.7	1333.3
4	8519	23.5	500	1000~	666.6	1333.3
5	8601	5.2	1000~	333.3	1000	2000
6	8602	21.5	1000~	500	666.6	2000
7	8717	12.1	500	1000~	666.7	1333.3
8	8722	124.8	333 3	500	666 7	2000
9	8723	16.4	500	500	666.7	1333.3
10	8725	9.3	1000~	500	666.7	1333.3
11	8726	18.0	500	333.3	666.7	2000
12	8806	19.8	500	500	500	2000
13	8816	15.2	500	500	1000	2000
14	8823	12.0	333.3	500	666.7	1333.3
15	8901	25.4	500	500	500	2000
16	8903	13.2	1000~	500	1000	1333.3

~ Un-reliable Estimate

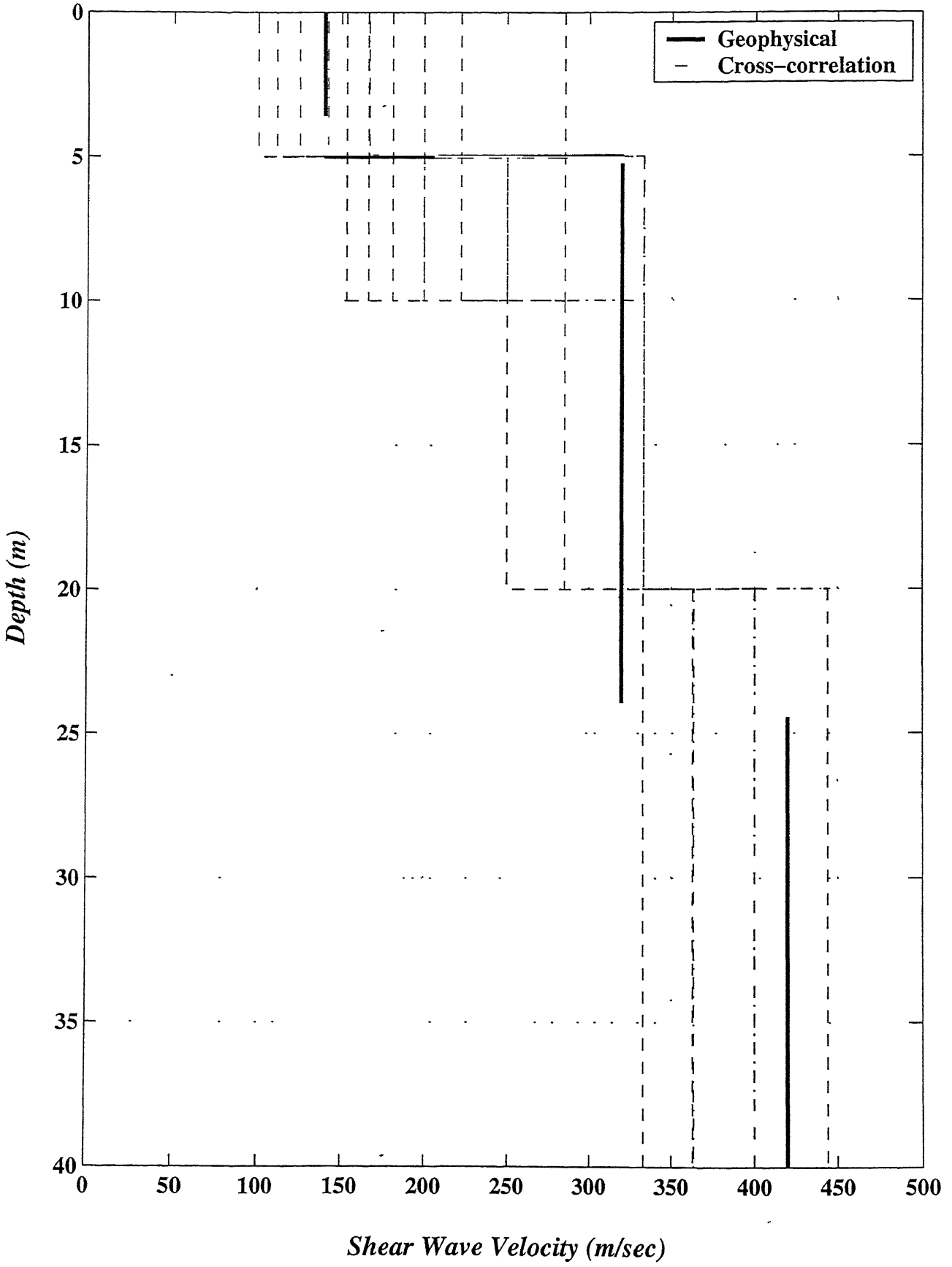

Figure 4.20: Estimated Shear wave velocity using Cross-correlation method

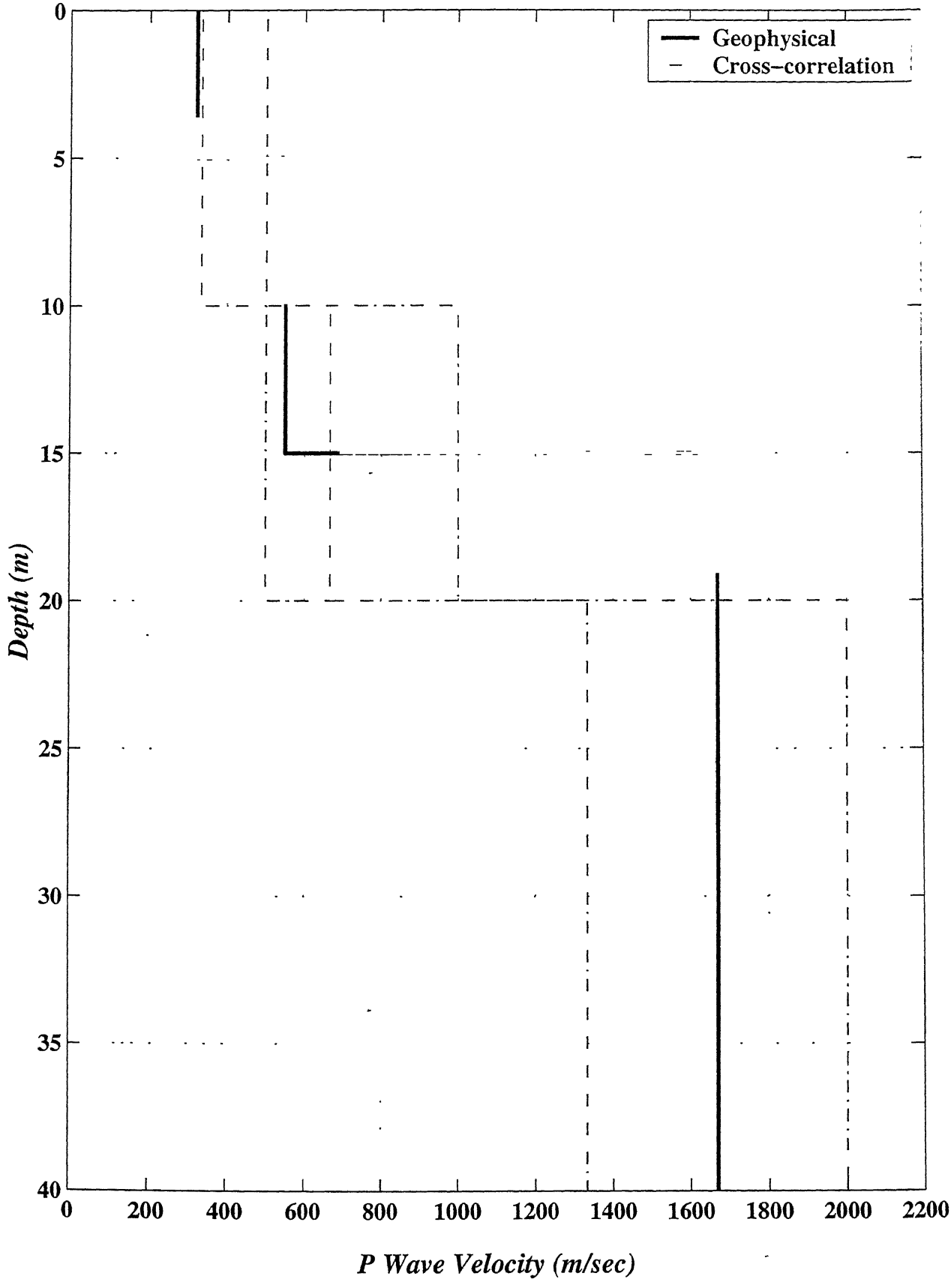

Figure 4.21: Estimated Primary wave velocity using Cross-correlation method

Chapter 5

SHEAR STRESS - STRAIN HISTORIES

5.1 Introduction

Calculating site shear stress-strain histories directly from the recorded acceleration histories enables to:

- understand the site amplification (linear or non-linear) under earthquake loading
- estimate the stiffness of the soil
- estimate the hysteretic damping of the soil
- estimate the induced strain in the soil.

Since the loading amplitude on soil varies with time during the dynamic loading, soil stiffness changes for each cycle. It influences the wave propagation velocity through soil media and is inversely proportional to the induced strain in the soil. Ground strain is effected by ground acceleration amplitude and ground displacements. In the present study One-dimensional shear beam idealization is used to describe the site seismic lateral response in line with other researchers. Similar studies by other researchers include:

- Abdel - Ghaffer et al. [2] employed a single degree of freedom system to calculate the shear moduli and damping values of Santa Felicia earth dam.
- Koya & Matsao [30] employed a force-relative displacement relation to study the results of shake table tests.
- Zeghal et al. [54] used One-dimensional shear beam idealization to study Lotung downhole array soil non-linear properties by calculating shear stress-strain histories.

In the current study as well as those reported in the literature review, longer period waves ($< 0.25 - 0.35$ HZ) were filtered out in calculating the ground stress-strain to estimate the soil dynamic properties.

5.2 Methodology

Using a shear beam model to describe site seismic lateral response, shear stress $\tau(z, t)$ at any level z can be expressed as:

$$\tau(z,t) = \int_0^z \rho \ddot{u}(\zeta,t)\, d\zeta \qquad (5.1)$$

where, ρ = mass density, and $\ddot{u}(\zeta,t)$ = absolute acceleration at level ζ.

Using the linear interpolation between downhole accelerations, the discrete counterpart of shear stress at level 2 is shown in Figure 5.1.

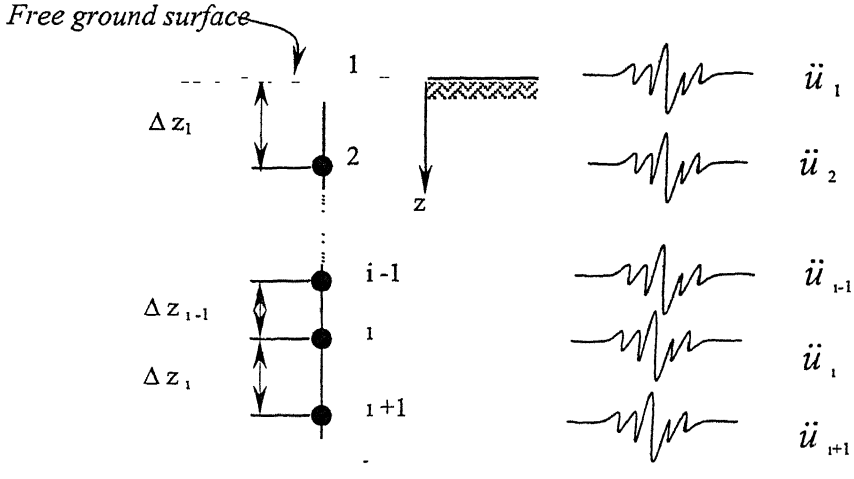

Figure 5.1: Site Discretization

From the Newton's Second Law of Motion (F = ma) and assuming unit area of shear beam in the calculation of stress,

$$F_2(t) = \frac{\rho_1}{g} \Delta Z_1 \frac{(\ddot{u}_1 + \ddot{u}_2)}{2} \qquad (5.2)$$

Stress is given as : $\tau_2(t) = \tau_1 + \rho_1 \frac{(\ddot{u}_1 + \ddot{u}_2)}{2} \Delta Z_1$ (5.3)

From the above equation the stress at any level z_i is expressed as,

$$\tau_i(t) = \tau_{i-1} + \rho_{i-1} \frac{(\ddot{u}_{i-1} + \ddot{u}_i)}{2} \Delta Z_{i-1} \quad (5.4)$$

Like wise the force at the mid point of levels 1 and 2 is given as,

$$\ddot{u}_{1-\frac{1}{2}} = \frac{(\ddot{u}_1 + \ddot{u}_2)}{2} \quad (5.5)$$

$$F_{1-\frac{1}{2}}(t) = \frac{\rho_1}{g} \frac{\left(\ddot{u}_1 + \ddot{u}_{1-\frac{1}{2}}\right)}{2} \frac{\Delta Z_1}{2} \quad (5.6)$$

Substituting $\ddot{u}_{1-\frac{1}{2}}$ from equation 5.5,

$$F_{1-\frac{1}{2}}(t) = \frac{\rho_1}{g} \frac{\left(\ddot{u}_1 + \frac{(\ddot{u}_1 + \ddot{u}_2)}{2}\right)}{2} \frac{\Delta Z_1}{2} \quad (5.7)$$

Stress is given as, $\tau_{1-\frac{1}{2}}(t) = \tau_1 + \frac{\rho_1}{g} \frac{(3\ddot{u}_1 + \ddot{u}_2)}{8} \Delta Z_1$ (5.8)

From the above equation the strain at any level $(z_{i-1} + z_i)/2$ is expressed as,

$$\tau_{i-\frac{1}{2}}(t) = \tau_{i-1} + \rho_{i-1} \frac{(3\ddot{u}_{i-1} + \ddot{u}_i)}{8} \Delta Z_{i-1} \quad (5.9)$$

In equations 5.4 and 5.9, i = 2,3... and i and i-1/2 refer to levels z_i (of the i^{th} accelerometer) and $(z_{i-1} + z_i)/2$ (halfway between accelerometers i and (i-1)) respectively, $\tau_i(t) = \tau(z_i, t)$, $\ddot{u}_i = \ddot{u}(z_i, t)$, Δz_i is spacing interval between accelerometers.

These stress estimates are second order accurate. And the corresponding second-order accurate shear strain between the levels 1 and 2 levels may be expressed as,

$$\gamma_{1-\frac{1}{2}}(t) = \frac{(u_2 - u_1)}{\Delta Z_1} \tag{5.10}$$

From the above equation the strain at any level $(z_{i-1} + z_i)/2$ is expressed as,

$$\gamma_{i-1/2}(t) = \frac{(u_i - u_{i-1})}{\Delta z_{i-1}} \tag{5.11}$$

Similarly strain at level 2 may be expressed as,

$$\gamma_2(t) = \left(\frac{u_2 - u_1}{\Delta Z_1} + \frac{u_3 - u_2}{\Delta Z_2}\right)\frac{1}{\Delta Z_1 + \Delta Z_2} \tag{5.12a}$$

$$= \left((u_3 - u_2)\frac{\Delta Z_1}{\Delta Z_2} + (u_2 - u_1)\frac{\Delta Z_2}{\Delta Z_1}\right)\frac{1}{\Delta Z_1 + \Delta Z_2} \tag{5.12b}$$

From the above equation the strain at any level z_i is expressed as,

$$\gamma_i(t) = \frac{1}{\Delta Z_{i-1} + \Delta Z_i}\left((u_{i+1} - u_i)\frac{\Delta Z_{i-1}}{\Delta Z_i} + (u_i - u_{i-1})\frac{\Delta Z_i}{\Delta Z_{i-1}}\right) \tag{5.13}$$

In equations 5.11 and 5.13, i = 2,3... and $u_1 = u(z_1, t)$ is absolute displacement evaluated through double integration of the recorded acceleration history $\ddot{u}(z_i, t)$.

5.3 Dynamic Site Properties

The evaluated shear stress strain histories at Chiba were used to estimate soil stiffness and material damping using the model,

$$\tau = G\gamma + \eta\dot{\gamma} \tag{5.14}$$

in which G and η are shear modulus and viscous damping.

These stiffness and damping parameters during a given time window (t_i, t_f) may be evaluated using a least squares fit to minimize the difference between shear stresses estimated from acceleration histories (Equations 5.15 and 5.16), and those predicted by linear model of Equation 5.14.

Thus, least squares minimization dictates:

$$G(t_i,t_f) = \frac{\int_{t_i}^{t_f}\tau\gamma\,dt\int_{t_i}^{t_f}\dot{\gamma}\dot{\gamma}\,dt - \int_{t_i}^{t_f}\tau\dot{\gamma}\,dt\int_{t_i}^{t_f}\gamma\dot{\gamma}\,dt}{\int_{t_i}^{t_f}\gamma\gamma\,dt\int_{t_i}^{t_f}\dot{\gamma}\dot{\gamma}\,dt - \left(\int_{t_i}^{t_f}\gamma\dot{\gamma}\,dt\right)^2} \tag{5.15}$$

$$\eta(t_i,t_f) = \frac{\int_{t_i}^{t_f}\tau\gamma\,dt\int_{t_i}^{t_f}\gamma\dot{\gamma}\,dt - \int_{t_i}^{t_f}\tau\dot{\gamma}\,dt\int_{t_i}^{t_f}\gamma\gamma\,dt}{\int_{t_i}^{t_f}\gamma\gamma\,dt\int_{t_i}^{t_f}\dot{\gamma}\dot{\gamma}\,dt - \left(\int_{t_i}^{t_f}\gamma\dot{\gamma}\,dt\right)^2} \tag{5.16}$$

where τ is stress history, γ is strain history and $\dot{\gamma}$ is strain rate history.

5.4 Results and Discussions

Site shear stress-strain responses were evaluated at four locations within the instrumented zone. Shear stress-strain hysterisis loops were shown in Figure 5.14 – 5.19. Overall, the employed linear model is seen to capture the essential features of recorded response. Calculated shear wave velocities and damping ratio values at different depths for the 25 events are shown in Table 5.1. Shear modulus & damping values were calculated using the Equations 5.15 and 5.16 and shear wave velocity was calculated based on the shear modulus mass density.

Displacement histories were calculated by double integrating the filtered acceleration histories and used to estimate the strain histories. These strain histories were calculated using the Equations 5.4 and 5.9 at halfway between accelerometers at 2.5, 7.5, 15.0 & 30.0 m depths in EW & NS directions and shown in Figure 5.2 & 5.9. These figures clearly show that shear stress was increasing with depth and the shear strain was decreasing with depth. Ground strain at surface (0 – 5 m layer) is significantly large increased compared to other layers, clearly indicating the surface soil amplification during the earthquake loading.

The optimized stresses calculated by assumed linear model with damping (Equation 5.14) are compared with the shear stress calculated using the one-dimensional shear beam model (Equations 5.4 and 5.9). The optimized shear stresses are in good agreement with the recorded shear stresses. These figures also show the variation in the stiffness of the material at various depths below the ground surface. The surface layer of loam is subjected to more ground strain compared to silty-clay and sand at other depths.

The calculated shear wave velocities are compared with the geophysical tests as shown in Figure 5.20. Shear wave velocities are found to be slightly lower than those obtained by geophysical method due to reduction in soil stiffness and mild non-linear behavior. Damping value for the top layer was also higher compared to other depths (Table 5.1). This phenomenon is supported by the Figures. 5.2 – 5.9. From these figures, It can be observed that shear stress was lowest at the top layer and increased with depth where as the shear strain was maximum at the surface and decreased with depth.

5.6 Summary

- The slight difference in the estimated shear wave velocities & geophysical measurements indicate that geophysical measurements induced much lower strains compared to earthquakes used in the analysis.

- Shear stress levels had increased with depth but the shear strain decreased with depth.

- Amplification in the top layer had produced high excitation levels and generated high strains due to loss of stiffness, which is supported by lower bound values estimated by the stress-strain imaging.

- The ranges of values of shear wave velocity profile estimated using this method were in good agreement with geophysical measurements except for top 5 m layer. It further corroborates that the behavior of soil at Chiba during the earthquake analyses was mildly nonlinear even during the strongest ground motion.

Table 5.1: Optimized Shear Wave Velocity and Damping Ratio using Stress-Strain Imaging

S no	Event (IEQK)	PGA (cm/sec^2)		Shear wave velocity V_s (m/sec) and Damping ratio η/G (%)															
				2.5 m				7.5 m				15.0 m				30.0 m			
		EW	NS	V_s (m/sec)		η/G (%)		V_s (m/sec)		η/G (%)		V_s (m/sec)		η/G (%)		V_s (m/sec)		η/G (%)	
				EW	NS	EW	NS	EW	NS	EW	NS	EW	NS	EW	NS	EW	NS	EW	NS
1	8307	47 4	55 7	80 5	98.3	2 08	2 16	98 3	163 8	4 86	2 28	230 6	300 2	2 22	2 32	404 4	393 9	2 13	2 25
2	8401	25 5	24 2	93 9	100 0	1.11	1.15	175.5	182 3	1.64	1 39	269 9	304 5	0 95	1 23	397 8	395 0	1 24	1 09
3	8406	22.3	28 0	81.4	79 9	0 45	0 78	83 9	130 0	3 54	1 72	244 3	251 6	0 41	1 72	401 3	395 9	1 25	0 6
4	8416	13.8	14.5	67 3	68 4	1 41	1 43	95 4	85 4	2 19	1 57	215 9	198 0	0 75	1 67	388.5	333 8	0.87	1 06
5	8420	22 1	24.1	95.8	105.7	1.23	1.13	187 3	189 1	1.31	1 49	292.8	302 5	0 88	1 13	400 1	394 4	0 91	1 36
6	8510	27.4	29.6	106 8	106 6	1 11	1 06	213 2	207 4	1.31	1.11	309 4	311 7	0 82	1 09	402 6	384 2	1.31	0 91
7	8519	59.2	82.2	94 6	111.1	1 10	1 08	231 9	213 3	1.34	1 20	299 2	320.0	1.04	1.10	398 7	398.9	0.92	0 75
8	8525	75.7	71 6	105 1	110 0	1.06	1 07	220 6	214 0	1 05	1.15	309 9	321.3	0 61	1 22	399 7	389 2	0 67	1 30
9	8601	15.4	14 3	83 2	73.8	1 31	1 42	137 7	107 4	1 79	1.55	270 8	211.5	1.16	1.75	391 2	361 5	1.18	1 31
10	8602	54 0	40 7	96.7	96 7	1 10	1.10	179 1	187 5	1 33	1 15	282 0	290.3	0.96	1 25	386 0	382 5	1.09	1 01
11	8706	11.3	14.0	73 8	73 4	1 34	1 08	120 8	144 2	1 27	1.16	211 3	223 4	1 44	1 32	371 5	345.7	0 98	1 33
12	8717	20.7	33.5	99 6	98 9	1 10	1.13	190 8	183 9	1.19	1 27	276 9	303 3	0.84	1.00	395 6	399 6	0 94	1 03
13	8722	213.6	327.1	105.0	111 3	1.18	1.09	230 1	210.5	1.24	1 23	284.3	300.1	1.51	1.22	367.3	381.9	1.13	1 3
14	8723	17.2	21.2	94.5	104 1	1.29	0 991	177.7	181 4	1.49	1.19	235.0	263.6	1 29	1 37	361.1	364 3	0.71	1 67
15	8725	23.8	13.8	108.9	98 2	1 08	1 41	192 8	182 2	1.24	1 83	264 6	250.5	0 83	1 02	388 9	358 4	0 89	0 71
16	8726	22.5	30.4	103 9	106 1	1.09	1 11	118 5	182.2	2 5	1 47	184 6	272 3	1.6	1 11	331 8	334 6	0.56	1 38
17	8802	40.6	40.8	106 4	102 5	1 28	1 26	208 1	212 8	1 49	1.37	287 0	315.0	0 66	0 82	413 4	384.3	0.56	1 04
18	8806	54 9	97 8	113 3	114 2	1.00	1 05	233 6	224 5	1 22	1 19	291 8	316 3	1.15	1 12	399.7	389.7	0.92	1 08
19	8808	19 0	26 2	80 8	62.2	1.70	2 12	138.1	117 6	2 67	2.49	184 2	165.7	2 58	2 87	338 2	321 3	0 49	0 96
20	8816	48.4	59.8	107 0	114.5	0 97	1 01	230 7	219 0	0.93	1.15	279 5	304 4	0 64	1 22	398 1	396 7	1.16	1 20
21	8823	46 4	35 2	103 1	105 9	1 12	1.06	220 1	211 5	1 18	1 28	296 9	312 9	1 45	1 26	411 5	399 0	1.18	1 28
22	8901	55.7	49.1	101 2	114 0	1 09	1 01	226 2	215 5	1 09	1.01	263.1	292 7	1.16	0 97	397 5	398 2	1.22	1 22
23	8903	27.5	28.9	101 5	110 7	1 05	1.07	215 4	208 1	1 09	1.15	253 5	291 3	1 15	1 4	396 5	390.2	1.24	1 37
24	8904	41 0	21 9	108 5	100 2	1 05	1 16	211 9	196 4	1 15	1 47	290 6	314.7	0 86	1 2	389 5	369 7	0.72	0 84

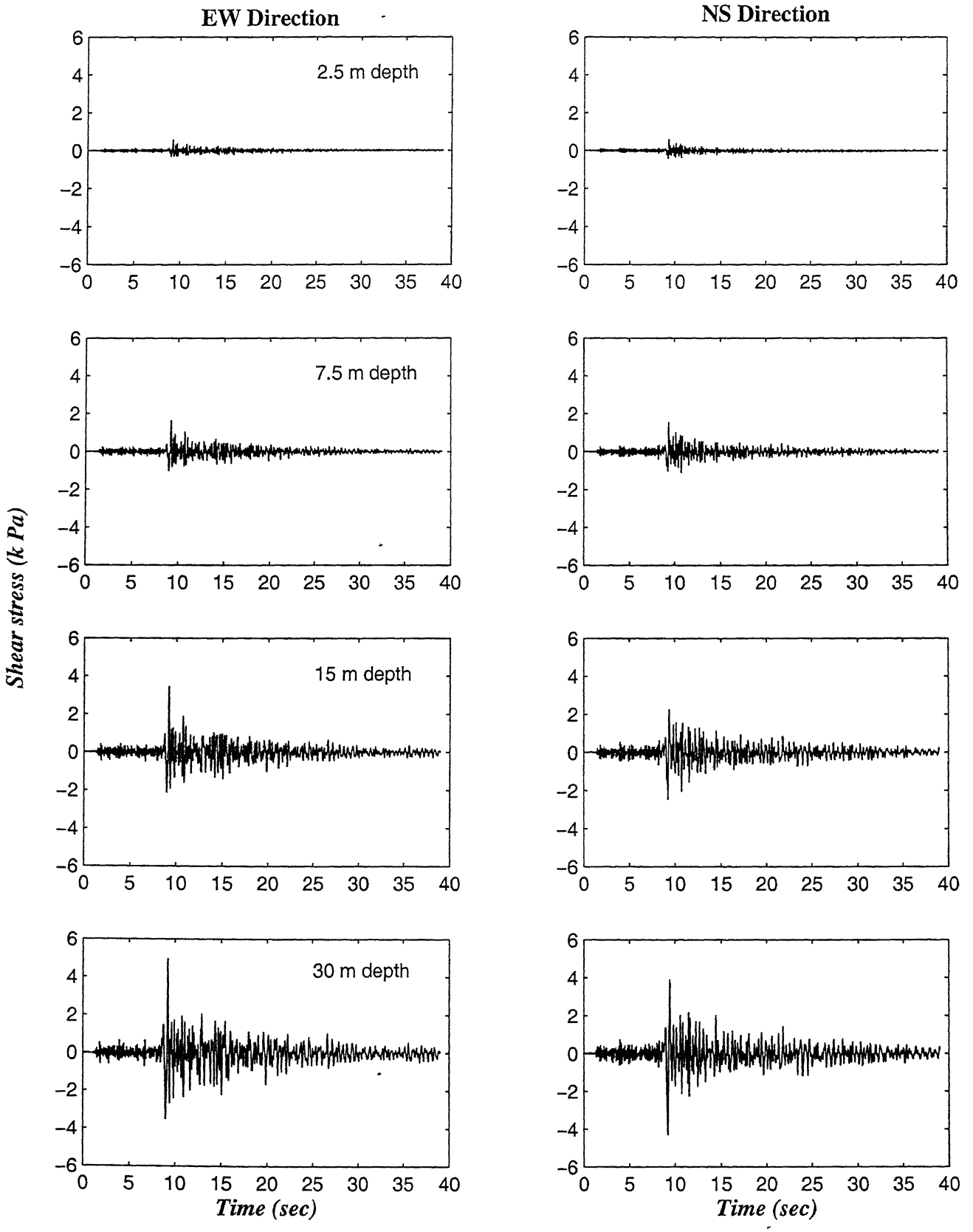

Figure 5.2: Computed stress histories at borehole C0 during the earthquake 8510

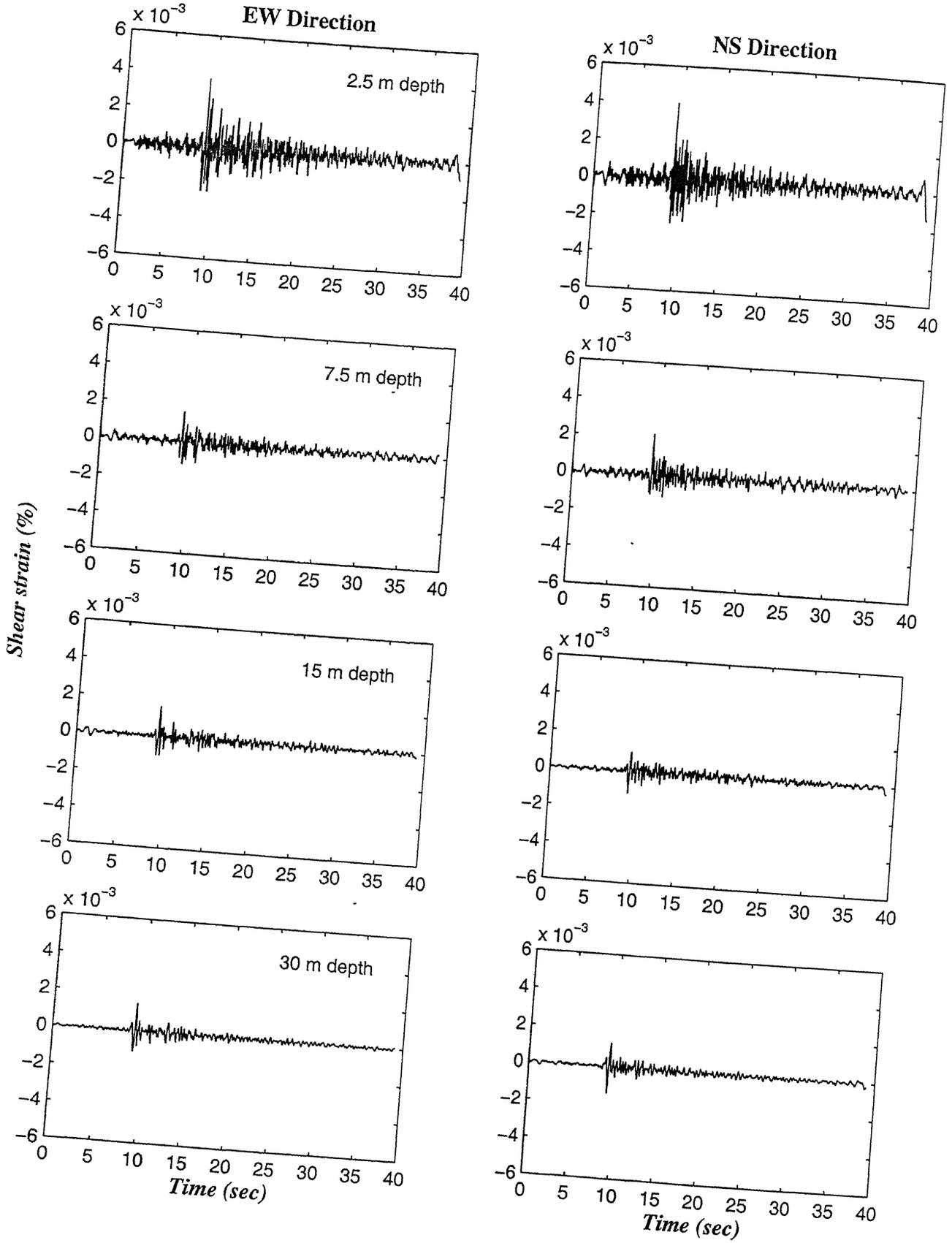

Figure 5.3: Computed strain histories at borehole C0 during the earthquake 8510

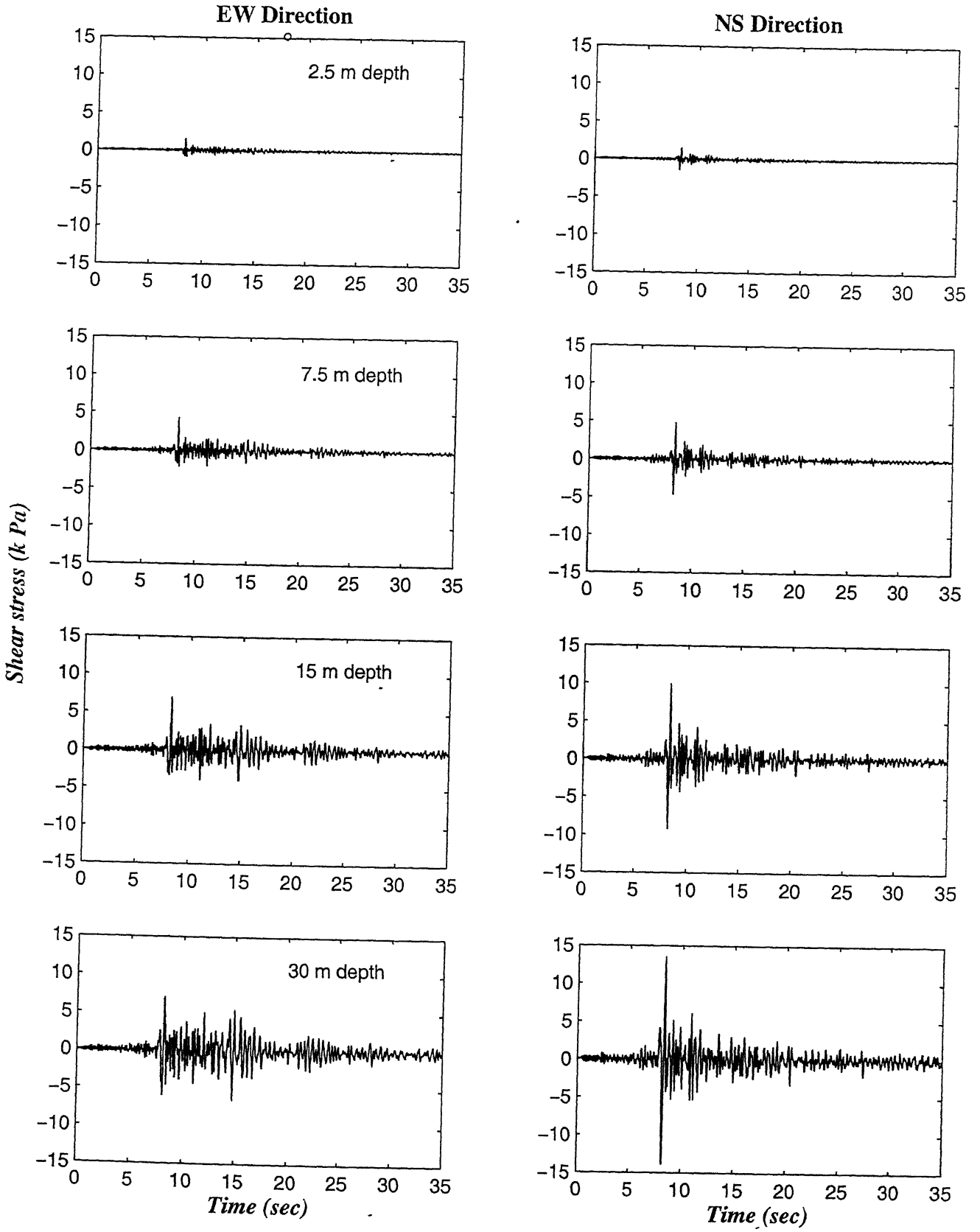

Figure 5.4: Computed stress histories at borehole C0 during the earthquake 8525

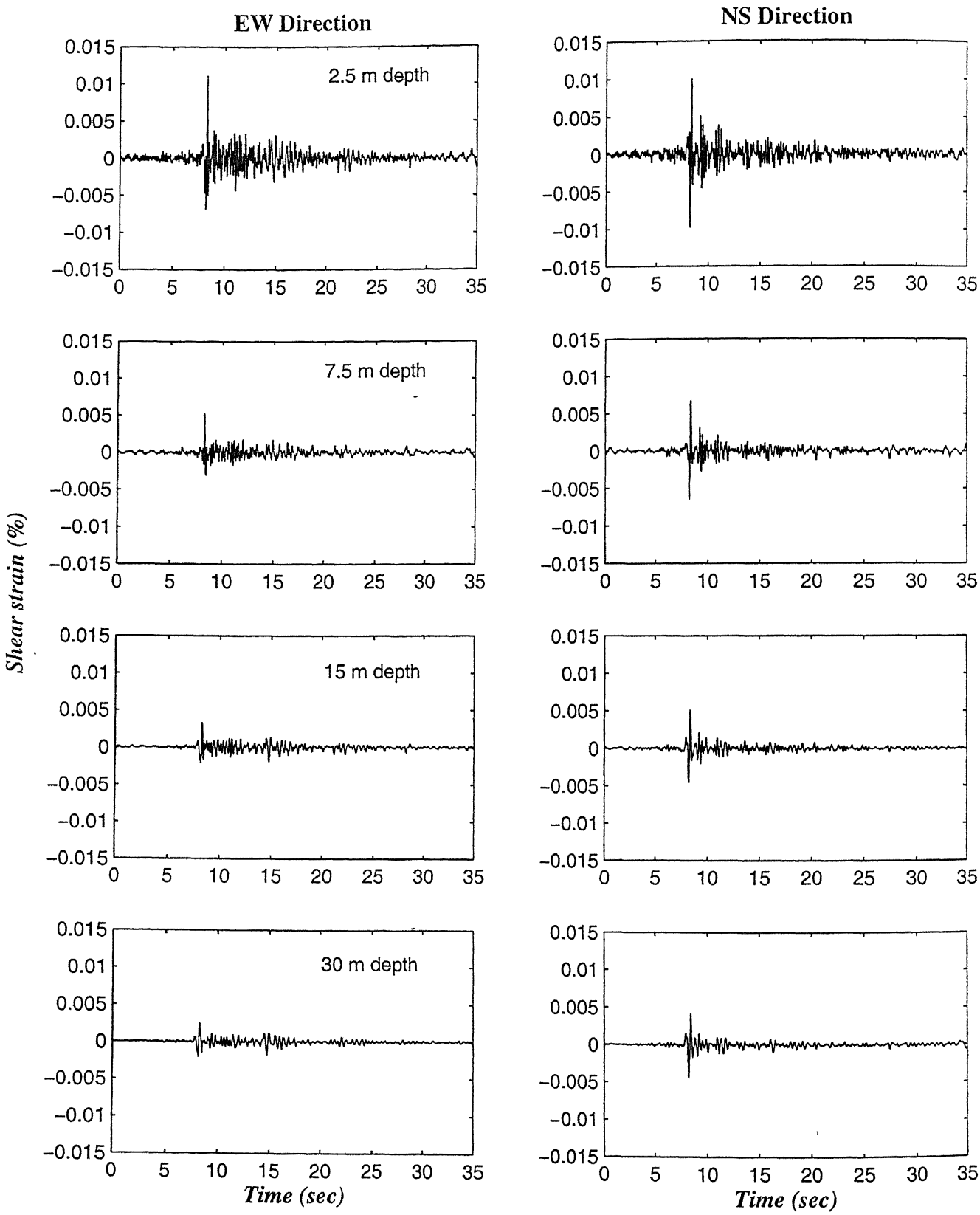

Figure 5.5: Computed strain histories at borehole C0 during the earthquake 8525

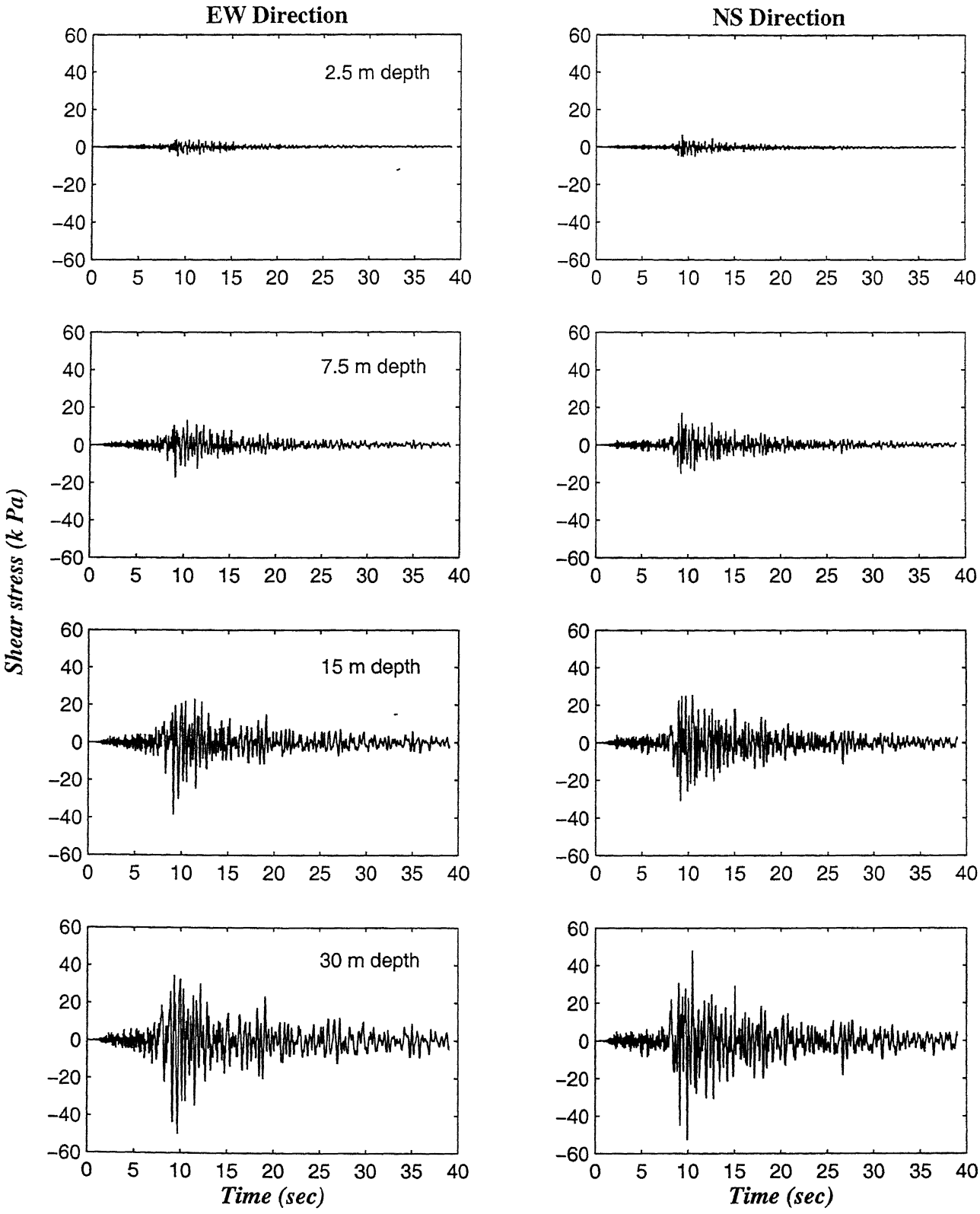

Figure 5.6: Computed stress histories at borehole C0 during the earthquake 8722

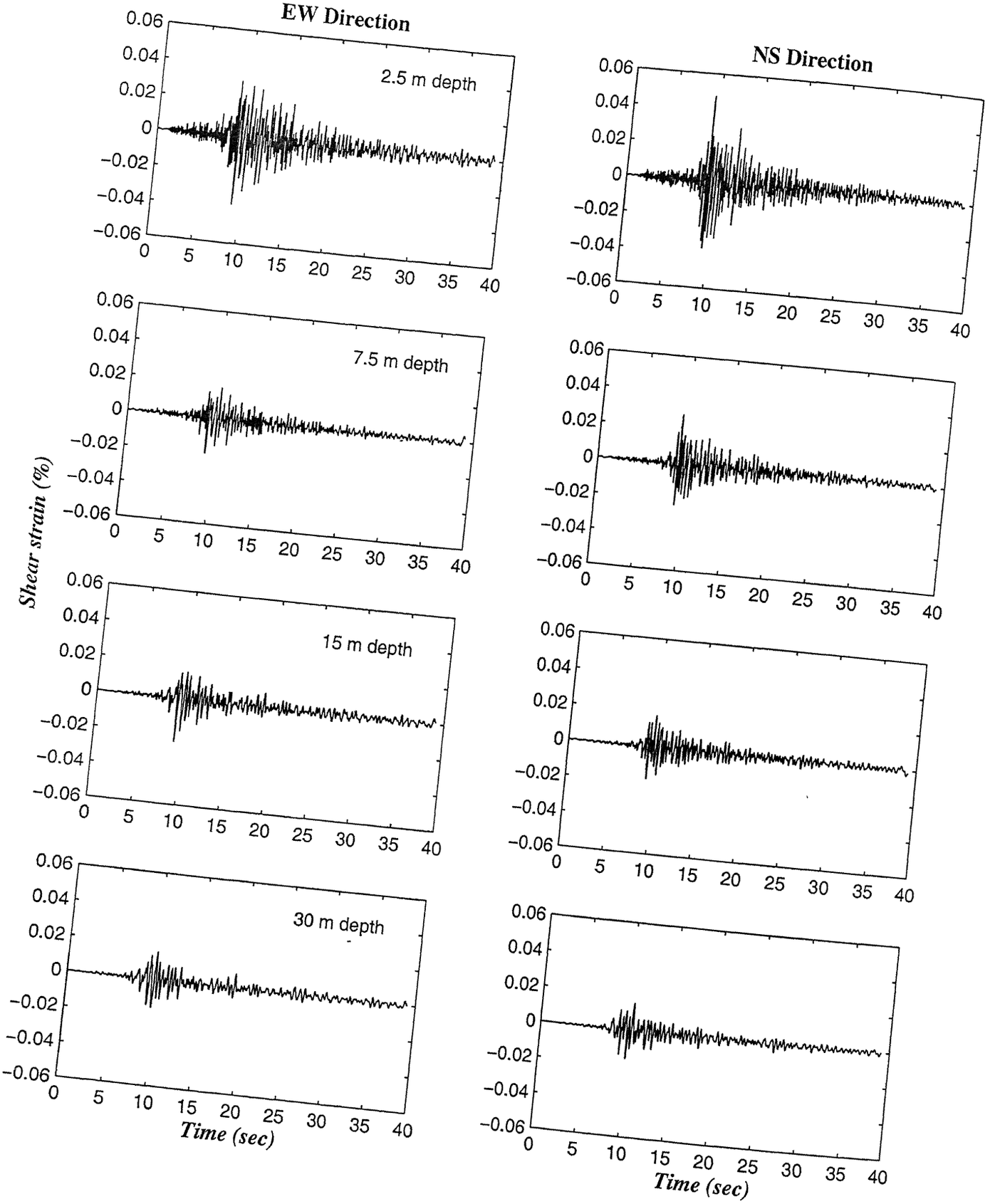

Figure 5.7: **Computed strain histories at borehole C0 during the earthquake 8722**

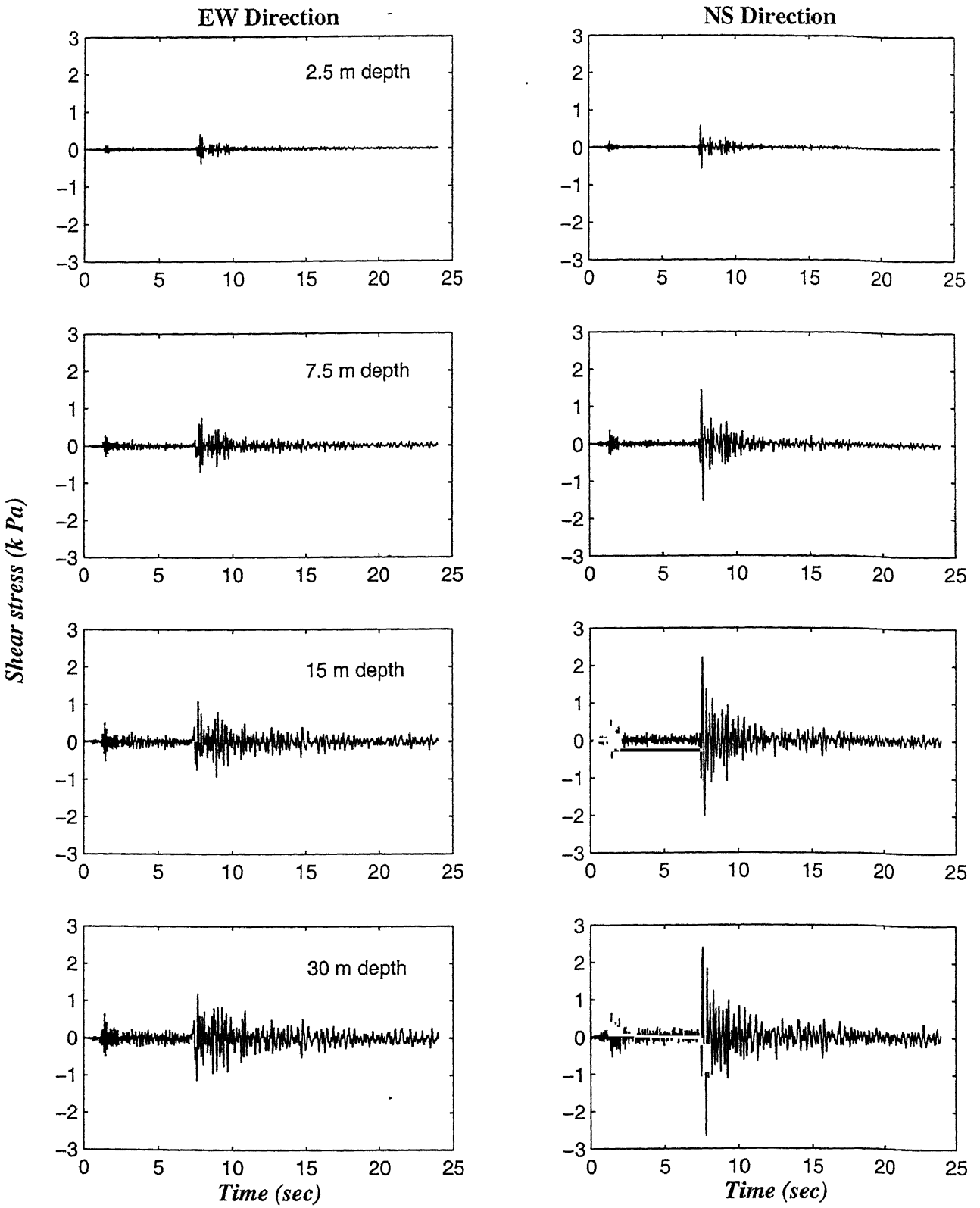

Figure 5.8: Computed stress histories at borehole C0 during the earthquake 8726

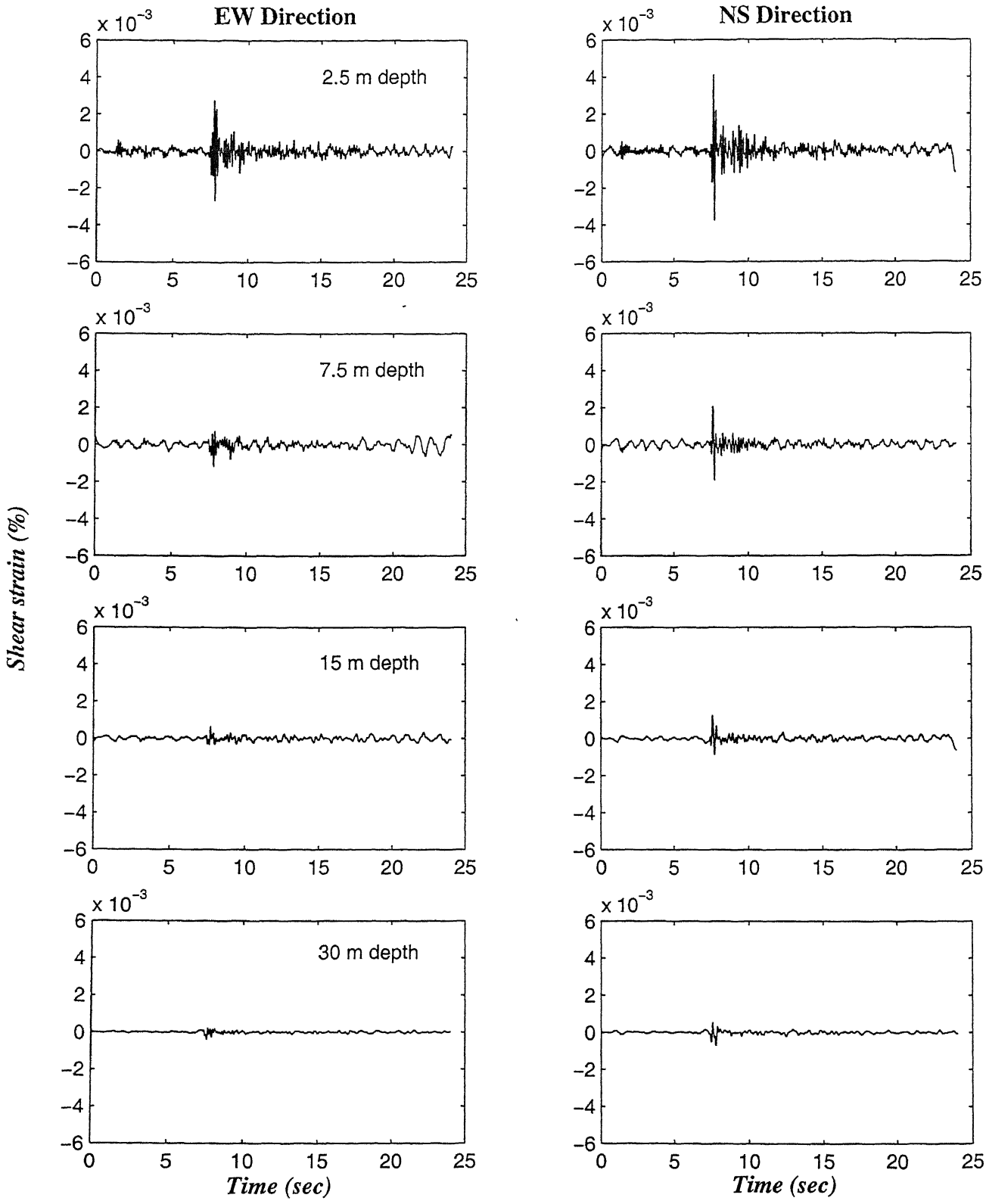

Figure 5.9: Computed strain histories at borehole C0 during the earthquake 8726

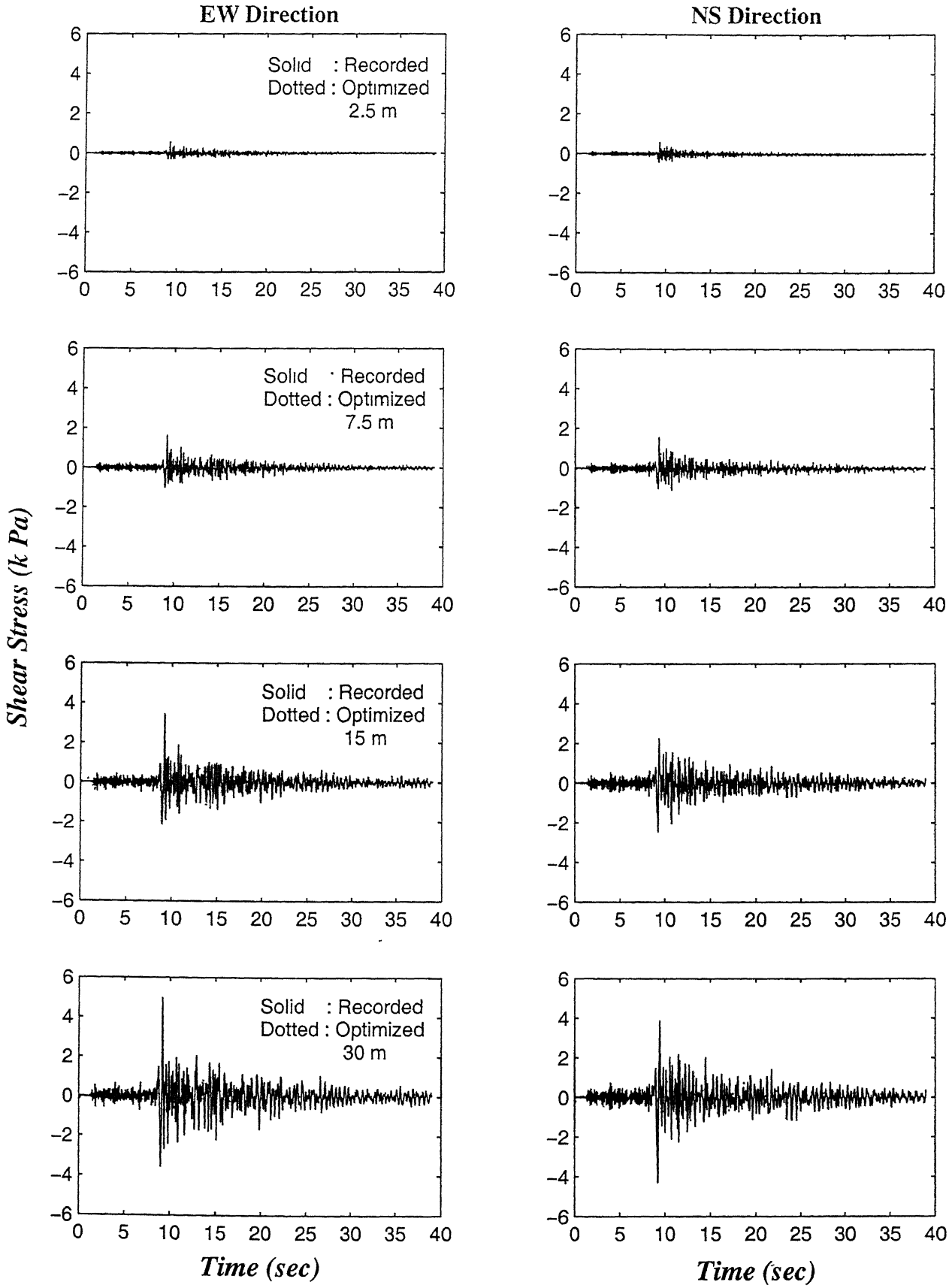

Figure 5.10: Evaluated and optimal stress histories at borehole C0 during the earthquake 8510

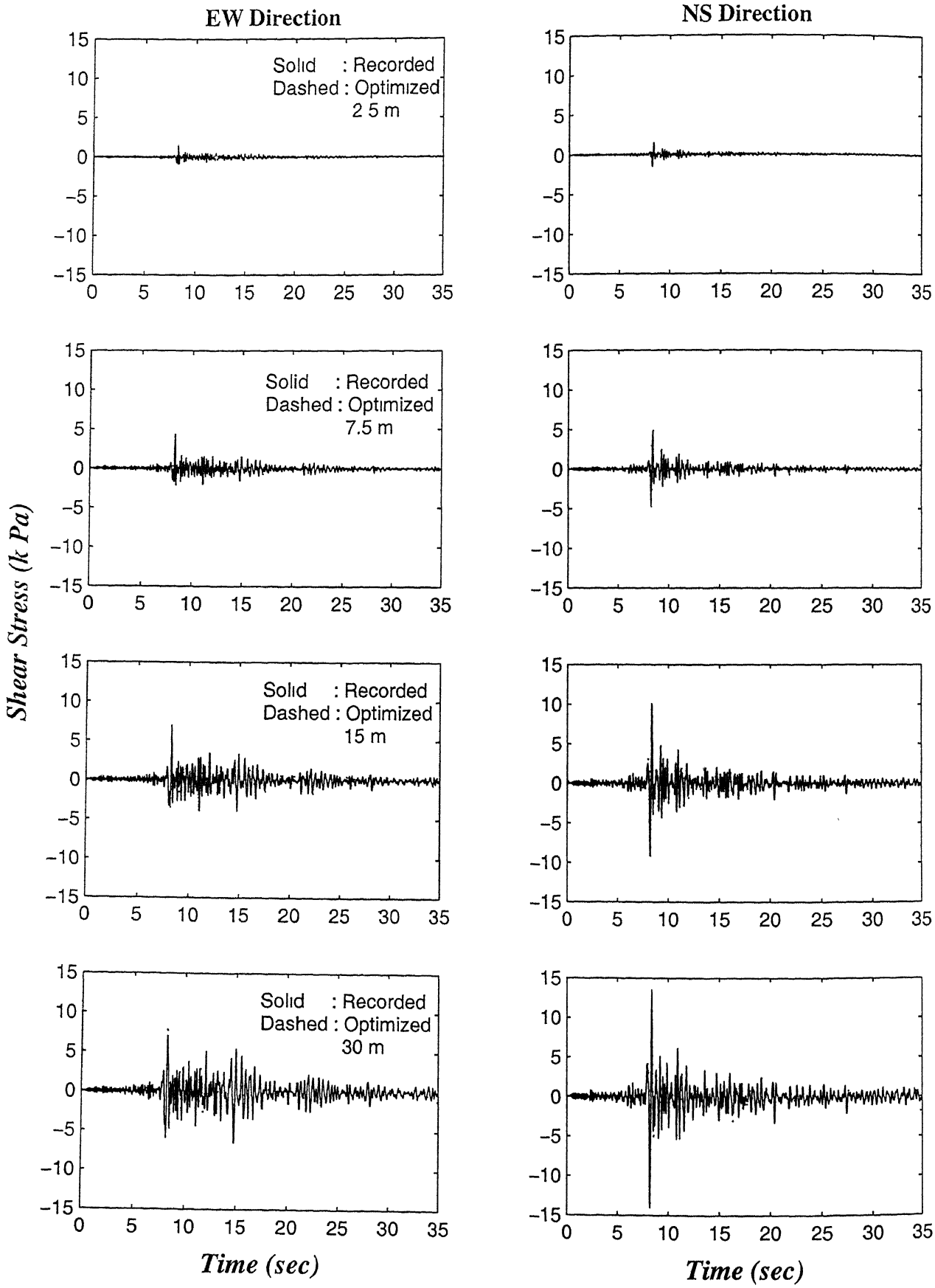

Figure 5.11: Evaluated and optimal stress histories at borehole C0 during the earthquake 8525

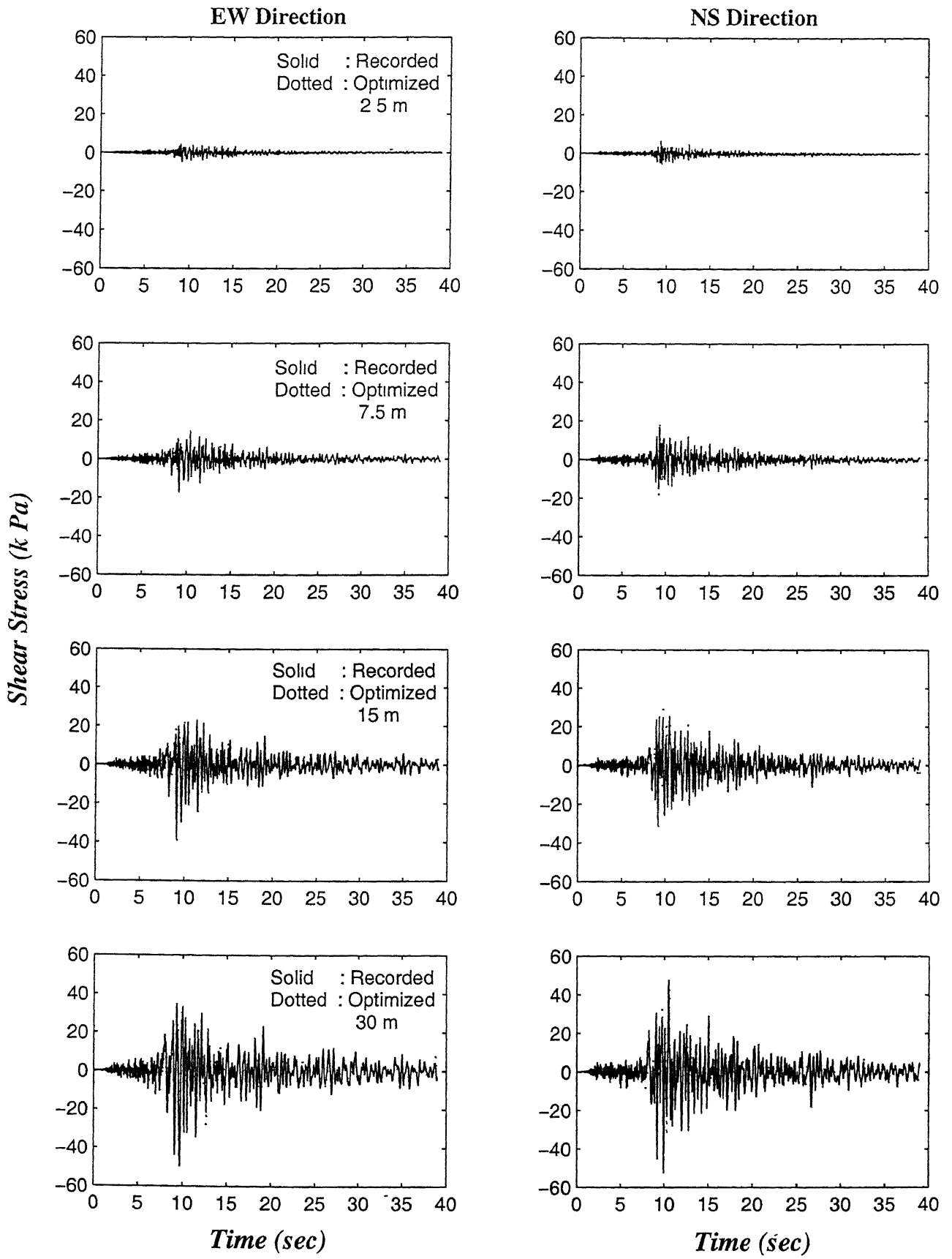

Figure 5.12: Evaluated and optimal stress histories at borehole C0 during the earthquake 8722

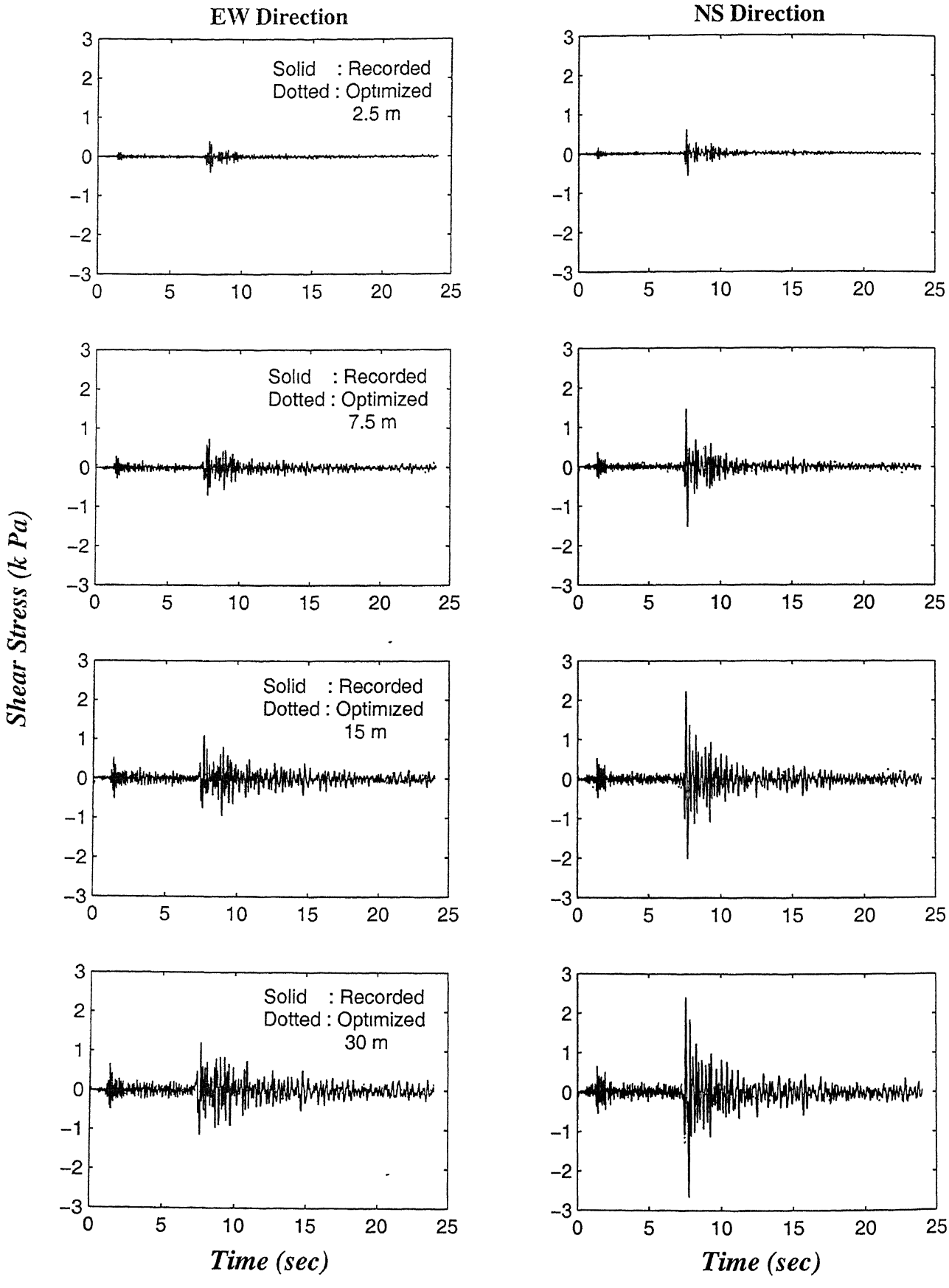

Figure 5.13: Evaluated and optimal stress histories at borehole C0 during the earthquake 8726

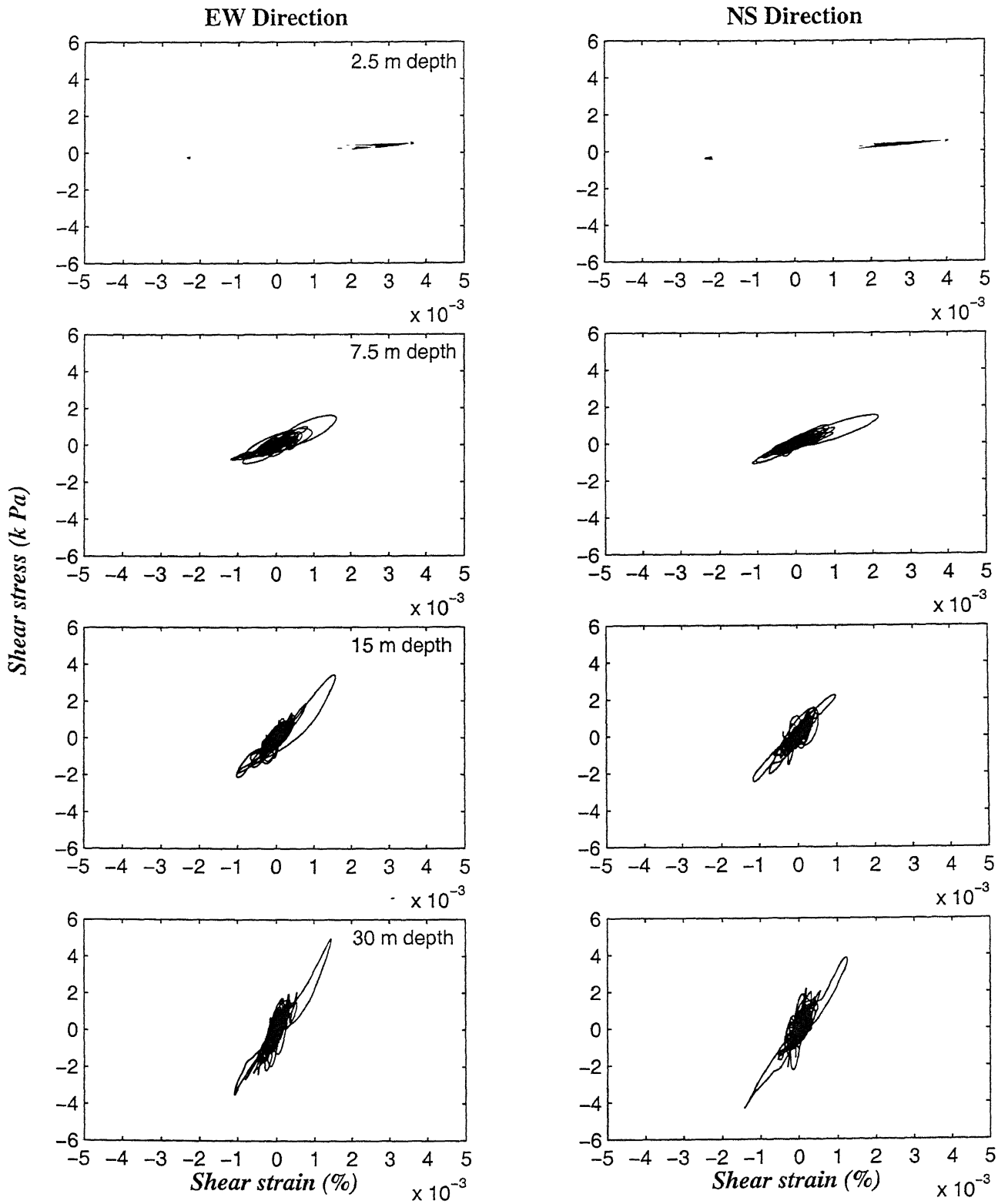

Figure 5.14: Computed shear stress-strain histories at borehole C0 during the earthquake 8510

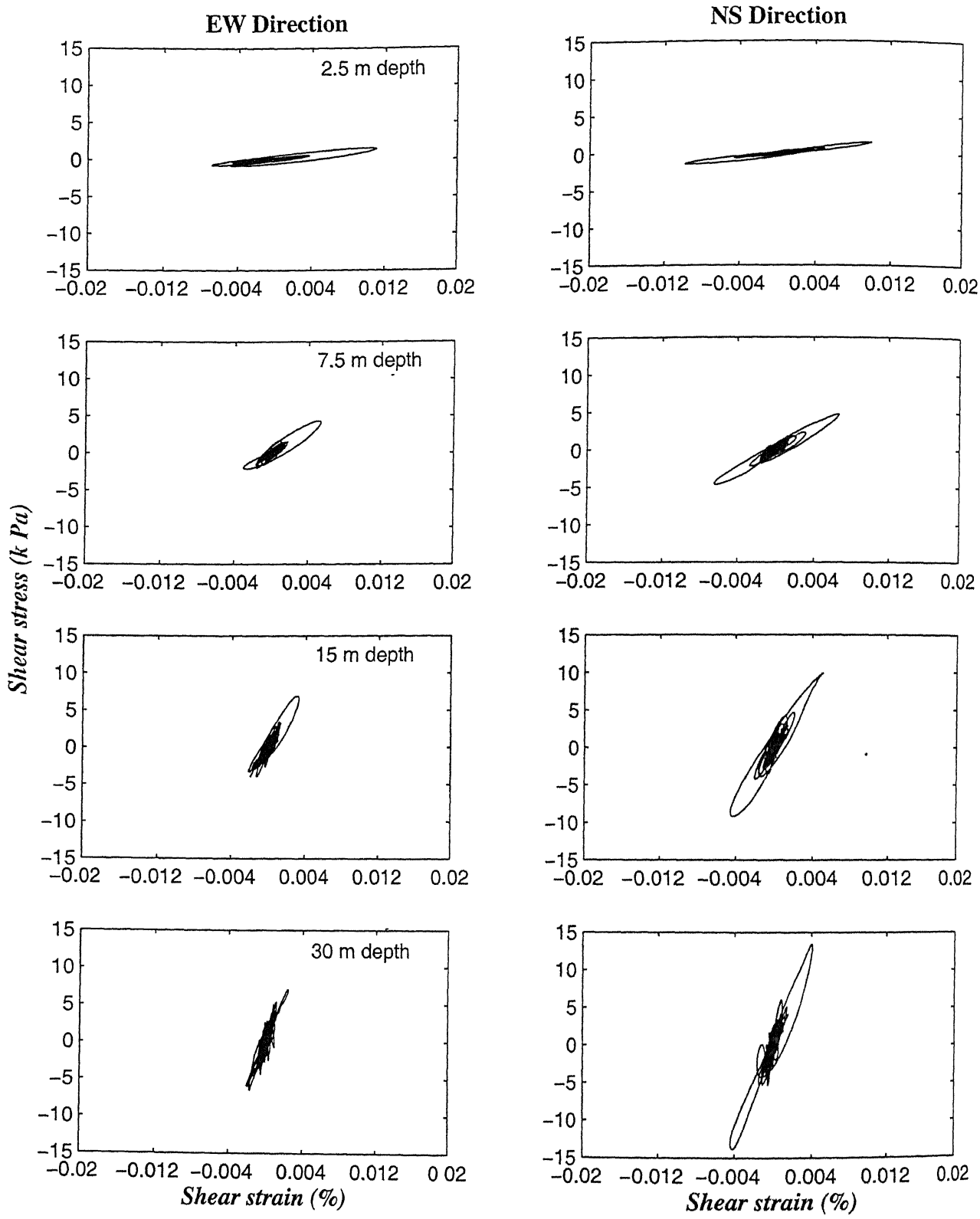

Figure 5.15: Computed shear stress-strain histories at borehole C0 during the earthquake 8525

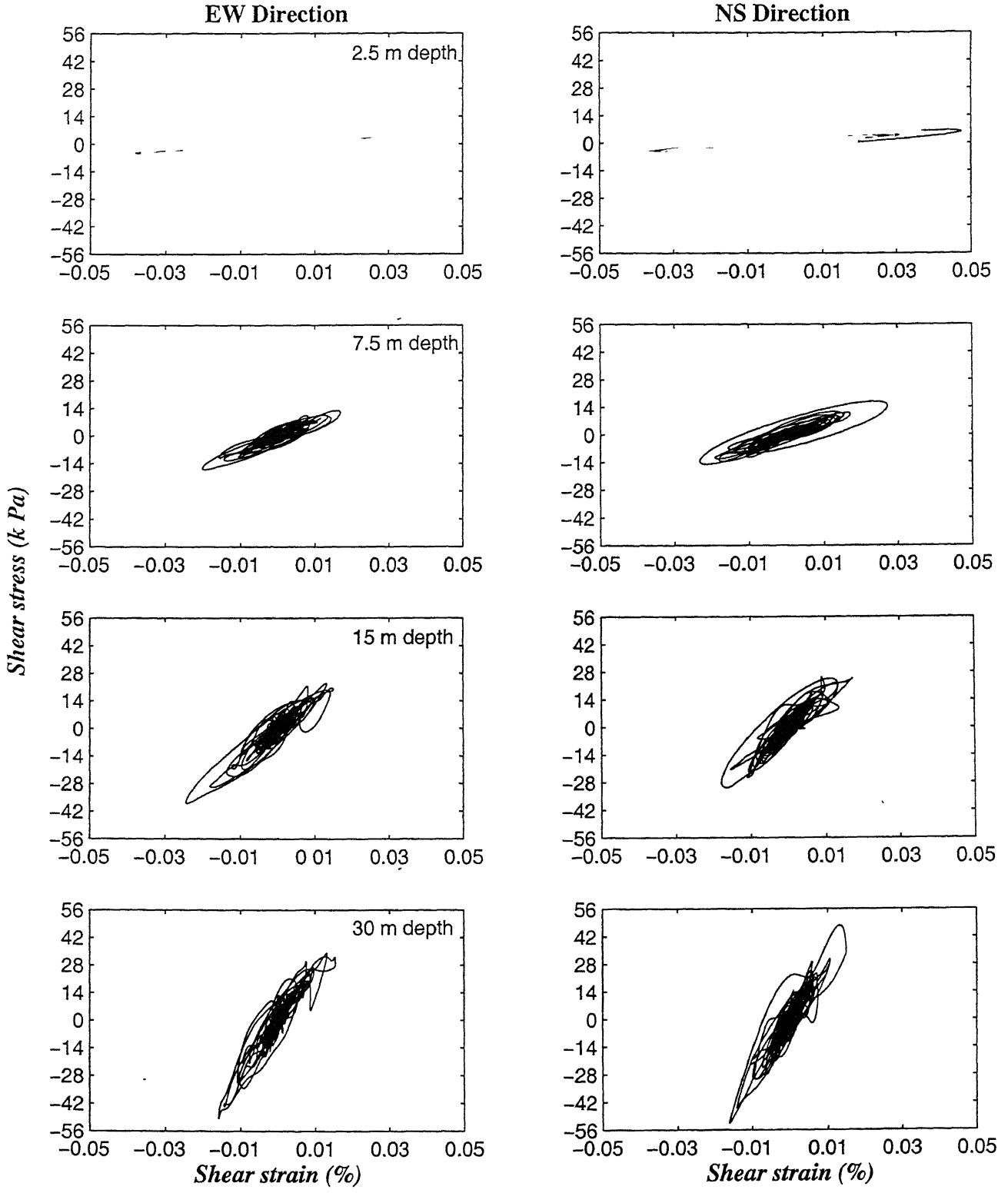

Figure 5.16: Computed shear stress-strain histories at borehole C0 during the earthquake 8722

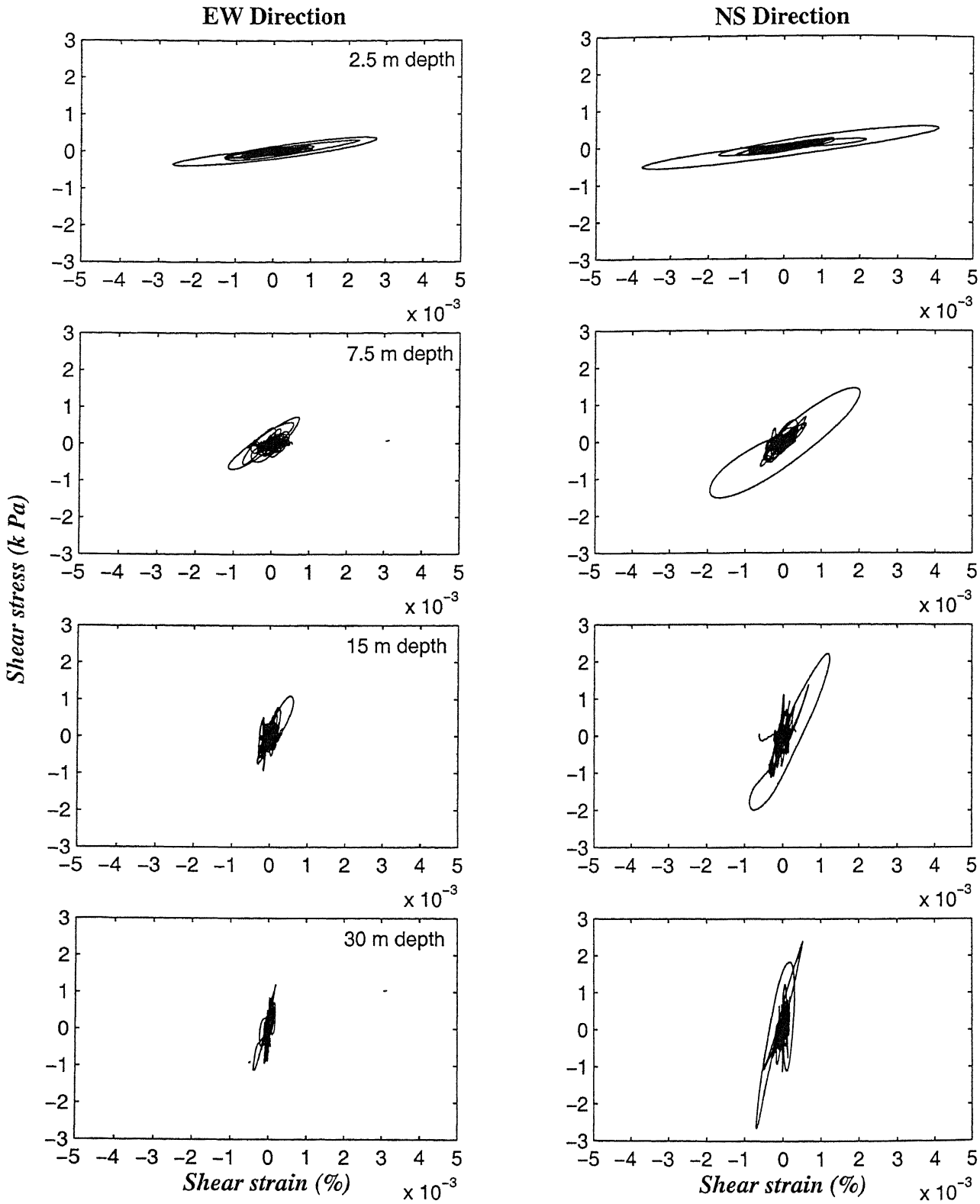

Figure 5.17: Computed shear stress-strain histories at borehole C0 during the earthquake 8726

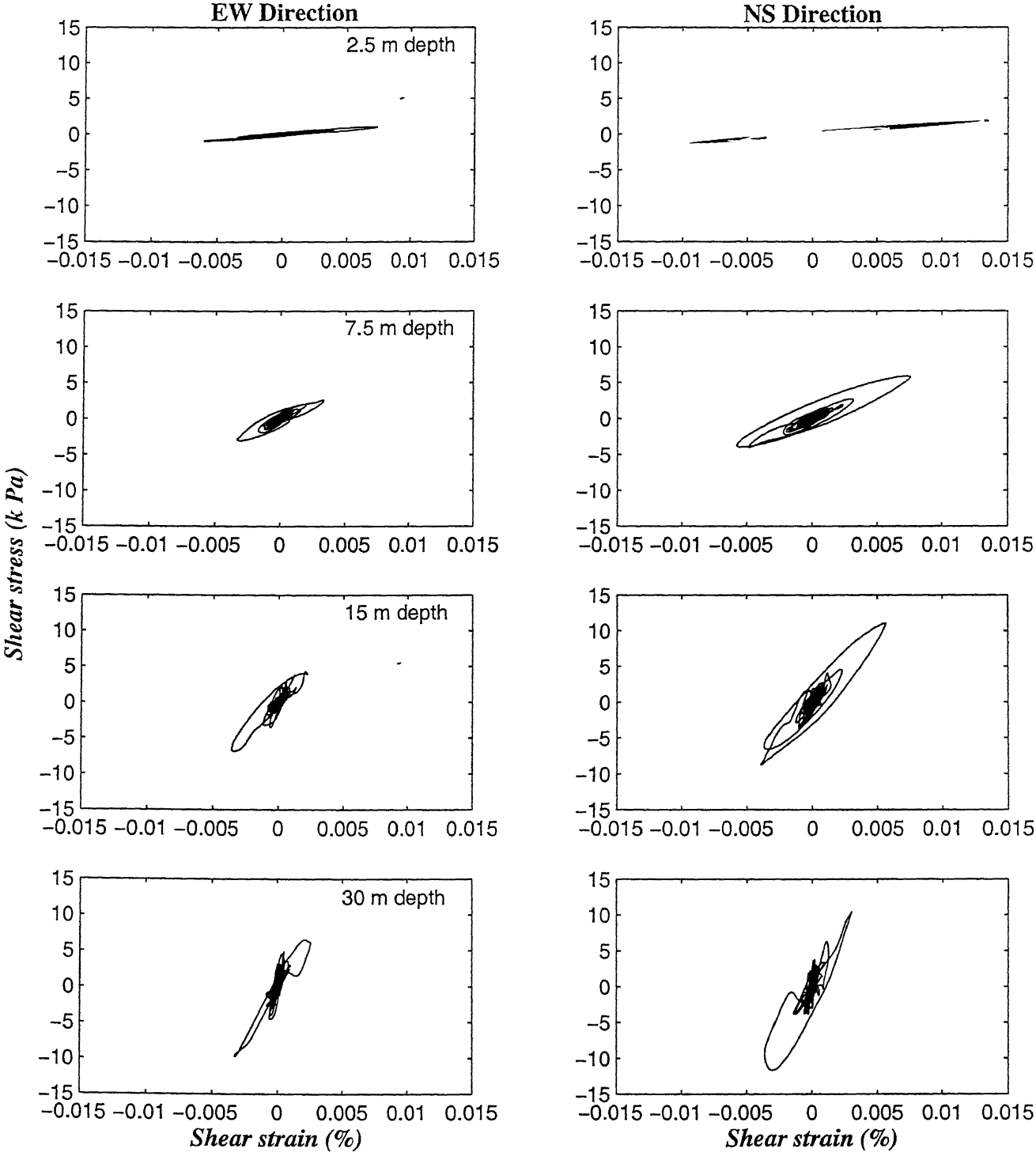

Figure 5.18: Computed shear stress-strain histories at borehole C0 during the earthquake 8806

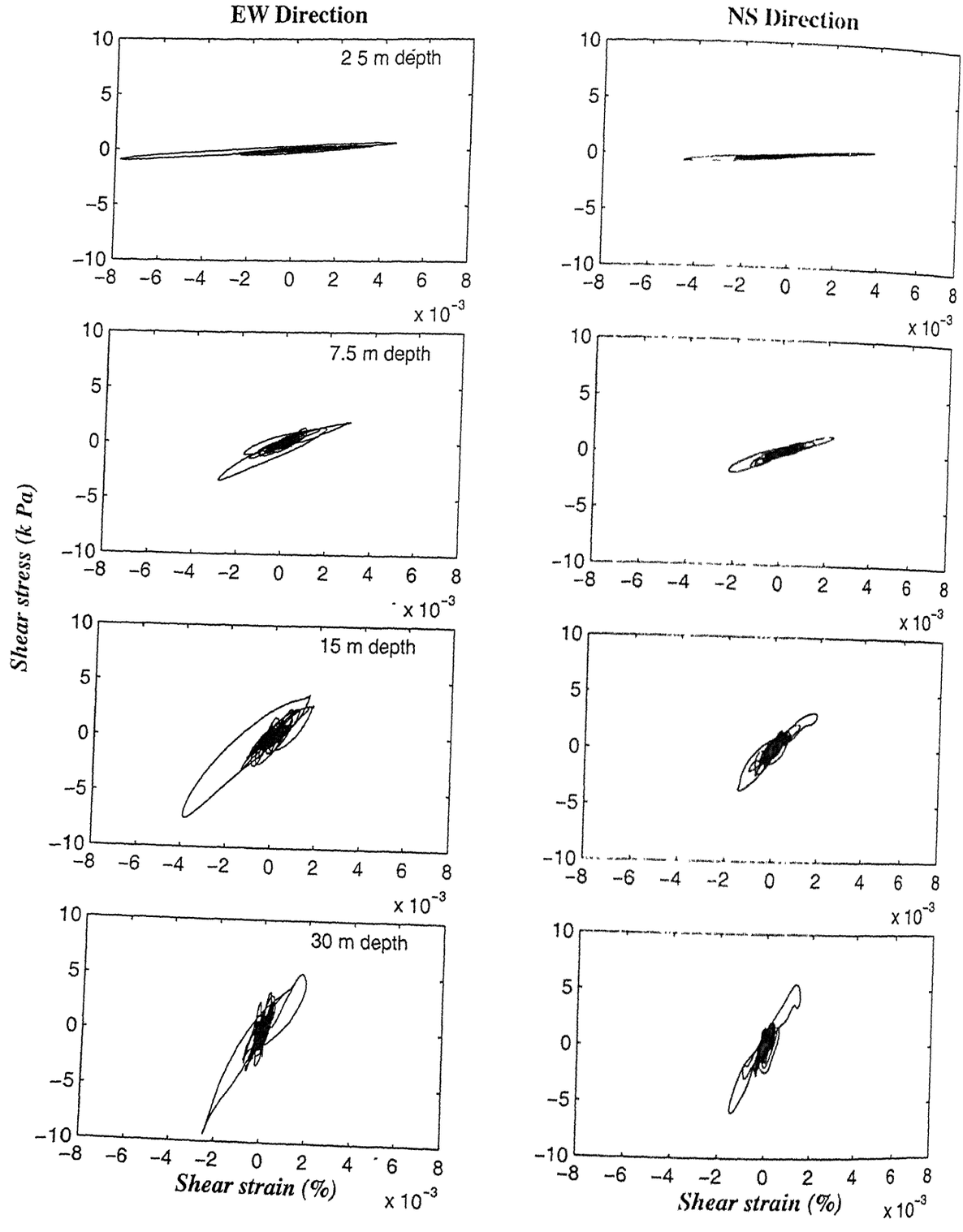

Figure 5.19: Computed shear stress-strain histories at borehole C0 during the earthquake 8823

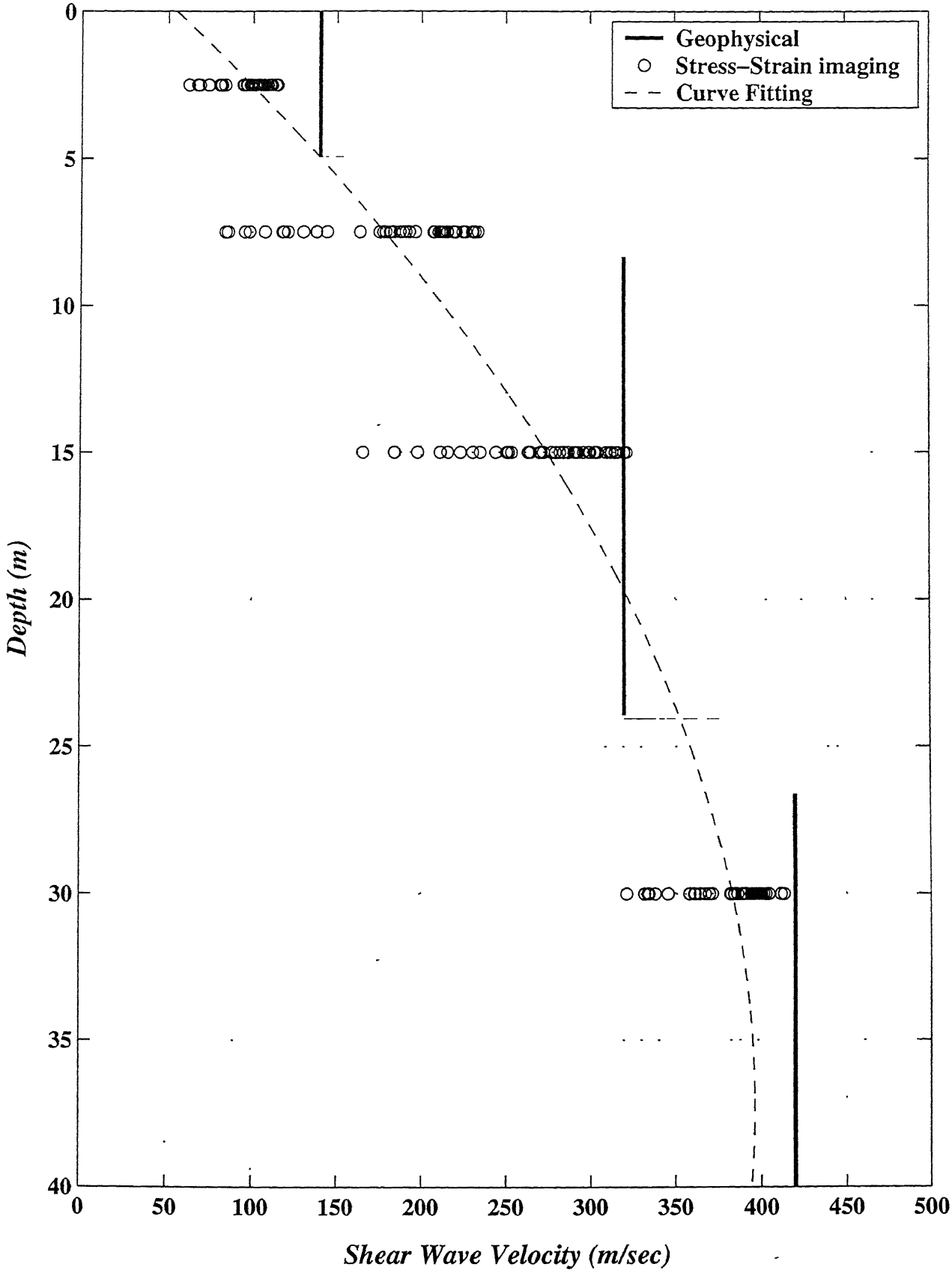

Figure 5.20: Estimated shear wave velocity using stress-strain imaging

Chapter 6
TWO-LAYER SOLUTION

6.1 Introduction

Strong ground motions at certain frequencies are largely affected by the amplification characteristics (shear wave profile) of subsurface layers. Amplification characteristics can provide information for the prediction of ground motion for a specific site and for the seismic safety assessment of existing structures.

In the present study, spectral ratio technique was used to study the response of the sub surface soil layers at borehole C0 of Chiba array. Two-layer solution was used to estimate the fundamental frequencies of soil layers and shear wave velocities between consecutive borehole stations.

Some other studies where spectral ratio techniques were employed to study amplification characteristics are:

- Chang et al. [9] in ground response analysis at Lotung downhole array.
- Chang et al. [10] in back calculating equivalent shear moduli (and their variations with shearing strains) from the resonant frequency of the Fourier spectral ratio at the Lotung site.
- Katayama et al. [28] in studying the ground amplification and calculation of natural frequencies.
- Wen et al. [48] studied the soil nonlinear seismic response by comparing the spectral ratios of surface to downhole horizontal accelerations on weak and strong motion based on the array records of SMART 1and SMART 2 in Taiwan.
- Huey-chu et al. [21] to investigate the site amplification of four level Dahan downhole recordings.

6.2 Methodology

The transfer function between the acceleration histories recorded at two depths can be calculated to investigate the characteristics of ground vibrations and to identify the modal frequencies of vibration of the soil layers. The transfer function was calculated between surface and other depths.

If a_i and a_j are surface and the depth at which ground motion is recorded (Figure 6.1), then Fourier spectral ratio is given as:

$$H_{a_i a_j}(f) = \frac{H_{a_i}(f)}{H_{a_j}(f)} \tag{6.1}$$

where $H_{a_i}(f)$ and $H_{aj}(f)$ are the Fourier transforms of the ground motion a_i and a_j

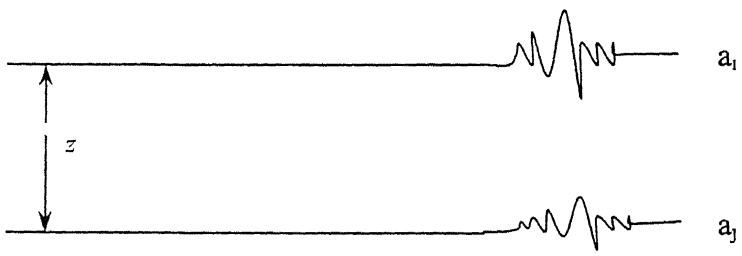

Figure 6.1: Recorded signals at z m apart for the calculation of transfer function

$H_{a_i a_i}(f)$ represents the transfer function of frequency f and $\left|(H_{a_i a_j}(f)\right|$ defines the amplitude spectrum. Arc tangent value of the ratio between the imaginary and real parts of the transfer function defines the phase spectrum. Amplitude and phase spectrums are used to identify the natural frequencies of vibrations of soil layers.

Since the spectral ratios calculated from the earthquake records are random in nature, Hanning window technique was used to smoothen the amplitude function and to locate the peak values for modal frequency identification.

The averaging operation is done on the spectral ratio function to calculate the smoothened function y (f) is given as:

$$y_i(f) = 0.25y_{i-1}(f)+0.5y_i(f)+0.25y_{i+1}(f) \quad (6.2)$$

where, i vary from 2 to N-1.

Smoothening procedure is repeated for the required number of times (8 to 10 times). The lowest frequencies at which the Fourier spectral ratio reaches its peak and where phase angle is 90^0 are identified. Equivalent / average shear wave velocities for each depth-interval were back calculated using resonant frequencies of the Fourier spectral ratios in conjunction with Two-layer solution derived by Madera (1970).

The equation of motion for a vertically propagating shear wave is:

$$\rho\frac{\partial^2 u}{\partial t^2} = \frac{\partial}{\partial z}\left(G\frac{\partial u}{\partial z}\right) \qquad \textit{where,} \quad (6.3)$$

ρ = *Mass density of soil*
x = $x(z,t)$ = *horizontal soil displacement*
z = *vertical coordenate*
t = *time*
$G = \rho v_s^2$ = *shear* mod*ulas of soil*
v_s = *shear wave velocity*

The solution of the above Equation with boundary condition of zero relative displacement at the bottom boundary of the layers A and B, and zero shear stress at the ground surface is:

$$\tan\left(\frac{\pi}{2}\frac{f}{f_A}\right)\tan\left(\frac{\pi}{2}\frac{f}{f_B}\right) = \frac{\rho_B}{\rho_A}\frac{H_B}{H_A}\frac{f_B}{f_A} \qquad (6.4)$$

Where f_A, f_B = *Fundamental frequency of layers A and B respectively*

f = *Fundamental frequency of the total soil layer*

ρ_A, ρ_B = *Mass densities of layers A and B respectively*

H_A, H_B = *Thickness of layers A and B respectively*

With the known fundamental resonant frequencies of layer A and the two layer profile (f_A and f respectively), fundamental frequency (f_B) of layer B is computed from Equation 6.4. Shear wave velocities of layers A and B are computed by $V_{SA} = 4H_A f_A$ and $V_{SB} = 4H_B f_B$ for a system of three layers of soil on top of an elastic half-space as shown is Figure 6.3.

The two upper layers are regarded as an equivalent uniform single layer of thickness $\overline{h}_A$ and mass density $\overline{\rho}_A$ where,

$$\overline{h}_A = h_A + h_B \qquad (6.5)$$

$$\overline{\rho}_A = \left(h_A\rho_A + h_B\rho_B\right) / \left(h_A + h_B\right) \qquad (6.6)$$

Upper 3 layers of soil are regarded as an equivalent two-layer system of thickness $\overline{h}_A$ and h_C (or $\overline{h}_A$ and h_D...), mass density $\overline{\rho}_A$ and ρ_C and resonant frequency $\overline{f}_A$ (is f^{th} fundamental frequency of the total soil layer above layer c) and f_C, where f_C is calculated using Equation 6.4. This procedure is followed for n number of layers and the velocity in each layer is calculated using $4H_n f_n$ where H_n, f_n are the thickness and fundamental frequencies of n^{th} layer.

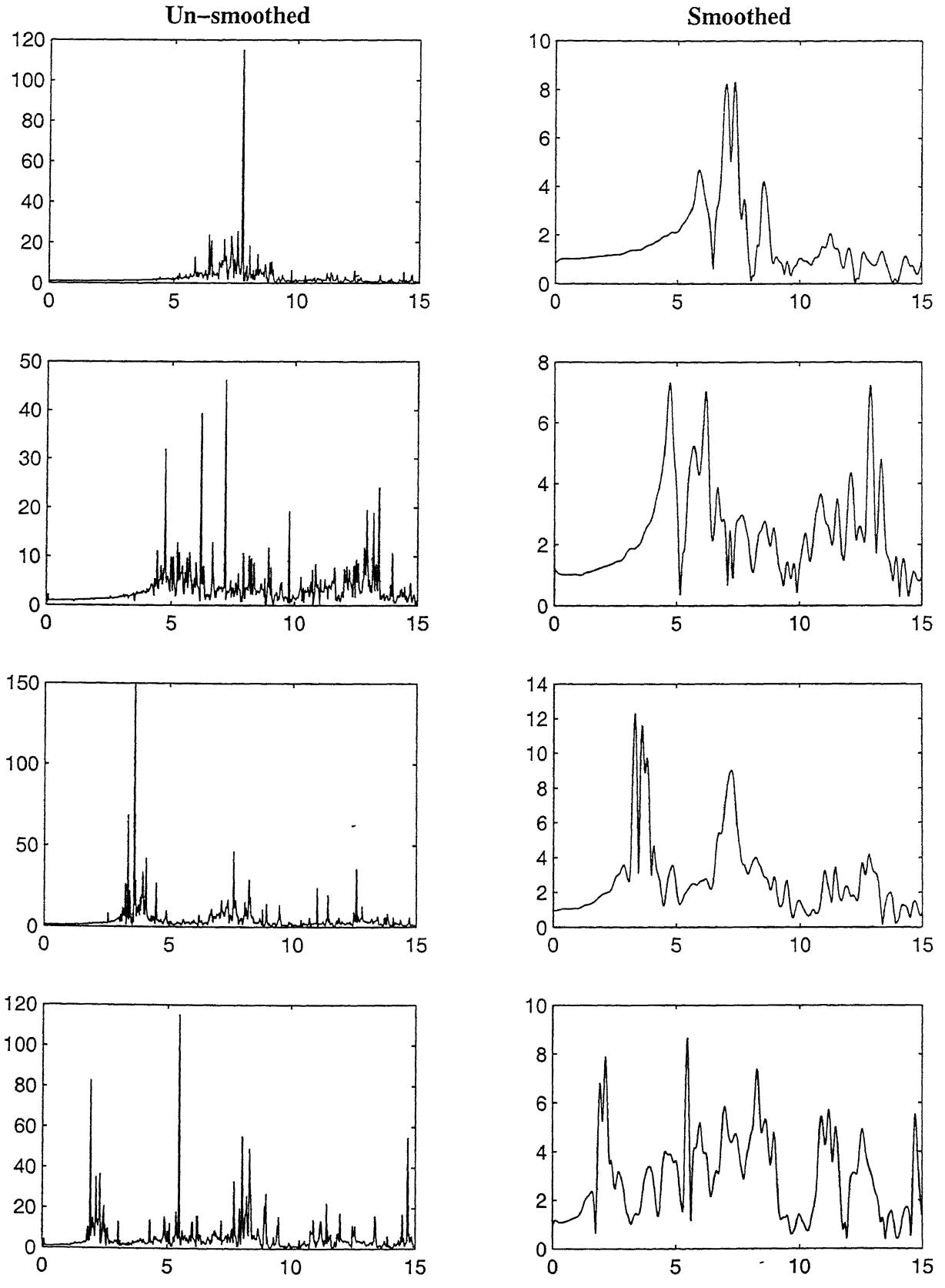

Figure 6.2: Transfer function of earthquake event 8722 before and after smoothening

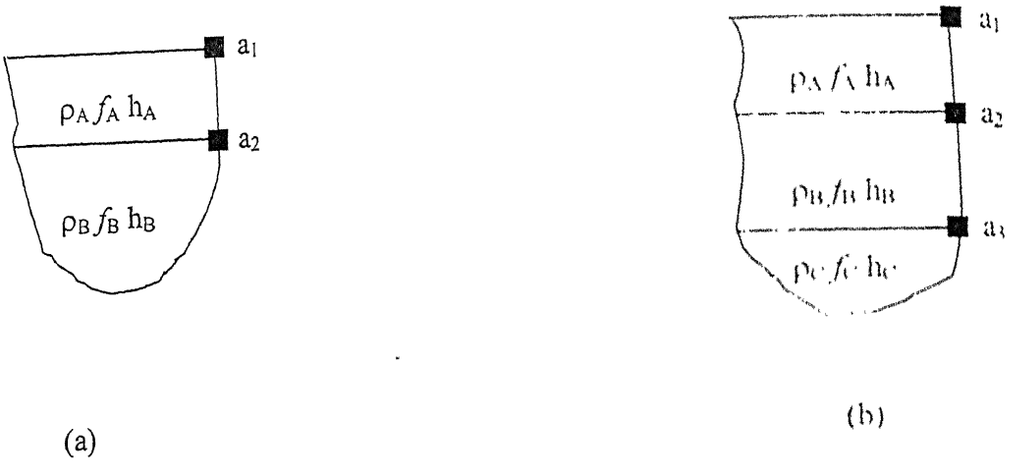

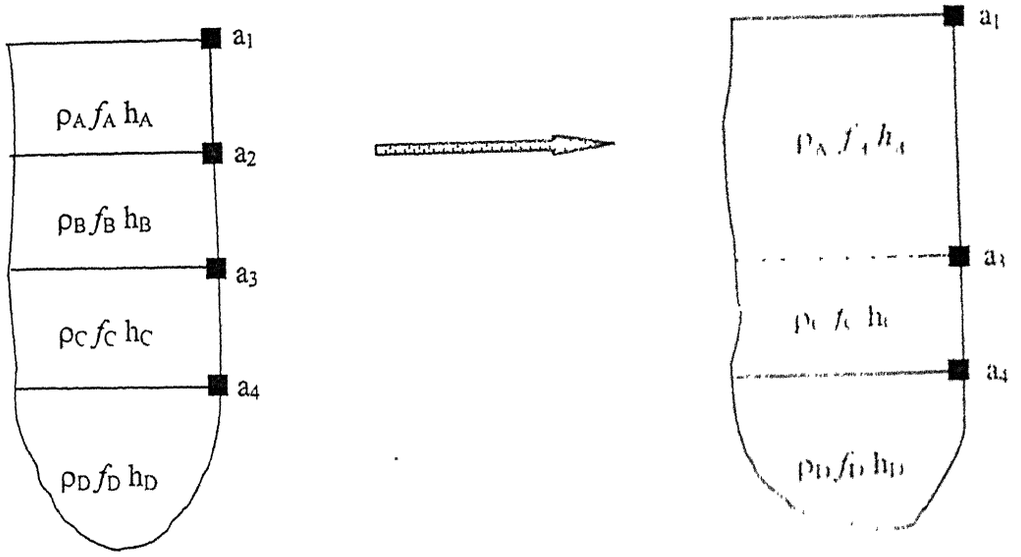

Figure 6.3: Models used for calculation of Shear wave velocity

(a) Single layer system (b) Two-layer system

(c) Three-layer system (d) Equivalent two-layer system

6.3 Results and Discussions

Simplified ground model adopted for estimating the shear wave profile the current analysis is shown in Figure 6.4.

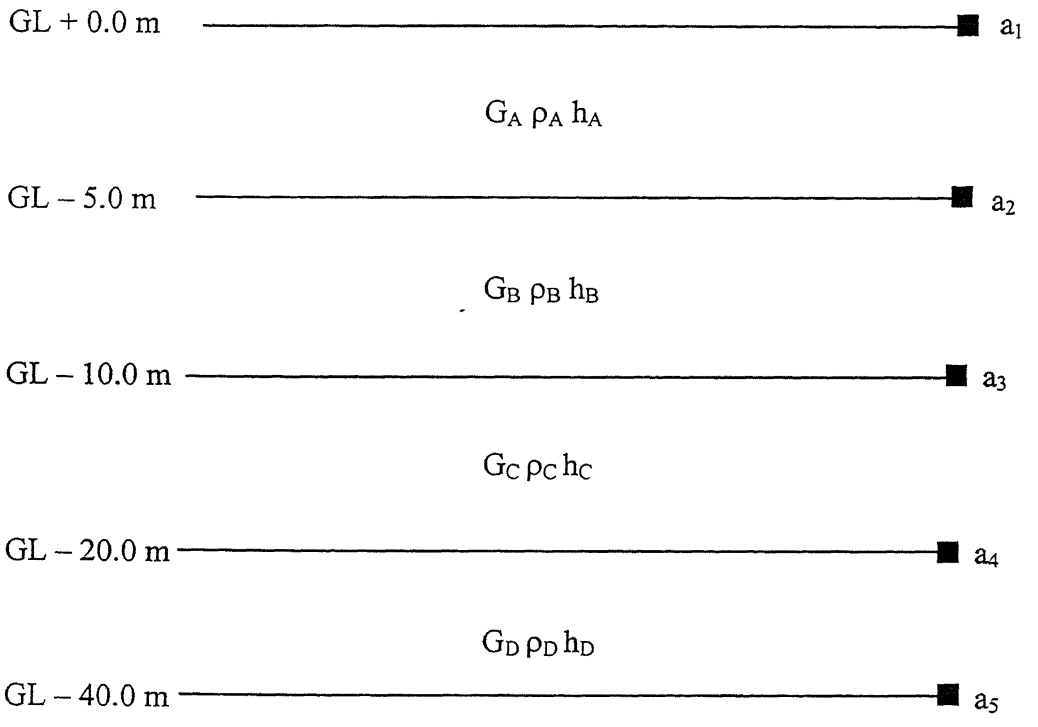

a_1, a_2, a_3, a_4 and a_5 are the accelerometers at surface, 5 m, 10 m, 20 m and 40 m respectively

Figure 6.4: Ground model used for system identification

Transfer functions were calculated between surface and 5 m, surface and 10 m, surface and 20 m and surface and 40 m for four events 8722 (PGA 327.1 cm/sec^2), 8706 (PGA 14.0 cm/sec^2), 8903 (PGA 28.9 cm/sec^2) and 8519 (PGA 82.2 cm/sec^2) and were compared in Figure 6.5.

As, can be seen from Figure. 6.5, peaks in transfer function between surface and 5 m and surface and 10 m exhibited some shifting with amplitude of PGA while this effect was not clear for other depths. This shows that there is no significant nonlinearity in the response for different input motions.

Table 6.1 presents the identified modal frequencies. EW and NS components of amplitude and phase spectrums of selected events are shown in Figures 6.6 – 6.15. Significant soil non linearity was not detected in layers below 10 m even during the peak event (PGA 8722, 327.1 cm/sec^2) due to the denser soil layer and the strain in these layers was not so large to soften the soils. Identified shear wave velocities are consistent with the geophysical measurements as shown in Figure 6.26.

6.4 Summary

- Fundamental frequency depends on PGA and is affected by the response of soil deposit.
- Fundamental frequency was higher in the top layers and decreased with depth.
- Changes in shear modulus or shear wave velocity were implied by the variation in fundamental frequencies and amplitude of ground acceleration.
- Reduction in fundamental frequency decreased with increasing thickness of the soil column.
- Shear wave velocities estimated during the earthquake excitation for the top layer (0 – 5 m) were substantially lower (2 – 37% variation) than the geophysical measurements implying the strains induced in the soil were higher than geophysical investigations.
- During the events with strong ground motions (>0.35g), shear wave velocity profile was consistent with the geophysical measurements implying no detectable nonlinear behavior.

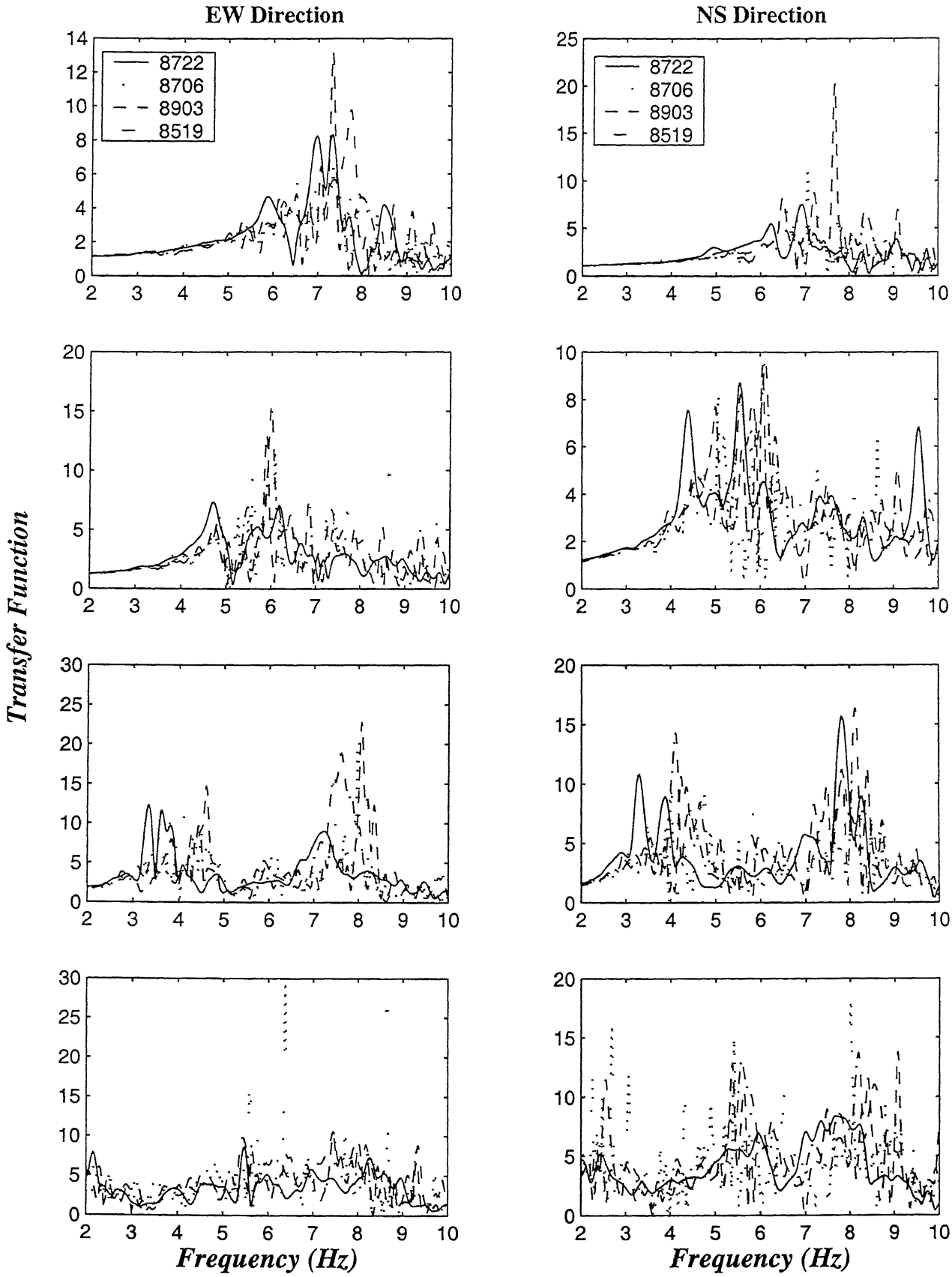

Figure 6.5: **Transfer functions estimated from NS component of the earthquake events 8519, 8706, 8722 and 8903 at borehole C0**

Table 6.1: Calculated Fundamental Frequencies and Estimated Shear Wave Velocities using Two Layer Solution

S no	Event (IEQ K)	PGA (cm/sec^2)		Fundamental Frequencies (Hz) and Shear wave velocity v_s (m/sec)															
				Fundamental Frequencies (Hz)								Shear wave Velocity V_s (m/sec)							
		EW	NS	Surface and		Surface and		Surface and		Surface and		Surface and 5m		5m and 10m		10m and 20m		20m and 40m	
				EW	NS	EW	NS	EW	NS	EW	NS	EW	NS	EW	NS	EW	NS	EW	NS
1	8205	28.3	26.1	7.80	6 84	6.26	5.12	4.59	4.45	2.26	2.71	127 5	109 5	286.7	222.2	373.2	463.1	333 9	425.1
2	8307	47 4	55.7	7.53	7.19	4 56	4.91	3.89	3.82	2.08	2.35	120.4	115.0	174.4	199.0	385.3	329.4	313.4	370 0
3	8401	25.5	24.2	7.32	7.51	5 94	5.70	4.26	4.29	2 43	2 40	117.1	120.2	283.5	251.0	340.7	356.7	373.3	366.9
4	8406	22 3	28 0	7.83	8.49	5 52	5.96	4.01	3.79	2.41	2.53	125.3	135.8	228 0	246 1	323.1	282.0	377.3	416.1
5	8416	13 8	14 5	7.50	7.54	6.09	6.32	4 35	5.01	2.26	3.01	120.0	120.6	291.0	319 5	346.1	441.0	338 0	469 2
6	8420	22 1	24.1	7.08	6.57	5.41	5.62	4.35	4.59	2 11	2.08	113.3	105 1	239.3	296.5	390.9	422.0	310.6	303.1
7	8510	27.4	29 6	8.36	8.49	6 13	5.85	3.77	3.51	2.49	2.74	133 7	135.8	261.2	238.9	277.1	256 0	405 3	512 1
8	8519	59.2	82 2	7.75	7.85	6.02	6.13	3.42	4.13	2 31	2.53	123 9	125.7	271.9	277.8	244 5	316 6	381.3	397 8
9	8525	75.7	71.6	8.97	8.66	6.09	5.51	4.37	4.46	2.23	2 14	143.5	138.5	245 5	215.3	349.5	402 7	331 9	315 3
10	8601	15.4	14.3	7.85	7.91	6.06	6 15	4.58	4.78	2 56	2.32	125.6	126.5	271.7	278 2	382.5	409.7	390.6	341 4
11	8602	54.0	40.7	7.26	7.37	5.22	6.23	3.41	4.13	2.15	2.69	116.2	117 9	219.2	320.0	257.4	314.1	343.3	434 3
12	8706	11.3	14.0	6.72	7.62	5.41	5.80	4.32	4.02	2.48	2.15	108.5	122 0	255.9	255.8	383.1	313.3	434.1	390 8
13	8717	20.7	33.5	7.49	6.74	6.37	4 91	4.02	3.47	2.79	2.77	119.8	107.9	331.7	207.8	298.9	273.7	468.5	531.6
14	8722	213.	327.1	6.97	7.79	4.74	6.10	3.62	3.28	1.92	2.38	111.6	124 7	191 6	277 9	304.3	231.3	289 3	414.3
15	8723	17.2	21.2	6.39	7.61	5.69	5.33	2.80	3.75	2.06	2.14	102.3	121.7	332.8	219.7	193.9	294.6	360 9	328.0
16	8725	23.8	13.8	7.86	8.71	5.46	5 43	3.82	3.04	2.29	1.87	125.7	139.4	223.9	209.8	299.8	216.2	356.5	295 5
17	8726	22.5	30.4	7.83	8.04	6.17	5 92	4.21	3.37	2.54	2.50	125.3	128.7	282.7	252.9	325.2	241.7	397.9	441.7
18	8802	40.6	40.8	7.82	7.76	6.24	6.00	4.41	4.59	2.59	2.41	125.2	124.2	290.5	269 1	348.9	387.5	400 9	361.7
19	8806	54.9	97.8	7.68	6.22	5.65	5.70	4.38	4.51	2.57	2.47	122.8	99.5	241.5	376.5	375 1	413.2	397.6	372.3
20	8808	19.0	26.2	7.84	6.42	6.21	5.16	3.32	3.58	1.89	3.26	125.5	102.7	286.9	242.9	233.3	279.4	290.9	863.7
21	8816	48 4	59.8	7.69	7.56	6.17	5.92	4.10	3.46	2.32	2.53	123.1	120.9	289.8	269 2	312.4	249.6	355.5	440.7
22	8823	46 4	35.2	7.52	7.64	6.14	6.02	3.73	4.05	2.84	2.23	120.4	122.2	295.7	276 8	272.7	309.8	515.9	338.2
23	8901	55.7	49.1	5.63	5.57	4.87	4.91	3.56	3.78	2.30	2.57	90.1	89.2	263.4	278.2	287.9	321.3	370.1	427.3
24	8903	27.5	28.9	7.07	7.67	6.28	6.06	4.60	4.23	2.32	2.41	113.2	122.7	366.1	279.4	373.9	332.0	344 8	369.0
25	8904	41.0	21.9	7.48	7.17	5.93	6.28	4.34	3.62	2.59	2 62	119.7	114.8	274.3	349 7	352 7	260.3	402 6	453 9

~ Unreliable Estimate

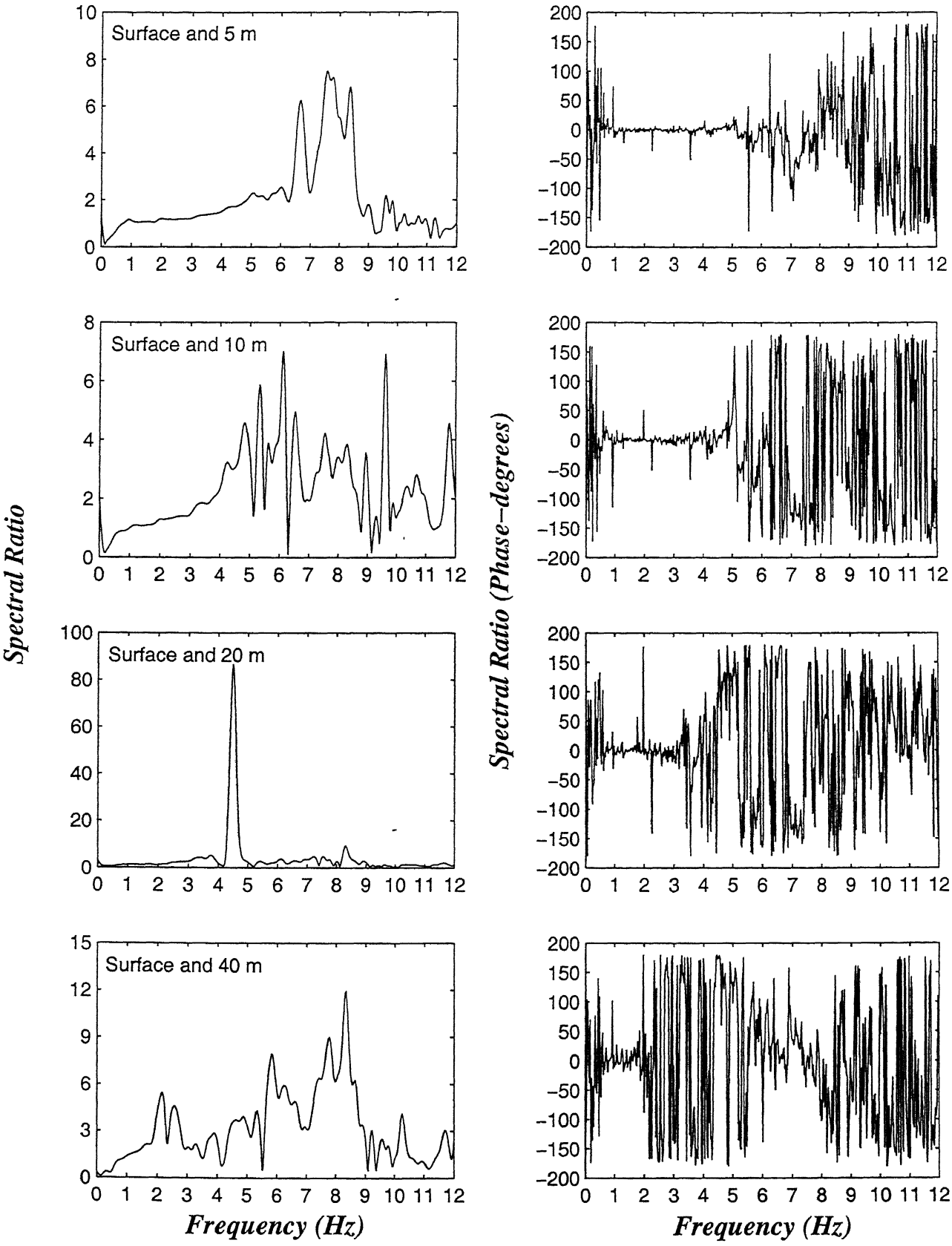

Figure 6.6: Amplitude spectrum and phase spectrum during the earthquake 8510 in east – west direction at borehole C0

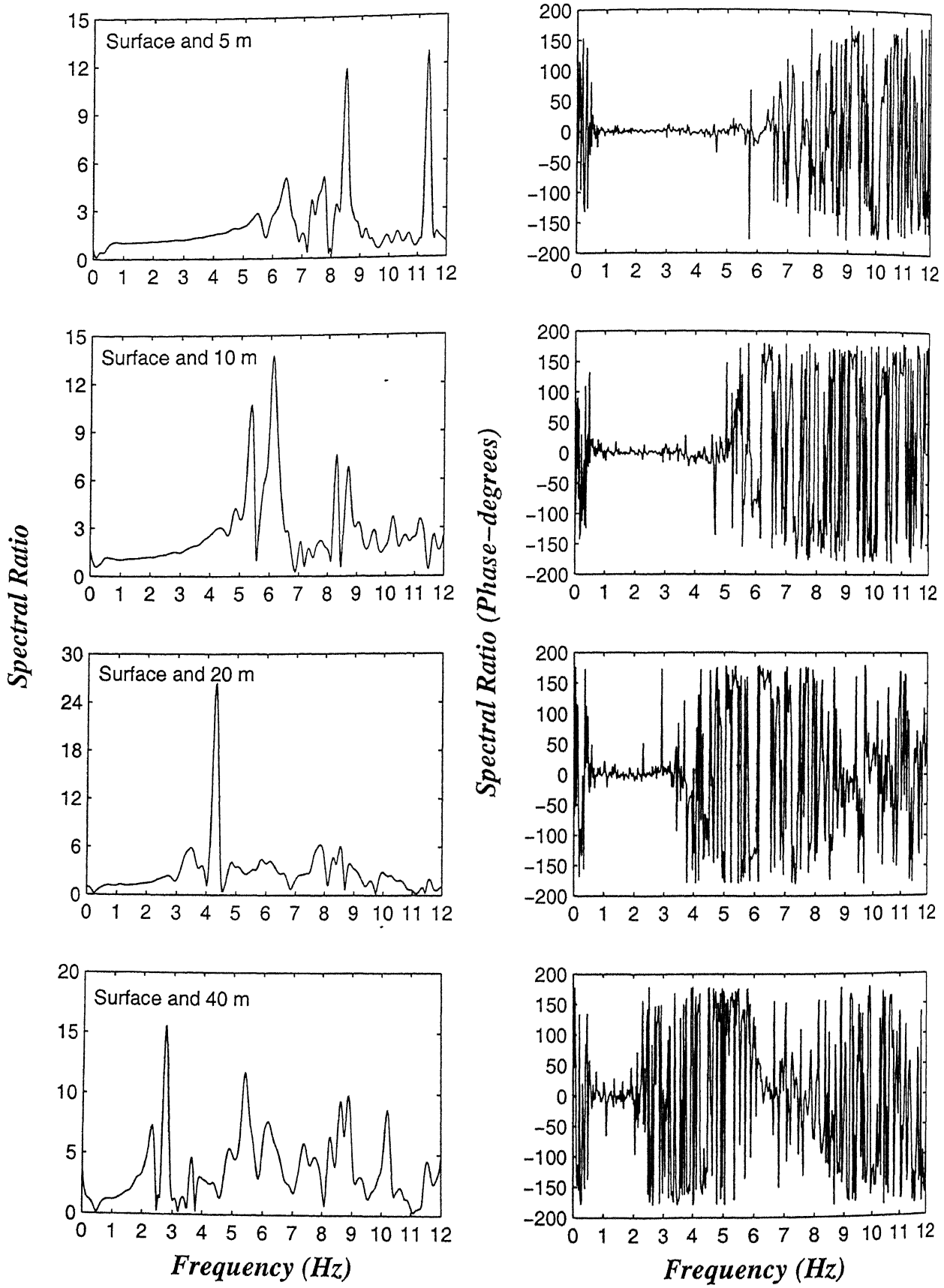

Figure 6.7: **Amplitude spectrum and phase spectrum during the earthquake 8510 in north – south direction at borehole C0**

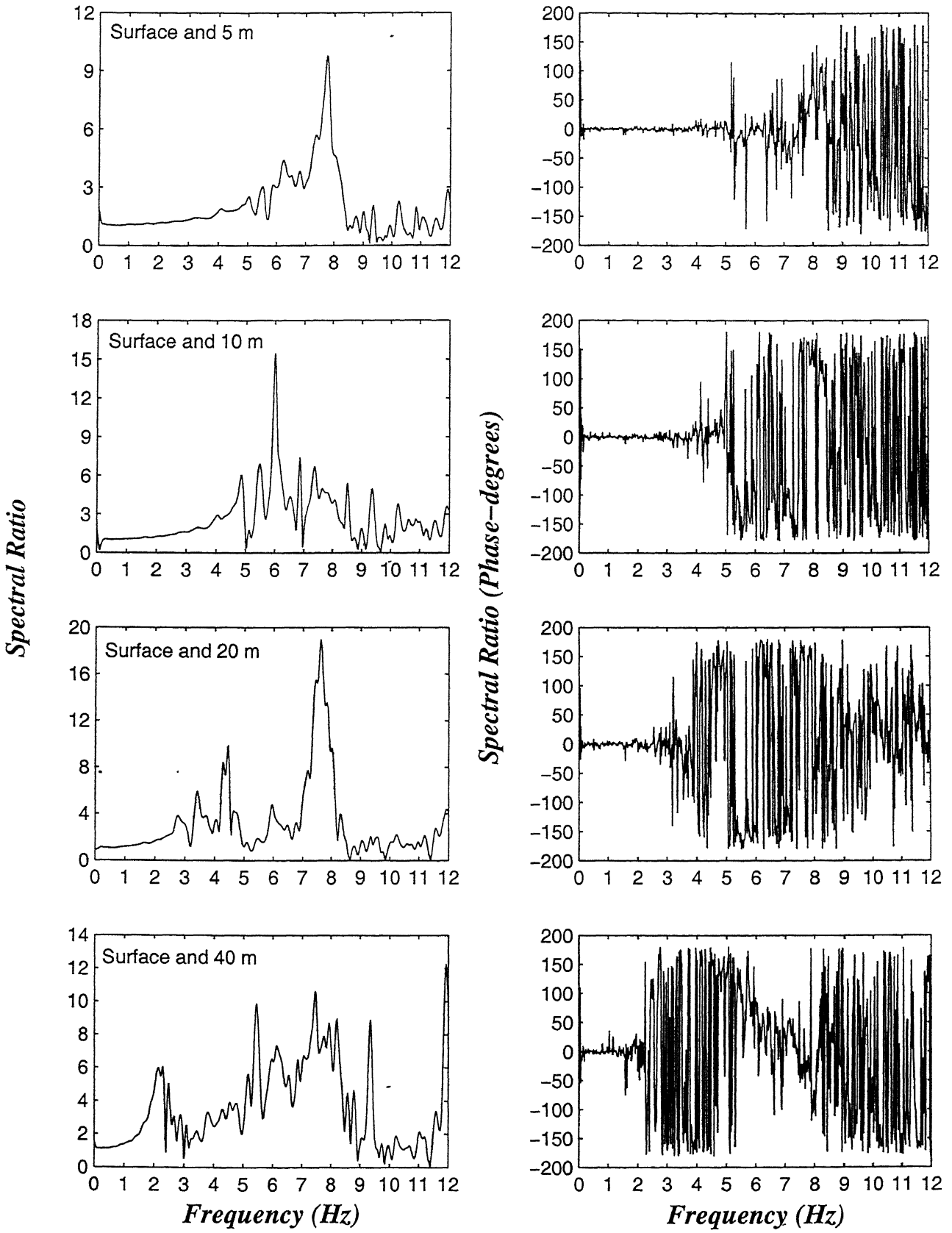

Figure 6.8: Amplitude spectrum and phase spectrum during the earthquake 8519 in east – west direction at borehole C0

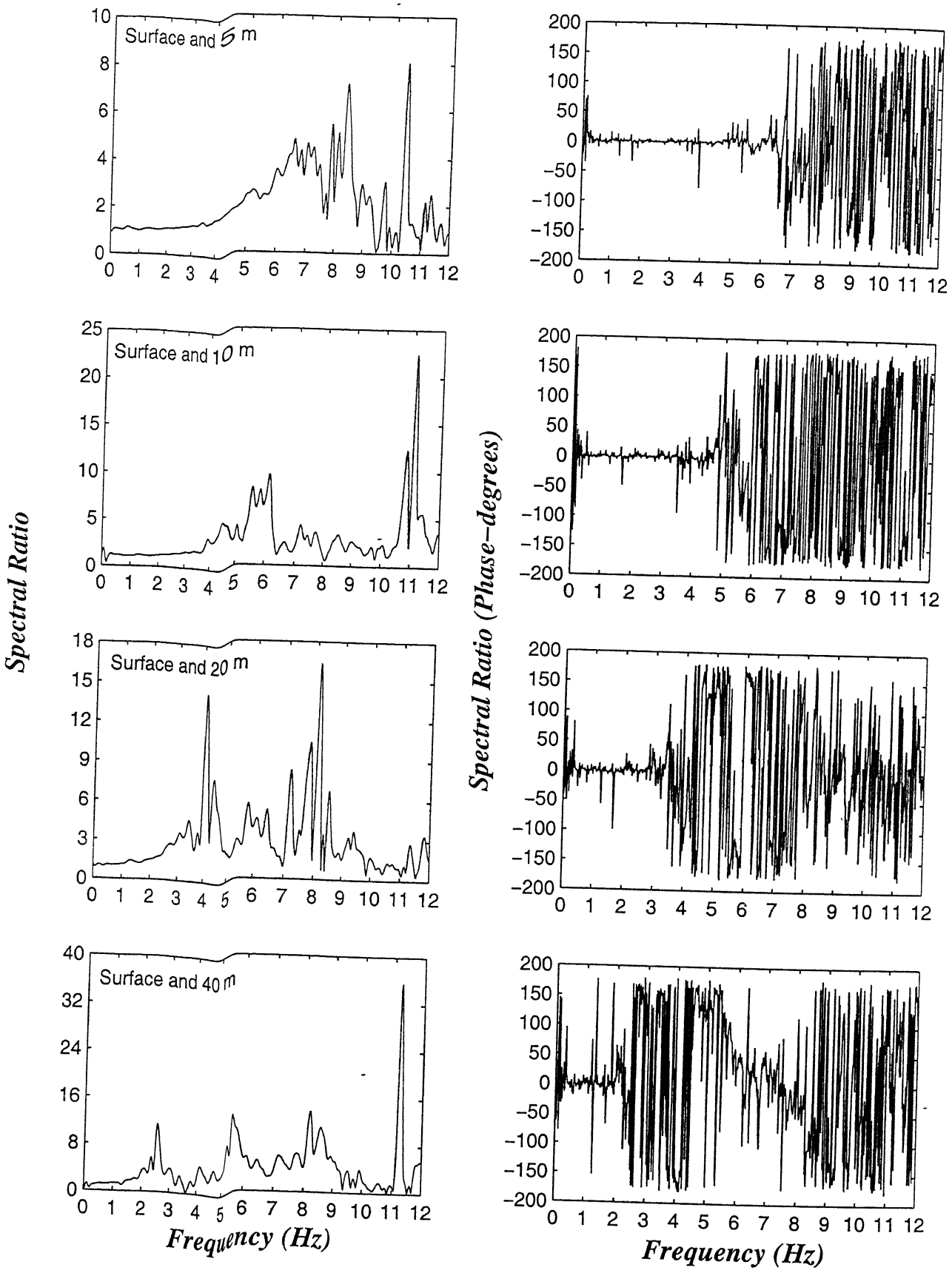

Figure 6.9: **Amplitude spectrum and phase spectrum during the earthquake 8519 in north-south direction at borehole C0**

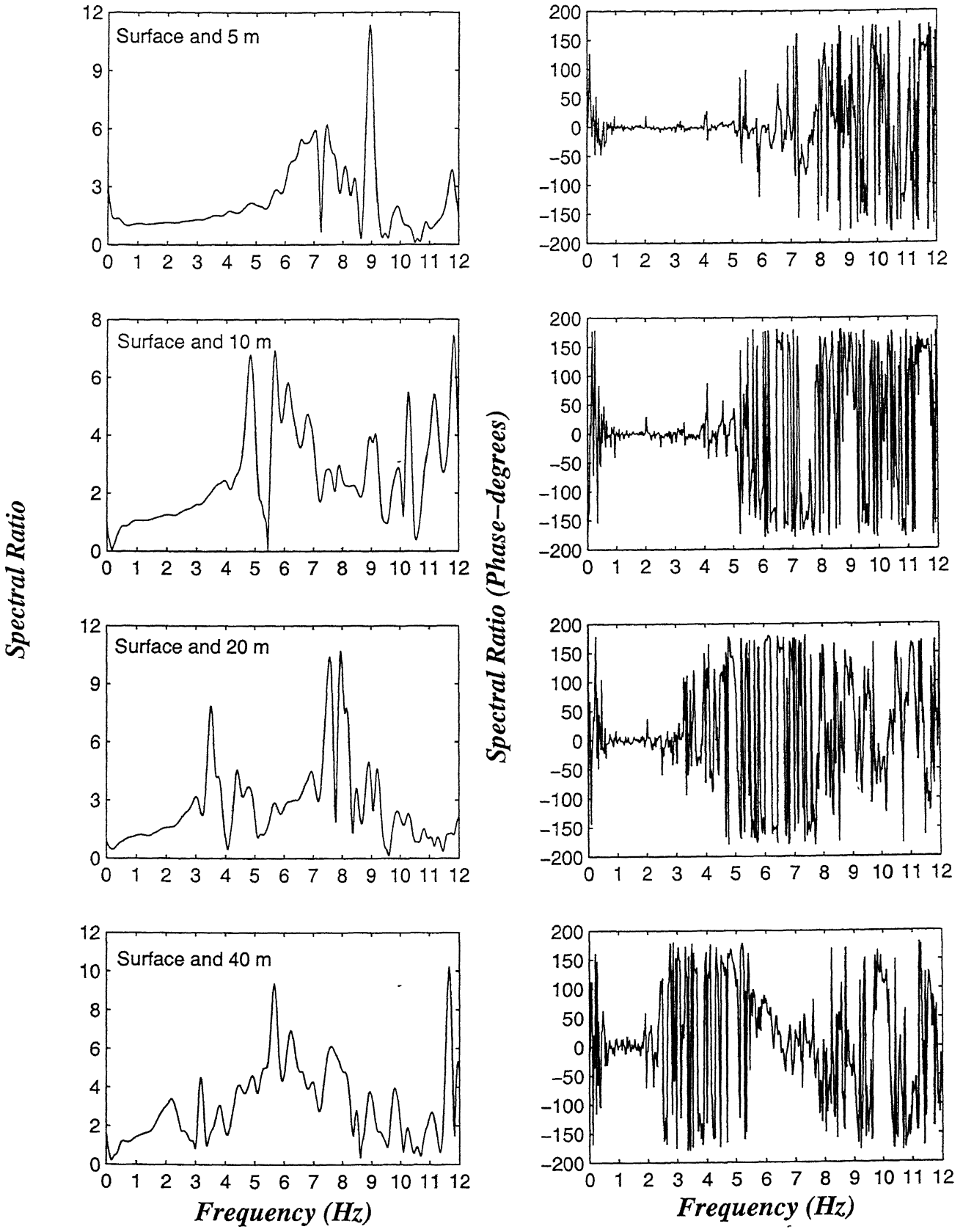

Figure 6.10: Amplitude spectrum and phase spectrum during the earthquake 8525 in east – west direction at borehole C0

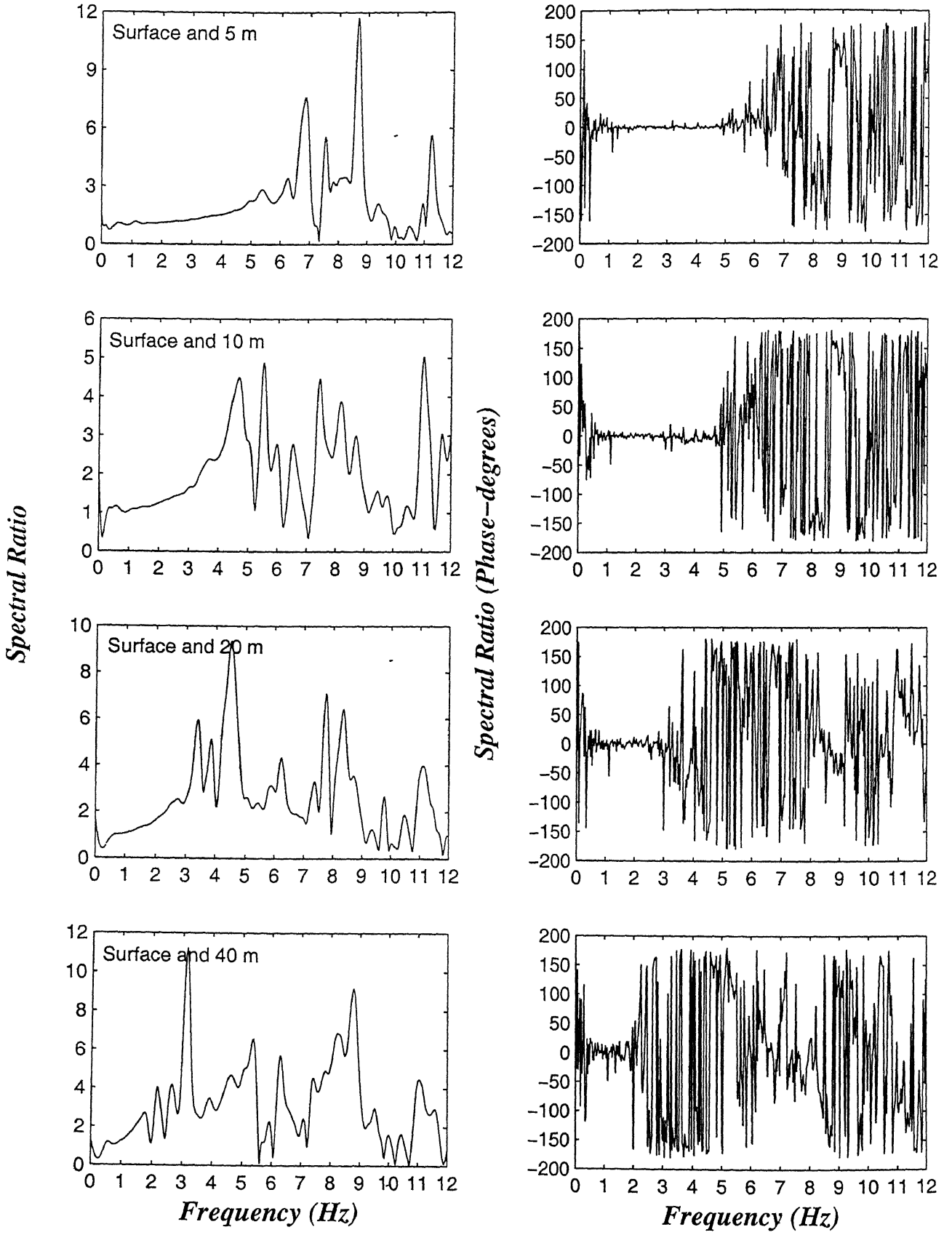

Figure 6.11: Amplitude spectrum and phase spectrum during the earthquake 8525 in north – south direction at borehole C0

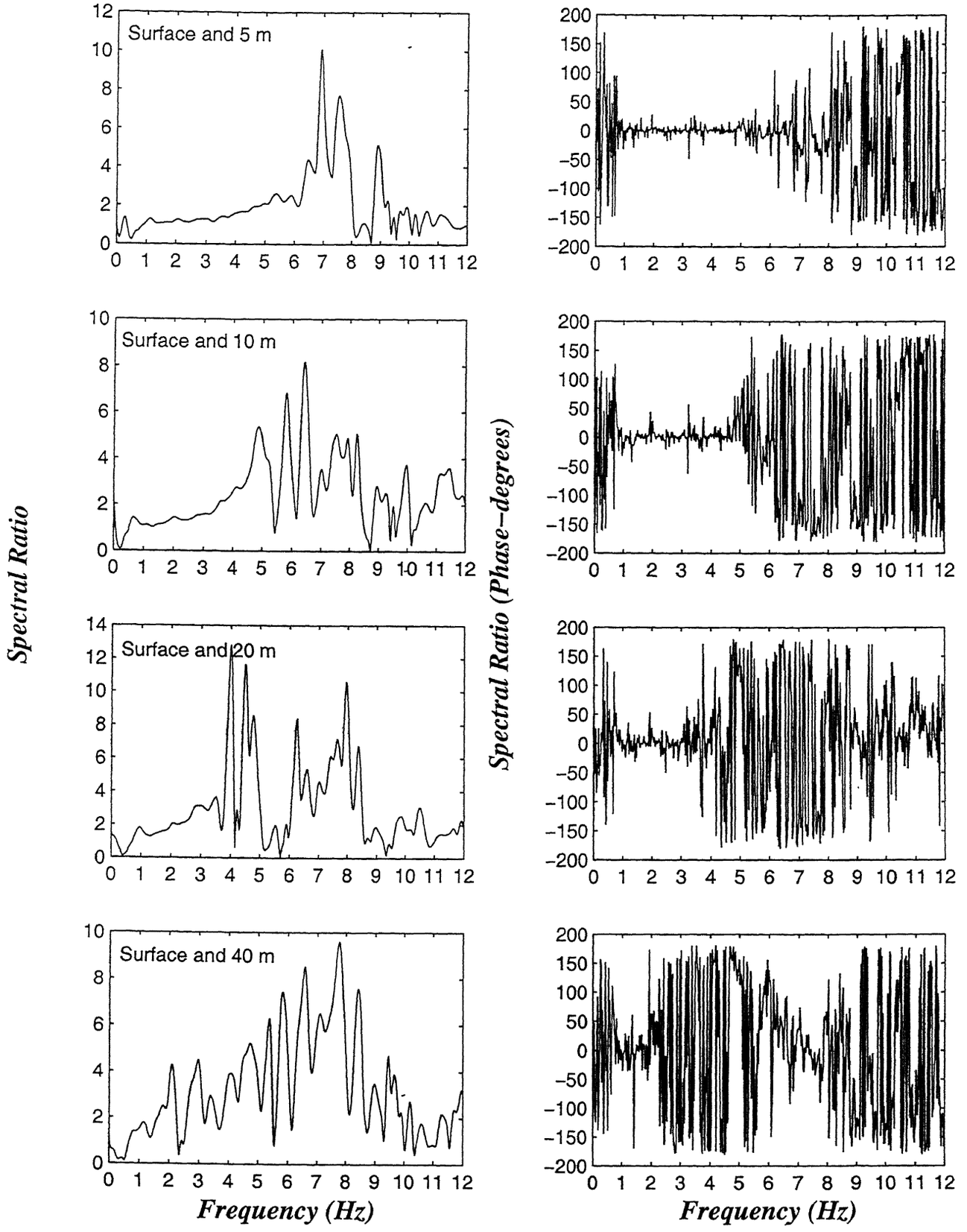

Figure 6.12: Amplitude spectrum and phase spectrum during the earthquake 8717 in east – west direction at borehole C0

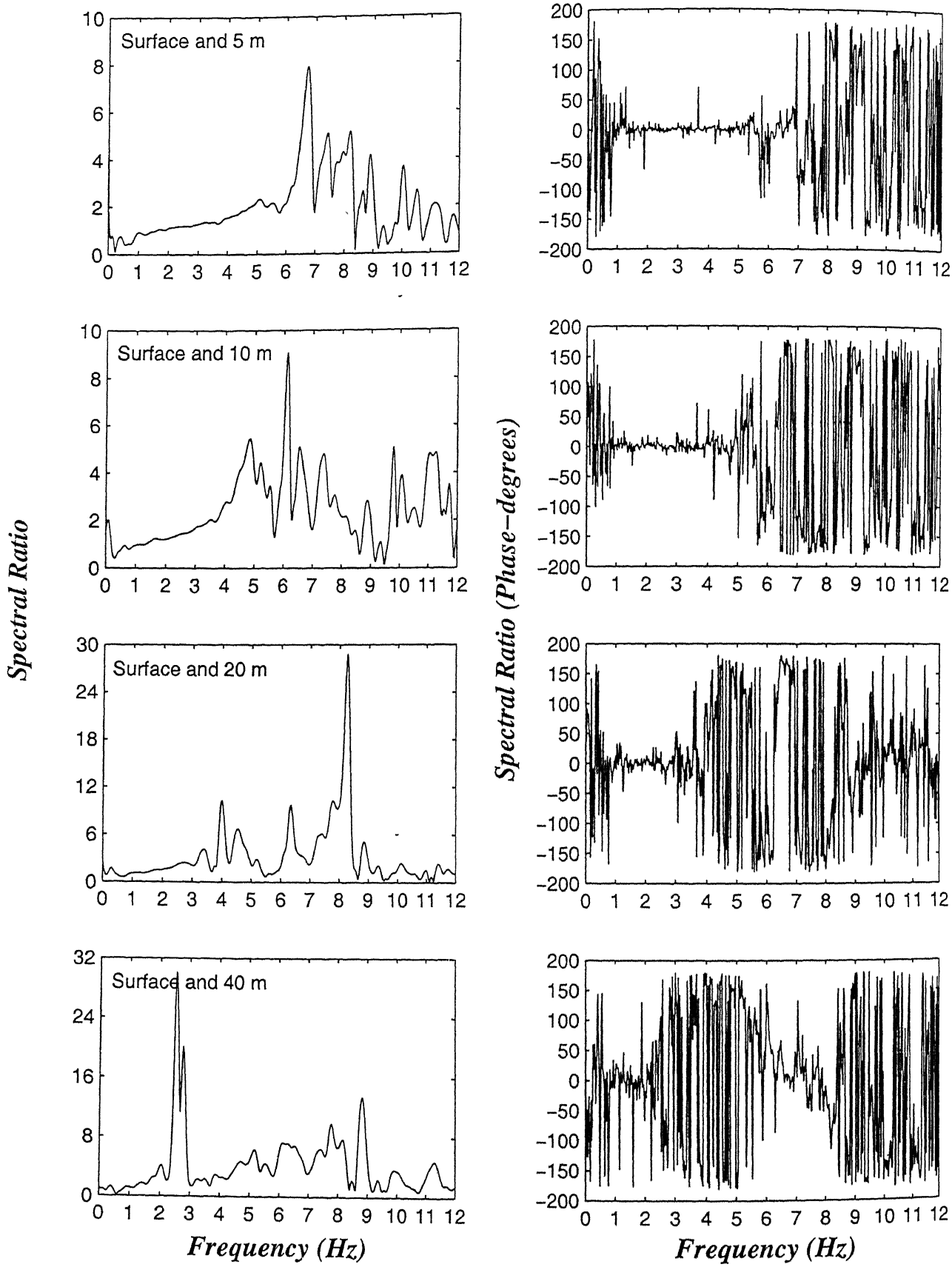

Figure 6.13: Amplitude spectrum and phase spectrum during the earthquake 8717 in north – south direction at borehole C0

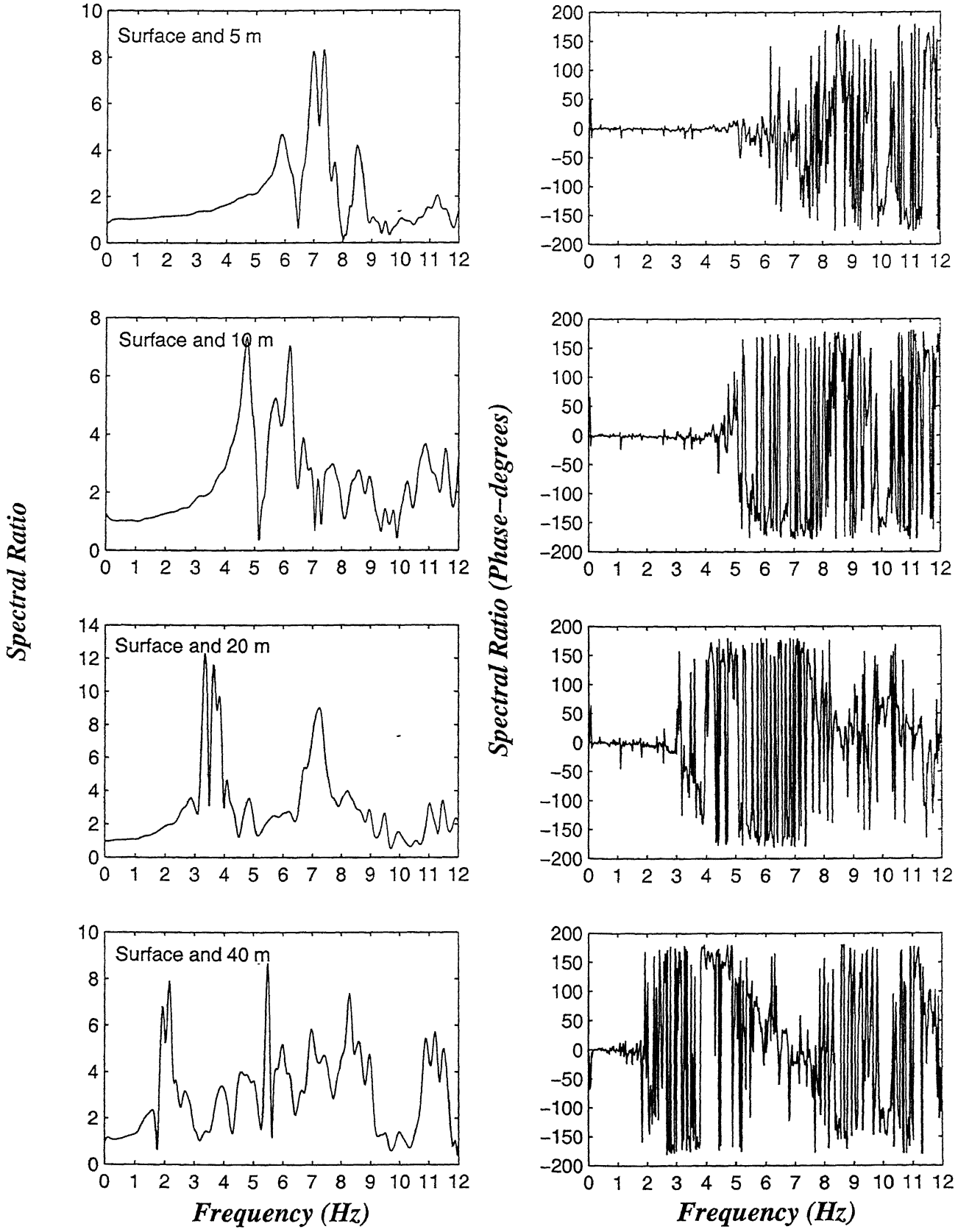

Figure 6.14: Amplitude spectrum and phase spectrum during the earthquake 8722 in east – west direction at borehole C0

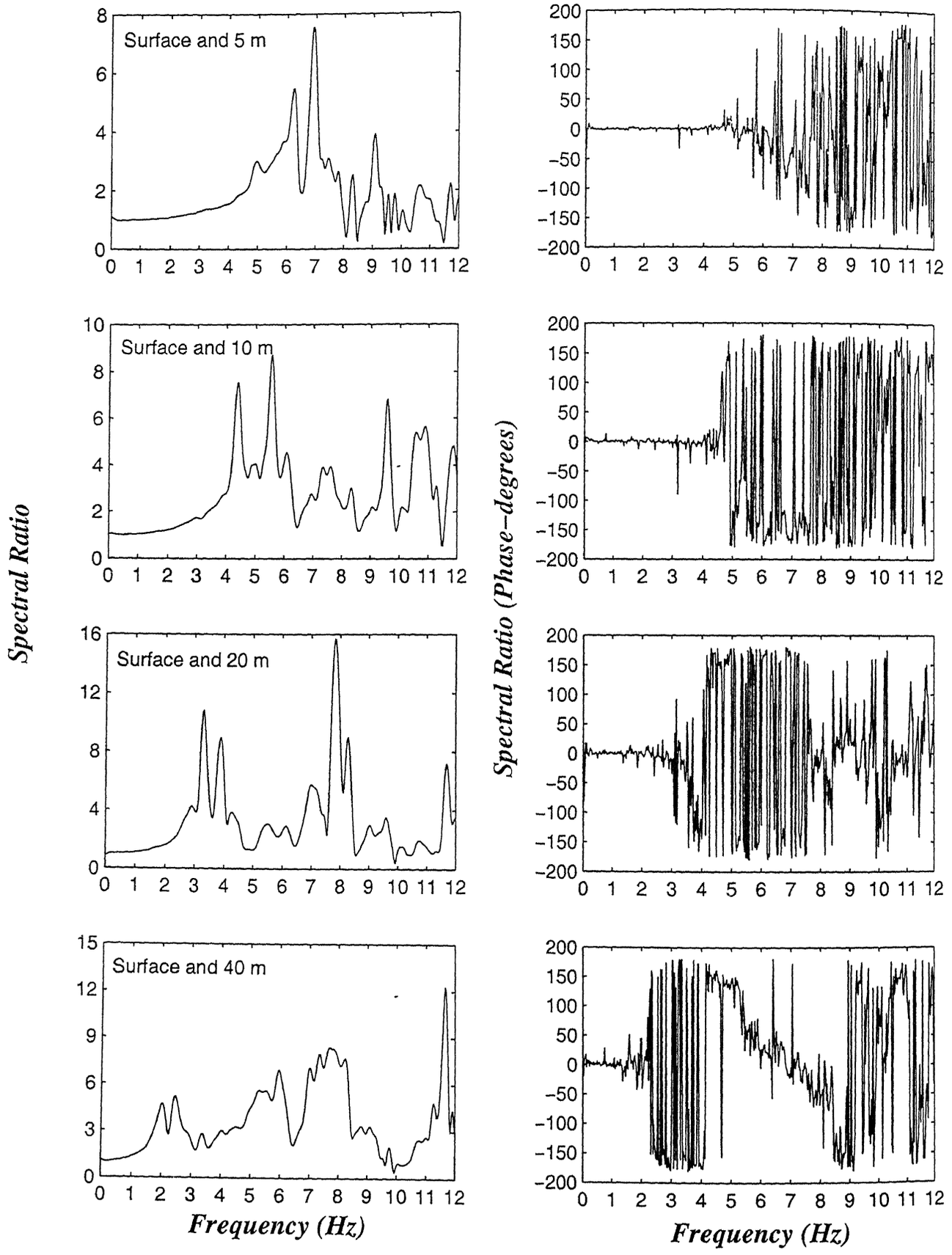

Figure 6.15: Amplitude spectrum and phase spectrum during the earthquake 8722 in north – south direction at borehole C0

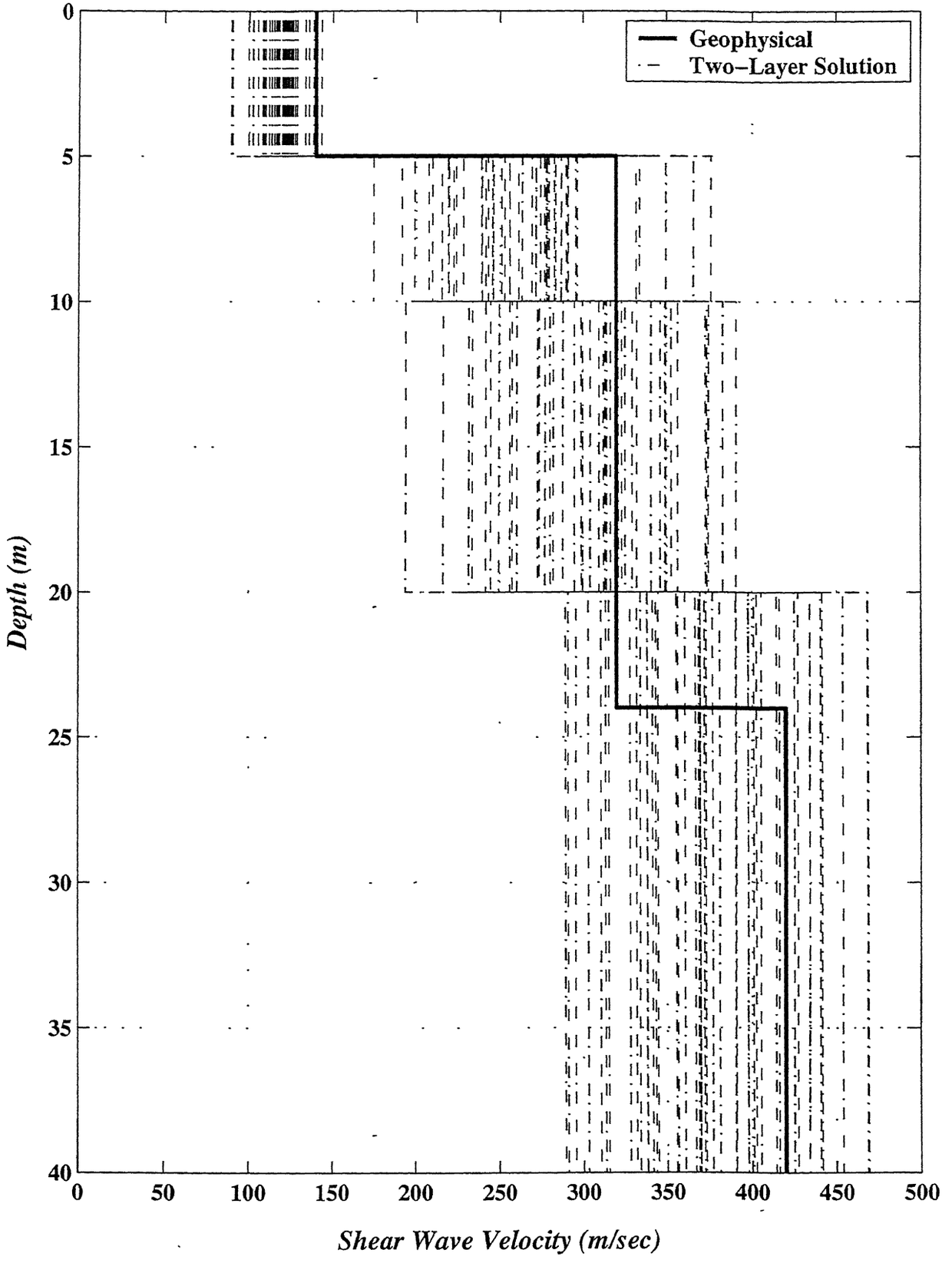

Figure 6.16: Estimated Shear wave velocities by Two-Layer solution at borehole C0

Spectral Ratio

Chapter 7
CONCLUSIONS AND FUTURE RESEARCH

7.1 Conclusions

In the research reported herein, the recorded free field surface and down-hole acceleration histories at Chiba array were utilized to:

- Evaluate shear wave propagation characteristics
- Estimation of Shear wave and Primary velocity with depth
- Evaluate site resonant frequencies
- Evaluate site shear stress-strain histories
- Estimate soil shear moduli and damping ratios

Shear wave velocities were evaluated using correlation analyses and a two-layer solution technique. Resonant frequencies were estimated using spectral analyses. Identified shear wave profile was in good agreement with geophysical measurements. Evidence of soil softening during moderate to strongest earthquakes in the top 10 m of soil was also shown.

A new non-parametric technique was used to directly evaluate soil seismic shear stress-strain histories from down-hole accelerations. The technique is based on interpolation between down-hole accelerations, and does not require the availability of bedrock or input motion records. The estimated shear stress and strain histories were employed to evaluate the soil shear stiffness and damping properties. The identified shear modulus and damping were able to capture the essential features of recorded response. There was a large scatter in identified damping in the top 10 m. This large scatter might be an actual reflection of the soft nature of top soil, along with other surface wave propagation characteristics that are not modeled by the employed simple one dimensional shear wave propagation concept.

A summary of the identified shear wave velocities and comparison with geophysical measurements is shown in Fig. 7.1. It is of interest to note that earthquake derived shear wave velocities were biased toward the lower geophysical velocity data in the top 10 m. This might reflect the fact that geophysical measurements were performed at lower strain amplitudes as compared to the employed seismic records. It is also observed that below 10 m depth soil softening was not observed even during the event 8722 where PGA exceeded 300 gals. Other researchers using different techniques also observed this fact. Figure 7.2 compares the identified shear wave profile with the results reported by Sawada et al. [44], which corroborates the above finding. This is attributable to the stiff nature of the soil below 5 m depth.

A thorough review of the literature and the results of this study suggest that the amount of information that can be inferred from the down-hole seismic records is a function of the site geology. The choice of the site is a function of the kind of information required i.e., whether the required information is on propagation paths; radiation pattern; magnitude and fault rupture; or nonlinear / liquefaction site behavior. The identified properties show the potential of down-hole records as a valuable source of information on dynamic site behavior. Simple tools such as correlation techniques can be utilized to identify the low-strain properties. In addition, down-hole acceleration records can be utilized to evaluate the seismic shear stress strain histories, to analyze the site response, and to estimate the soil dynamic properties such as shear modulus and damping properties. Finally it is emphasized that the techniques that were used herein may also be conveniently employed in conjunction with well-instrumented soil systems such as earth dams, retaining walls etc.

7.2 Future Work

The information and site properties provided by this study will be utilized in a parametric system identification of Chiba site seismic response characteristics. The estimation will account for the two dimensional horizontal shear response. Parameter identification will be formulated on the basis of optimality criteria that related the observed and predicted seismic histories. Further research is required to fully quantify the effect of dense lower layers on site amplification.

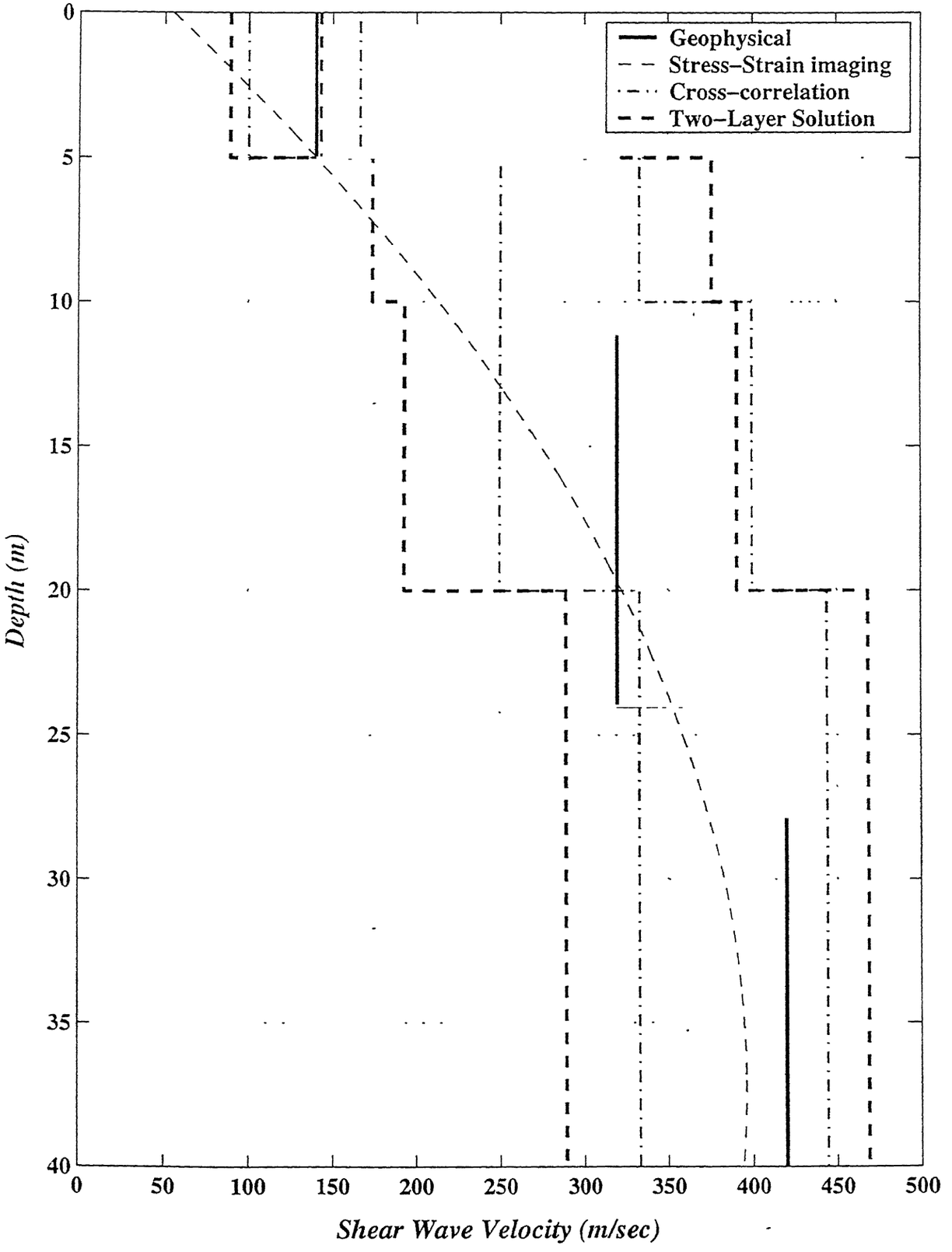

Figure 7.1: Range of shear wave velocities estimated by various methods

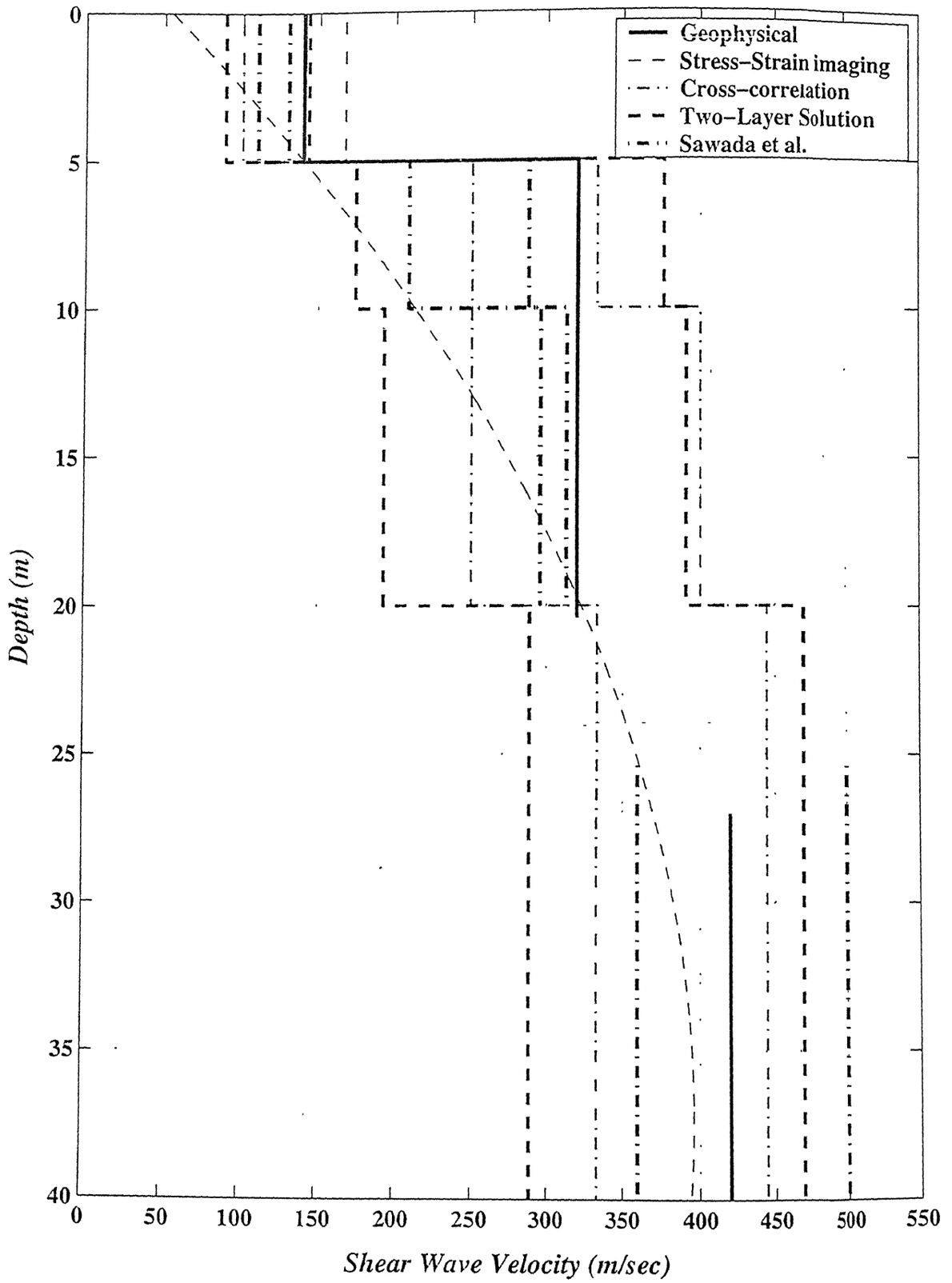

Figure 7.2: Comparison of shear wave velocities with the results reported by Sawada et al. [44]

REFERENCES

1. Abdel - Ghaffer, A. M., and Scott, R. F., *"Investigation of the Dynamic Characteristics of an Earth Dam."* Report No. EERL 78-02, Earthquake Engineering Laboratory, Pasadena, California, 1978.

2. Abdel - Ghaffer, A. M., and Scott, R. F., *"Shear Moduli and Damping Factors of Earth Dam."* Journal of the Geotechnical Engineering, ASCE, Vol. 105, No. GT12, pp. 1405 – 1426, December 1979.

3. Ansary, M. A., Yamazaki, F., Kokusho, T., and Ueshima, T., *"Microtremor Observation at Haulien LSST Array Site, Taiwan."* Proceedings of 3rd International Conference on Recent Advances in Geotechnical Earthquake Engineering and Soil Dynamics, Columbia, pp. 357 – 362, November 1996.

4. Archuleta, R. J., and Seale, H. S., *"Analysis of Site effects at Garner Valley Downhole Array near the San Jacinto Fault."* Proceedings of 2nd International Conference on Recent Advances in Geotechnical Earthquake Engineering and Soil Dynamics, St. Louis, Missouri, pp. 1203 – 1206, March 1991.

5. Archuleta, R. J., Seale, H. S., Sangas, P. V., Baker, L. M., and Swain, S. T., *"Garner Valley Downhole Array of Accelerometers: Instrumentation and Preliminary Data Analysis."* Bulletin of the Seismological Society of America, Vol.82, No.4, pp.1592-1621, August 1992.

6. Beck, J. L., *"Structural Identification using Linear Models and Earthquake Records."* Earthquake Engineering and Structural Dynamics, Vol. 8, 1980.

7. Beresnev, I.A., Kuo-Liang, W., and Yeong, T.Y., *"Nonlinear Soil Amplification: Its Corroboration in Taiwan."* Bulletin of the Seismological Society of America, Vol. 85, No. 2, pp. 496 – 515, April 1995.

8. Campanella, R. G., and Stewart, W. P., *"Downhole Seismic Cone Analysis using Digital Signal Processing."* Proceedings of 2nd International Conference on Recent Advances in

Geotechnical Earthquake Engineering and Soil Dynamics, St. Louis, Missouri, pp. 77 – 92, March 1991.

9. Chang, C. Y., Mok, C. M., Power, M. S., Tang, Y. K., Tang, H. T., and Stepp, J. C., "*Equivalent Linear versus Nonlinear Ground Response Analysis at Lotung Seismic Experiment Site.*" Proceedings of 4th U.S. National Conference on Earthquake Engineering, Palm Springs, California, Vol.1, pp. 327 – 336, May 1990.

10. Chang, C.Y., Mok, C. M., Power, M. S., Tang, Y. K., Tang, H. T., and Stepp, J. C., "*Development of Shear Modulus Reduction Curves based on Lotung Downhole Ground Motion Data.*" Proceedings of 2nd International Conference on Recent Advances in Geotechnical Earthquake Engineering and Soil Dynamics, St. Louis, Missouri, pp. 111 – 118, March 1991.

11. Chang, C.Y., Mok, C. M., and Tang, H. T., *"Inference of Dynamic Shear Modulus from Lotung Downhole Data.*" Journal of Geotechnical Engineering, Vol. 122. No. 8, pp. 657 – 665, 1996.

12. Cheng, H. C., and Hwang, C. C., "*Anisotropic Seismic Ground Responses Identified from the Hualien Vertical Array.*" Soil Dynamics and Earthquake Engineering, Vol. 17, pp. 371 – 395, 1998.

13. DiPasquale, E., and Cakmak, A. S., *"Identification and Serviceability Limit State and Directions of Seismic Structural Damage."* Technical Report CNEER-88-0022, National Center for Earthquake Engineering Research, Buffalo, NY, 1988.

14. Elgamal, A. W., Zeghal, M., Tang, H. T., and Stepp, J. C., *"Lotung Downhole Array I: Evaluation of Site Dynamic Properties.*" Journal of Geotechnical Engineering, ASCE, Vol. 121. No. 4, pp. 350 – 362, 1995.

15. Francois, E. H., Ueng, T. –S., Lawrence, J. H., Stephen, P. J., and Paul, W. S., *"A New Seismic Geotechnical Strong Motion Approach.*" Lawrence Livermore National Laboratory, Livermore, CA, pp. 125 - 132.

16. Ghanem, R., and Shinozuka, M., *"Structural System Identification 1: Theory,"* Journal of Engineering Mechanics, ASCE, Vol.121. No.2, pp. 255 - 264, February 1995.

17. Ghayamghamian, M. R., and Hideji, K., *"On-site Nonlinear Hysteresis Curves and Dynamic Soil Properties."* Journal of Geotechnical and Geoenvironmental Engineering, Vol. 126. No. 6, pp. 543 – 555, 2000

18. Glaser, S., *"System Identification and its Applications to Estimating Soil Properties."* Journal of Geotechnical Engineering, Vol. 121. No. 7, pp. 553 – 560, July 1995.

19. Hart, G. C., and Yao, J. T. P., *"System Identification in Structural Dynamics."* Journal of Engineering Mechanics, ASCE, Vol. 103, No. 6, June 1977.

20. Honjo, Y., Satoru, I., Michio, S., Sadatomo, O., and Mutsuhiro, Y., *"Inverse Analysis of Dynamic Soil Properties based on Seismometer Array Records using the Extended Bayesian Method."* Soils and Foundations, Vol. 38. No. 1, pp. 131 – 143, 1998.

21. Huang, H. -C., and Chiu, H. -C., *"Estimation of Site Amplification from Dahan Downhole Recordings."* Earthquake Engineering and Structural Dynamics, Vol. 25, pp. 319 – 332, 1996.

22. Katayama, T., Yamazaki, F., Nagata, S., Lin, L., and Turker, T., *"A strong Motion Database for the Chiba Seismometer Array and ts Engineering Analysis."* Earthquake Engineering and Structural Dynamics, Vol. 19, pp. 1089 – 1106, 1990.

23. Katayama, T., Turker, T., Yamazaki, F., *"Analysis of Seismic Wave Propagation based on the Chiba Array Data."* Proceedings of 8th Japan Earthquake Engineering Symposium, pp. 505 – 510, 1990.

24. Katayama, T., Yamazaki, F., Nagata, S., Lin, L., and Turker, T., *"Development of strong Motion Database for the Chiba Seismometer Array."* Earthquake Disaster Mitigation Engineering, Institute of Industrial Science, University of Tokyo, Japan, Report No. 90 – (14), 1990.

25. Katayama, T., Villacis, C., yamazaki, F., *"Analysis of Seismic Ground Strain Observed at the Chiba Experiment Station."* International Symposium on National Disaster Reduction and Civil Engineering, University of Tokyo, Japan, pp. 207 – 216, 1991.

26. Katayama, T., "*Use of Dense Array in the Determination of Engineering Properties of Strong Motions.*" Structural Safety, Vol. 10, pp. 27 – 51, 1991.

27. Katayama, T., Yamazaki, F., Turker, T., "*Spatial Correlation Study on Earthquake Ground Motion Based on Array Data.*" International Symposium on National Disaster Reduction and Civil Engineering, University of Tokyo, Japan pp. 197 – 206, 1991.

28. Katayama, T., Yamazaki, F., and Lin, L., "*Soil Amplification based on Array Observation in Chiba, Japan.*" Proceedings of 2nd International Conference on Recent Advances in Geotechnical Earthquake Engineering and Soil Dynamics, St. Louis, Missouri, pp. 1181 – 1188, March 1991.

29. Katayama, T., Yamazaki, F., and Lin, L., "*Soil Amplification based on Seismometer Array and Microtremor Observations in Chiba, Japan.*" Earthquake Engineering and Structural Dynamics, Vol. 21, pp. 95 – 108, 1992.

30. Koya, Y., and Matsuo, O., " Shaking Table Tests of Embankments Resting on Liquefiable Sandy Ground." Soils and Foundations, Vol. 30, No. 4, pp. 162 – 174, 1990.

31. Kozin, F., and Natke, H. G., "*System Identification Techniques.*" Structural Safety, Vol. 3, 1986.

32. Kramer, S. L., "*Geotechnical Earthquake Engineering.*" Prentice Hall International Series, 1996.

33. Lin, J-S., and Chao, B. K., "*Estimation of Shear Modulus and Damping Factors of Earth Dam Material.*" Earthquake Engineering and Structural Dynamics, Vol. 19, pp. 891-910, 1990.

34. Lin, J-S., "*Extraction of Dynamic Soil Properties using Extended Kalman Filter,*" Journal of Geotechnical Engineering, ASCE, Vol.120, No.12, December 1994.

35. Matsunaga, Y., Iai, S., Morita, T., Sakurai, H., and Hitachi, S. "*Seismic Array Observation of S wave Propagation Phase Velocity And Direction.*" 5th US National Conference on Earthquake Engineering, pp. 141 – 148, 1996.

36. Nagata, S., Katayama, T., Yamajaki, F., Lin, L., and Turker, T., "*A Dense Seismograph Array in Chiba, Japan and its Strong Motion Database*" Proceedings of 4th US National Conference on Earthquake Engineering, Palm Springs, California, Vol. 1, pp. 357 – 366, May 1990.

37. Natke, H. G., *"Recent Trends In System Identification."* Structural Dynamics W.B. Kratzig et al. Eds., A. A. Balkema, Rotterdam, The Netherlands, 1991.

38. Pecker, A., "*Validation of Small Strain Properties from Recorded Weak Seismic Motions.*" Soil Dynamics and Earthquake Engineering, Vol.14, pp. 399 – 408, 1995.

39. Peng C. Y., and Iwan, W. D.,- "An Identification Methodology for a Class of Hysteritic Structures," Earthquake Engineering and Structural Dynamics, Vol.21, pp. 695 – 712, 1992.

40. Peter, G., and Archuleta, S., *"Array Analysis Of Seismic Signals."* Geophysical Research Letters, Vol.14. No. 1, pp. 13 – 16, January 1987.

41. Pilkey, W. D., and Cohen, R. E., "System Identification of Vibrating Structures: Mathematical Models from Test Data." Winter annual meeting of ASME, New York, 1972.

42. Safak, E., *"Discrete-time Analysis of Seismic Site Amplification."* Journal of Engineering Mechanics, Vol. 121. No. 7, pp. 801 – 809, 1995.

43. Santamarina, J. C., and Danta, F., *"An Introduction to Discrete Signals and Inverse Problems in Civil Engineering."* ASCE Press – New York, 1999.

44. Sawada, T., Hirao, K., Taniguchi, T., and Tsujihara, O., "*A Localized Identification of Dynamic Soil Properties of Subsurface Layers in Ground by Vertical Array Records.*" Earthquake Geotechnical Engineering, Ishihara, Balkema, Rotterdam, pp. 493 – 498, 1995.

45. Sayed, H. S., Abdel – Ghaffer, A. M., and Masri, S. F., *" Parametric System Identification and Seismic Performance Evaluation of Earth Dams during The October 17, 1989 Loma Prieta, California Earthquake."* Department of Civil Engineering, University of Southern California, July 1991.

46. Toshimi, S., Hiroshi, K., and Toshiaki, S., Evaluation of Site Effects and their Removal from Borehole Records Observed in the Sendai Region, Japan." Bulletin of Seismological Society of America, Vol. 85. No. 6, pp. 1770 – 1789, December 1995.

47. Tsujihara, O., Sawada, T., and Sugito, M., "*Identification of Subsurface Layers of the Ground by Using Vertical Array Records.*" Proceedings of 4th U.S. National Conference on Earthquake Engineering, Palm springs, California, Vol. 1, pp. 395 – 404, May 1990

48. Wen, K. L., Beresnev I, A., and Yeong, T. Y., "*Investigation of Nonlinear Site Amplification at Two Downhole Strong Ground Motion Arrays in Taiwan.*" Earthquake Engineering and Structural Dynamics, Vol. 24, pp. 313 – 324, 1995.

49. Yamazaki, F., Lin, L., and Katayama, T., "*Orientation Error Estimation of Buried Seismographs in Array Observation.*" Earthquake Engineering and Structural Dynamics, Vol. 21, 679 – 694, 1992.

50. Yasuyuki, K., and Osamu, M., "*Shaking Table Tests of Embankments Resting on Liquefiable Sandy Ground.*" Soils and Foundations, Japanese Society of Soil Mechanics and Foundation Engineering, Vol. 30. No. 4, pp. 162 – 174, 1990.

51. Yeong-Tein, Y., and Hung-Chie, C., "*Two New Strong-Motion Arrays in Haulien, Taiwan.*" Tenth World Conference on Earthquake Engineering, Balkema, Rotterdam, pp. 6947 – 6950, 1994.

52. Zeghal, M., *"System Identification of the Nonlinear Seismic Response of Earth Dams "* Ph.D. Dissertation, Princeton University, New Jersey, June 1990.

53. Zeghal, M., Elgamal, A. W., *"Analysis of Site Liquefaction Using Earthquake Records."* Journal of Geotechnical Engineering, ASCE, Vol.120, No.6, pp. 996 – 1017, June 1994.

54. Zeghal. M., Elgamal. A. W., and Tang. H. T., and Stepp. J, C., *"Lotung downhole array II: Evaluation of Soil Nonlinear Properties."* Journal of Geotechnical Engineering, ASCE, Vol.121, No.4, pp.363 – 378, April 1995.

55. Zeniou, C., *"System Identification using Correlation and Spectral Analysis of Earthquake Records of an Earth Dam,"* Master's Thesis, Princeton University, New Jersey, 1985.